NPL Report CMMT (A) 175

May 1999

Fine Scale Abrasion Testing of Hardmetals and Ceramics

M G Gee, A Gant and L Van der Berg

Centre for Materials Measurement & Technology
National Physical Laboratory
Teddington, Middlesex, UK, TW11 0LW

SUMMARY

This report describes the results of tests performed on a range of hardmetals and ceramics using tests which are relevant to the abrasion of these hard wear resistant materials by fine abrasives.

The three techniques that were examined are:

- High load single pass scratch testing
- Low load single and multiple pass scratch testing
- Ball cratering

The scratch tests provide a method of examining the response of the test materials to the model abrasion provided by a test indenter under carefully controlled conditions. In the case of the single pass high load tests this is relevant to severe abrasion from highly loaded abrasive particles. The low load scratch tests are relevant to less severe abrasion. In particular, the multiple pass scratch testing shows how abrasion damage builds up as repeated abrasion occurs.

In the scratch testing it was found that fracture was a predominant form of damage to both hardmetals and ceramics. In the case of the hardmetals the fracture was on a fine scale, but with the ceramics fracture occurred on a larger scale, often removing large fragments of material.

There was a general decrease in the scratch damage to the samples as the hardness of the materials was increased, but the results were not clear cut.

By contrast, in the ball cratering tests on the hardmetals, there was a small increase in wear as the hardness of hardmetals was increased. Wear occurred by a two stage process with mechanical removal of the binder phase followed by fracture of the WC grains.

ISSN 1361-4061

National Physical Laboratory
Teddington, Middlesex, UK, TW11 0LW

Approved on behalf of Managing Director, NPL, by Dr C Lea,
Head, Centre for Materials Measurement and Technology

CONTENTS

1 INTRODUCTION

Ceramics and hardmetals are used in many wear resistant applications. Project CAM 9, *Performance Related Wear Testing of Ceramics and Hardmetals*, is concerned with the development of wear testing procedures which are relevant to the industrial application of hardmetals and ceramics.

Wear by abrasion is the largest cause of wear problems in industry [1]. For this reason most of the testing that was carried out in project CAM 9 is concerned with abrasive wear. A companion report [2] describes the results of macroscopic abrasion tests where abrasion occurs through the action of many relatively large abrasive particles simultaneously. Although these tests can simulate the abrasion that occurs in industrial applications quite closely, it is difficult to obtain clear information on the details of the mechanisms of wear because of the complexity of the multiple interactions that occur.

Scratch testing is a technique that has potential for addressing the need for a simpler test to provide more fundamental information on wear mechanisms. It can be used as a test which simulates the interaction of a material with a single abrasion scratch event. The indenter tip is then a model of the abrasive particle. The load acting between the abrasive particle and the component (or in the scratch testing model between the indenter and the test-piece) is a crucial test parameter, and tests can be broadly divided into two categories. When the load is high, considerable fracture occurs to the material and the abrasive particle, and the wear process is termed high stress abrasion; when low loads are operating less fracture damage is caused and the wear process is termed low stress abrasion.

These two different extremes have been examined by using scratch tests with a relatively high stress of 50 N to simulate high stress abrasion, and further tests have been carried out at a lower load of 4 N to simulate low stress abrasion.

The scratch tests mentioned so far have consisted of single scratch events. Another modification to this test which was explored was carry out multiple scratches along the same scratch path, and monitor the build up of damage as the repeated abrasion events occur.

Ceramics and hardmetals are used in applications where fine scale abrasion are occurs. The recently developed ball cratering (micro-abrasion) test [3] is relevant to wear under these conditions, and tests have been carried out to explore the variation in wear that occurs for different hard materials.

The test methods and the rationale behind their choice are listed in Table 1 and a summary of the overall test conditions that are used is given in Table 2.

2 MATERIALS

The materials that were tested are listed in Table 3. Hardmetals with a wide range of grain sizes, % volume fraction binder phase, and different binder phase composition (cobalt and nickel) were tested. A selection of different ceramics were also tested and are listed in Table 4.

The sample size was 40 mm x 20 mm x 5 mm. This accommodated all the test systems described here.

3 TEST DESCRIPTION AND RESULTS

3.1 High Load Scratch Testing

3.1.1 Description of Test System

Scratch testing was developed originally as a quality control test for the measurement of the adhesion of coatings. It is still widely used in this role, but also offers potential as a model abrasion test method where the abrasion is caused by a single abrasive point (the indenter). The advantage of this approach is that the response of a material to this single point abrasion under these simple conditions can be controlled and modelled much more easily than in conditions where a high number of abrasive particles are acting in very close succession.

The test system employed, Figure 1 is based on an early CSEM [4] automatic loading system. The system was originally supplied without friction measurement capabilities, but these had been fitted, and data-logging is now carried out with a PC based data acquisition system. These modifications pre-dated project CAM 9.

The test-pieces were polished before the test. Careful polishing procedures were used for ceramic test-pieces to minimise surface damage and surface residual stresses. Hardmetal test-pieces were additionally annealed at 800 °C for 30 minutes under vacuum to ensure that an undamaged surface was produced.

3.1.2 Tests Results

For the hardmetals, the scratch width decreases with increasing hardness (Figure 2, Table 5). The different types of hardmetals (different binder phase volume fractions and composition) follow the same broad trend. There is also a decrease in friction coefficient with increasing hardness (Figure 3), but there is more scatter in the friction results and the trend is less clear.

A scratch hardness parameter H_s can be defined as

$$H_s = \frac{P}{A_p}$$

where P is the contact load and A_p is the projected contact area of the indenter with the surface (calculated from scratch width) as the scratch is formed [5]. There is an approximately linear relationship between scratch hardness and the conventional indentation hardness of the material (Figure 4).

As the scratch is formed, work is done by moving the indenter against the resistance of the material. This energy is dissipated through the generation of heat and the production of increased surface area of the scratch and associated debris.

The specific scratch energy (energy dissipated per unit volume of scratch formed) E_d, is given by

$$E_d = \frac{\mu F}{A_c}$$

where μ is the friction coefficient, F is the applied normal force, and A_c is the cross-sectional area of the scratch.

An approximately linear increase in the specific scratch energy dissipated density with increasing hardmetal hardness was observed (Figure 5).

When results for the ceramics are considered, there seem to be similar trends in results for scratch width and friction coefficient (Figures 6 and 7). However, a relatively small number of materials was examined by comparison with the hardmetals, so the trends are not so clear[1].

3.1.3 Surface Examination

3.1.3.1 Optical Examination

Optical micrographs of typical scratches are shown in Figure 8. For the hardmetals, the roughness of the scratches increases as the grain size of the hardmetal gets larger. This is particularly noticeable at the edges of the scratches where the shape of the edge is dictated by the grain structure of the material.

Grooving is present at the base of the scratches. The amount of grooving increases as the grain size of the hardmetal increases. This indicates that although the roughness of the surface of the indenter may cause some of the grooving, the majority is caused by the movement of debris over the surface. The condition of the indenter was checked after the series of experiments and was unaltered in appearance.

[1] Because the ceramic materials crack when indented under high loads, it is not possible to use the 30 kg Vickers indentation measurements to obtain hardness values for the ceramics. For this reason a lower indentation mass of 0.1 kg was used for the ceramics. This means that the two different hardness scales are not directly comparable.

The appearance of the scratches in the ceramics varied considerably with the microstructure of the materials (Figure 9). Scratches for the Sintox and the SSN materials were similar to those observed with hardmetals. However, the RBSC scratch was very rough, showing signs of gross fracture. The α-SiC scratch was also very rough, but with some fragments of material at the side of the scratch which showed curved cracks. These cracks were likely to be the remaining traces of Hertzian cracking caused by the movement of the loaded indenter over the surface of the sample.

3.1.3.2 Scanning Electron Microscope Examination

Low magnification SEM micrographs of the scratches on the hardmetal samples show similar features to the optical micrographs (Figure 10). However, in the coarse grained materials, it was clear that the microstructure revealed at the base of the scratch was considerably disturbed by comparison with the original structure (seen at the edges of the scratch).

Higher magnification examination of the fine grained hardmetal material (Figure 10a) shows little obvious change to the overall microstructure over most of the surface apart from some obvious grooving over the scratch surface. There are some areas where grains of WC appear to have been removed from the surface.

Coarse grained hardmetal samples show considerable microstructural damage with most WC grains fractured, and many grains have fragmented into small particles which are embedded in the binder phase (Figure 10b). It is noticeable that in some of the larger carbide grains which were fractured, the fracture planes are typically perpendicular to the scratch direction.

As previously noted, the scratch tests on the ceramics showed different behaviour depending on the structure of the material (Figure 11). The RBSC scratch shows a highly fractured surface, with some small fragments of material visible at the base of the scratch. The vitox scratch shows intergranular fracture over most of the scratch surface with only isolated areas of unfractured material remaining. The α-SiC scratch is also heavily fractured, but the fracture here seems to be transgranular. It is noticeable that there is a circular form to many of the fracture paths in the scratch, presumably due to Hertzian cracking.

3.2 Low Load Scratch Testing

3.2.1 Test Description

The low load scratch test system was designed to enable tests to be carried out accurately at low applied loads. The rationale that lies behind this test system is that the abrasion that occurs in many applications takes place through low load contacts. Key features of the test system, Figure 12, are the frictionless bearings for the lever arm, full computer control and data acquisition, measurement of frictional load by a horizontal axis of a dynamometer, measurement of the applied load by a static load cell in addition to the vertical axis of the dynamometer, measurement of the horizontal position of the test-piece, and the vertical position of the indenter.

In addition the test system is designed to allow multiple repeat scratches to be performed. This enables the build-up of damage to be studied as repeated abrasion of the same position on the test-piece takes place. The same test-pieces were used in both the high load and low load scratch tests (section 3.3).

3.2.2 Results

The results of the low load scratch tests are given in Tables 6-13.

One of the key results obtained is the variation of average friction coefficient with number of repeat scratches. The behaviour observed varied considerably (Figure 13) for the hardmetals. In some cases the average friction coefficient rose steadily with number of repeats (13a; TC222 with 200 μm indenter, 13d; CWC15C with 200 μm indenter). In other cases there was an initial increase in average friction coefficient over the first few repeats followed by a plateau in the average friction coefficient (13b; MA10 with 200 μm indenter, 13e; SHMUF with 50 μm indenter). There were also some cases where the fiction coefficient initially reduced to a plateau value for the rest of the repeat scratches (13f; SHMUF with 200 μm indenter). In most cases the repeatability in the tests was quite good with the data points for the different scratches falling well within the error bands describing the variation in friction within a single repeat scratch. However, in a few cases the results for the different scratches did not agree so that there were significant differences in the data values from one scratch to another (Figure 13d).

Similar results are seen for the ceramic samples, but the most common behaviour is for an initial fairly rapid increase in friction to a maximum followed by a drop to a steady value (Figure 14).

The variation of initial scratch width (width of a single with scratch) hardness was examined, but no obvious trend in results was observed for either the hardmetals or the ceramics (Figures 15 and 16). However, it was quite noticeable that for most materials the initial scratch width for the 50 μm indenter was larger than the initial scratch width for the 200 μm indenter.

One of the key purposes in performing repeated scratches with the low load test system is to examine the build up of damage as the number of passes of the diamond indenter over the same path on the sample increases. Figure 17a shows that for the hardmetals with a 50 μm indenter, as the number of repeats increases the width of the scratch increases (with the rate of increase in width decreasing as the number of repeats increases). Figure 17b shows the same data with a logarithmic scale for the number of repeats. This shows an approximately linear relationship for many of the hardmetals.

The width of the scratches in the ceramics with the 50 μm radius indenter increases in a similar way to the hardmetals (Figure 17c). However, the increase in scratch width is greater for most of the ceramics than for most of the hardmetals.

With the 200 μm radius indenter there is very little increase in scratch width with number of repeats for the hardmetals (Figure 18a). By contrast, the scratch width increases considerably with the number of repeats for most of the ceramics (Figure 18b).

Figure 19 shows the variation in final friction coefficient (friction coefficient at the end of a scratch with a certain number of repeat passes) with final scratch width (scratch width at the end of a scratch with a certain number of repeat passes) for the hardmetals and ceramics for scratches performed with the 50 μm and 200 μm indenters. Different types of behaviour are observed. The final friction coefficient for the hardmetals with the 50 μm indenter decreases initially then increases as the number of repeats increases (and thus the scratch width increases). With the ceramics and a 50 μm indenter the final friction coefficient rises as the final scratch width increases for the RBSC, but decreases for the other materials (Figure 19b).

For the 200 μm indenters the final friction coefficients increase as the final scratch width increases for most hardmetals (Figure 19c), but decrease for a few materials. RBSC shows a progressive increase while for the other ceramics there is an increase to a maximum followed by a decrease (Figure 19d).

3.2.3 Surface Examination

Optical micrographs of scratches on hardmetals are shown in Figures 20-23. There is a build up of gross damage to the microstructure of the samples as the number of repeats increases for all the hardmetals. However, the severity of this damage seems to be greater for the coarse grained materials (eg Figure 22c) than for the fine grained materials.

Gross damage builds up much more quickly for the ceramics (Figures 23-27). For the Vitox tested with the 50 μm indenter gross fracture of the material has taken place at the base of the scratch even for a single scratch (Figure 24a). By comparison, with the 200 μm indenter damage on this scale only occurs after a few repeat scratches have taken place (Figure 25b).

The build up of damage on the RBSC sample with the 200 μm indenter is particularly interesting (Figure 26). Even with a single pass, some fracture has occurred to the sample. Fracture damage rapidly increases with curved cracks aligned roughly perpendicular to the direction of scratching for the scratches with 2 and 10 repeats. Eventually the scratch surface suffers from gross failure (Figure 26d).

Scanning electron microscopy (SEM) provided a considerable amount of additional information on the build up of damage.

On the N15 hardmetal sample tested with a 200 μm indenter with 100 repeat passes there was a dark contrasting film had build up on the surface of the scratch (Figure 27a). This film was also visible on the surface of the scratch made with the 50 μm indenter for 100 repeat passes (Figure 27c). However, when the same sample tested with the 50 μm radius indenter for 20 repeated passes was examined there was no sign of this film but there was evidence for break-up of carbide grains and fracture of the scratch surface (Figure 27b).

Further evidence of the formation of the dark contrasting films after a large number of repeat scratches are seen on examination of a number of other scratches on hardmetals (Figures 28, 29d, and 30c).

For the CWC20C sample tested with the 200 μm indenter, there is a clear progression in fracture damage to the material as the number of repeat scratches increases (Figures 29a, 29b, 29c and 29d). The WC grains become progressively broken up and fragmented until after 200 repeat scratches have taken place a film of material is left on the surface of the scratch which contains a few larger fragments of WC with a very large number of small WC fragments. Some of these fragments of WC are 100 nm or less in size (Figures 29e-29g).

The ultrafine hardmetal material (SHMUF) shows damage on the first traverse with the 200 μm indenter (Figure 30a). As the number of traverses increases the film noted earlier forms (Figures 30b and 30c). Figure 30e shows the edge of this film on the 50 repeat scratch and shows that the film is composed of small fragments of WC embedded in a dark contrasting film. The size of the WC fragments in the film is much less than the size of the WC grains in the unaltered microstructure (which is visible towards the base of this micrograph). The edge of the 100 repeat scratch with the 200 μm radius indenter also shows breakaway of material (Figure 30f).

Scanning electron micrographs of the surface of the scratches produced in low load experiments on ceramics are shown in Figures 31-38. Normally the build up of damage is slower (in terms of number of scratch repeats) for the 200 μm radius indenter than for the 50 μm radius indenter.

Quite severe fracture damage has already occurred after a single pass for the α-SiC sample (Figure 31a), and builds up as the number of repeats increases (Figures 31b and 31c). By contrast, the first isolated pockets of significant fracture damage for the 200 μm indenter only occurs after 50 repeat passes (Figure 31e). This damage extends along the length of the scratch and becomes more marked as the number of repeats increases (Figures 31f and g).

A similar picture emerges for the RBSC where significant damage occurs after only a single pass for the 50 μm radius indenter(Figure 32), but only a small amount of fracture occurs after two repeat passes for the 200 μm radius indenter (Figure 32b).

Vitox also behaves similarly, but it is interesting that the fracture observed for the material is predominantly intergranular (Figure 33), although there is clear evidence for some transgranular fracture of grains (Figure 33d).

3.3 Ball Cratering

3.3 Test Description

Ball cratering is a miniaturised abrasion test method which has been developed over the last few years from two earlier techniques. These were the production of TEM test-pieces by dimpling with a wheel or ball to produce a spherical depression which was more easily thinned; the second was the use of a ball and appropriate grinding media to produce a spherical crater with known geometry which cuts through a coating. From measurements of the diameter of the crater in the substrate and the coating the thickness of the coating can be readily calculated.

Through better control of test parameters such as load, speed, abrasive type and suspension etc these techniques have been developed into wear tests [2,5]. There is now great interest in the use of the test for thin hard coatings such as TiN, polymeric films such as paints, and other monolithic materials.

One of the key points with the test is that it enables a small area (about 0.5-1 mm across) to be evaluated, with little damage to a component that in many cases can remain in service. The test could in principle be made portable, to carry round to the component rather than vice-versa.

The commercial test system [6] used at NPL is shown in Figure 34 and is a lever arm loaded test system which uses a ball fixed in a split shaft. The test-piece is pressed against the rotating ball. Abrasive is drip fed onto the contact interface between the ball and the test-piece.

Some modifications to the test system as supplied were found to be necessary. These were the addition of a separate peristaltic pump to supply the abrasive feed to the test. In the supplied test system, the main test motor that also rotated the ball drove the peristaltic pump. This arrangement meant that the abrasive feed rate could not be adjusted separately from the ball rotation speed, giving lack of control of the test conditions. The second modification that gave better usability of the test system was to replace the supplied ball revolution counter with a counter which shut off power to the drive motor and peristaltic pump when the preset number of revolutions had been reached. The third modification was to add a video camera system with video printer that enabled images of craters to be captured while test-pieces were still clamped in place in the test system so that evolution of the craters could be examined without removing the test sample. An image capture board also allowed immediate digitisation of images of the craters for analysis of crater size.

3.3.2 Results

The overall results of ball cratering tests on hardmetals are given in Figure 35 and Table 14. When all the hardmetal results are considered, considerable scatter was evident with no obvious trend in results. When only the hardmetals with a 6% Co binder phase composition were considered, there was again considerable scatter in the results, but there was also a slightly surprising indication of a small increase in wear as the hardness increased. To check the scatter in results, some tests were repeated and were found to give a similar variation.

Figure 36 shows the results of performing tests in a range of different suspension fluids. No obvious effect of the different fluids was seen, but again it was found that there was some evidence for an increase in wear as the hardness of the material increased.

The effect of changing the test duration was also examined and it was found that the wear normally increased as the test duration was increased (Figure 37). However, there was again considerable scatter in the results which meant that the results were not clear cut.

With the ceramic samples, tests were performed using two different abrasives and two different test loads (Figure 38a, Table 15). By contrast with the hardmetal samples, there was

a marked decrease in wear for the ceramics tested using SiC abrasive as the hardness of the ceramic was increased. However, when silica abrasive was used the wear was much reduced at low values of hardness for the ceramics, with a maximum in wear for the ceramics at a ceramic hardness of about 1600 HV0.1.

Some tests were also performed on the ceramics using a commercial 0.25 μm diamond abrasive suspension. Again, it was found that there was a maximum in wear, but this now occurred at a higher hardness of about 1800 HV0.1 (Figure 38b).

To examine the effect of load on wear a series of experiments was performed at different loads on a hardmetal sample (Figure 39). This showed no variation in wear with increase in test load as the test load was increased from 0.1 to 10N.

3.3.3 Surface Examination

Some optical micrographs of wear scars on hardmetal samples are shown in Figure 40 and confirm that there is a clear-cut consistent relationship between wear and hardness of the hardmetal. It is also clear that the edge of the scar is not distinct but is feathered and diffuse, potentially one of the reasons for some of the scatter observed in test results for the hardmetals.

Figure 41 shows a scanning electron micrograph of a typical wear scar on a hardmetal. The grooving that is seen across the middle of the scar is visible on many of the hardmetal wear scars.

A higher magnification view of the grooves is shown in Figure 42a. The grooves are about 15-25 μm wide. The edge of a crater is shown in Figure 42b and shows isolated areas of damage which became more frequent in the direction of the centre of the scar.

The rest of the micrographs in Figure 42 show the response of the hardmetal microstructure to the abrasion. The binder phase seems to have been completely removed from thesurface region. There is also considerable microfracture damage to the WC grains in the form of "pock-marks" over their surface.

Examples of wear scars for the ceramic samples are shown for the Vitox and α-SiC in Figures 43 and 44. There is only a small amount of fracture damage to the ceramics with the majority of the wear scar relatively smooth and flat. In the Vitox, where fracture has occurred this is by an intergranular process.

Figure 45 shows the wear scar on a hardmetal sample tested at a load of 5N. A large area can be seen which is much smoother than the rest of the scar running back from a point fairly close to the leading edge of the wear scar. High magnification examination of this scar shows that the hardmetal in this region has not worn significantly, indicating that abrasive has not reached this region of the sample.

4 DISCUSSION

4.1 Scratch Testing

4.1.1 Correlation between scratch hardness (scratch width) and sample hardness.

One of the significant results for the high load scratch testing tests performed on both the hardmetals and the ceramics is the correlation that is observed between scratch hardness and hardness of the sample (Figure 5). (Note that this is equivalent to the observed inverse correlation between scratch width and sample hardness (Figure 3) due to the assumption of a conformal geometry between the scratch and the diamond indenter). This suggests that conventional hardness measurements can be used to give a reasonable estimate of the magnitude of the damage to the sample that is caused by scratching under the conditions used in the high load test.

By contrast, there is very little if any correlation between the scratch width and the sample hardness for the single pass low load scratches (Figure 16). There are several possible reasons for this. The first possibility is that any trend may be obscured by instrumental scatter.

A second possibility is that any trend is masked by changes in the indenter geometry and the effect that this would have on the resultant width of the scratch. This might occur over a period of time within one test, or when the indenter was changed. It is certainly true that damage to indenters was observed in the repeated low load scratch testing experiments, and this was the reason for trying to minimise the effect of indenter damage through the frequent introduction of new indenters.

The verification of the shape of indenters is a technical problem that has still not been completely solved. Thus recent work on scratch testing of TiN coatings has shown that the measurement of indenter shape is still a concern and can have a detrimental effect on the quality of results [7]. Work is now underway to try to address this issue [8].

The third potential reason why there is little correlation between the scratch width and the sample hardness is that because of the lower load, the indenter penetrates into the surface of the sample much less than in the case of the high load scratch tests. This means that surface adhesion effects are much more important than for the high load scratches, with the possibility that small variations in surface condition or composition may have a large effect on the results that are obtained.

4.1.2 Friction

An inverse correlation was also observed between friction coefficient and sample hardness. This correlation was quite strong for the high load hardmetal scratches, but was nothing like as clear-cut for the low load scratches. Friction is known to be dependent on two general contributions. These are:

- The force needed to induce deformation (including fracture as far as this discussion is concerned).
- The force needed to overcome the adhesion that is generated between the two surfaces.

The deformation term can be identified with the force that is used to generate the permanent scratch.

The better correlation for the high load scratches is perhaps not surprising, as it is likely that the deformation term will be larger for the high load scratches, with surface effects being more important for the low load scratches as discussed earlier with respect to the initial scratch width.

The consideration of the force required to generate the scratches suggests that another way of looking at the friction data is to consider the energy dissipated in the generation of the scratch (Figure 5). This was also found to give a reasonable correlation with hardness for the hardmetal samples tested at high load.

The changes in average friction with number of repeats gave a number of different types of behaviour, with decreases for some samples, increases for others and thresholds in average friction for a third group of materials. In many cases this behaviour was repeatable, but the reasons for the different types of behaviour are not understood and more work will clearly be required before this can be fully developed.

4. 3 Development of scratch widths in repeated low load scratch tests

One of the most important measurements obtained in the low load scratch tests is the development of the width of the scratch as the number of repeated passes in the same scratch path is increased. This increase in scratch width is directly related to the development of the volume of the scratch and the increase in damage as repeated abrasion events occur. The increase in scratch width is not linear with the number of scratch repeats, and in fact in most cases is quite well described by a linear dependence on the logarithm of the repeat number.

It may be argued that this is due to the fact that the parameter that is really important is the volume per unit length V_s of the scratch which is clearly a non-linear function of the scratch width w and is expressed by the relationships:

$$V_S = \frac{1}{2}R^2\theta - w\left(R^2 - \frac{w^2}{4}\right)^{\frac{1}{2}}$$

where

$$\theta = \arcsin\left(\frac{w}{2R}\right)$$

and R is the radius of curvature of the indenter (and therefore also of the base of the scratch which is assumed conformal to the indenter).

When the measured values of scratch width are used to calculate scratch volume for some selected samples, a non-linear increase in scratch volume with increasing number of repeat scratches is found, with the rate of increase in volume decreasing as the number of repeat passes increases (Figure 46).

One reason why the relationship between scratch volume and repeat number is not linear is that although the applied test load is constant, the contact area is increasing with every repeat pass, so that the stress acting on the sample is decreasing as the test proceeds. Thus if the amount of damage that is caused is dependent on the applied stress rather than the applied load, the observed dependence of scratch volume on repeat passes is quite likely. Another reason is that for many different materials an altered surface layer is formed which may have a better capacity to resist further surface damage than the original material. This can occur through plastic deformation processes such as work hardening, or by the mechanical compaction of crushed material at the surface. Thus the observed volume dependency is simply due to the build up of this altered surface layer.

It is clear that the progressive increase in the width of the scratch for the ceramic materials is much greater in most cases that that for the hardmetals. An easy way to compare the rates of increase is to examine the slope parameter B obtained by fitting the logarithmic relationship $w=B \log(r)$ (where r is the number of repeat scratches) to the scratch width data.

These results are shown in Figure 47, and show:

- The rate of increase in scratch width as described by the slope parameter B (which is measure of damage) is always greater for the 50 μm indenter than the 200 μm indenter. The slope parameter B is nearly always greater for the ceramics than for the hardmetals with similar hardness (there are some exceptions), with particularly large slope parameters for some of the ceramics.

These results imply that although the initial ability of some ceramics to withstand scratching damage is better than many hardmetals, because the scratch damage to the ceramics increase more rapidly (in most cases) than the hardmetals, the hardmetals prove to be better at withstanding repeated abrasion damage.

4.1.4 Mechanism of damage

In the hardmetals the main mechanisms of damage are through the fracture of WC particles to form small fragments of WC which are then embedded in a film of dark-contrasting film which was observed to form at the surface of scratches. This dark contrasting film is likely to be binder phase material (cobalt for most of the hardmetals tested here), and it is known from the literature that the surface layers of hardmetals subjected to scratching form a layer near the surface which is depleted in binder phase with the binder reforming on the surface of the hardmetal [9,10].

In the case of the high load tests, this damage takes place in a single scratch. For the low-load scratches the damage builds up more slowly as the number of passes increases. What is quite remarkable is the small size of the particles that are formed which can be as small as 50-100 nm.

The mechanisms of fracture for the WC grains are not yet clear, and further work would be required to develop an understanding of this process.

A clear dependence of the damage mechanisms on grain size was observed, with fracture of WC grains much more evident for the large grained materials than the fine grained materials.

In the case of the ceramics, fracture was a major form of damage. Two distinct types of damage were observed. These were partial Hertzian ring cracking. This has been observed previously, and is a well understood form of damage for brittle materials due to the stress fields that are generated underneath a spherical indenter. The cracks are partial due to the alteration of the stress fields due to the movement of the indenter. Ceramics where signs of Hertzian cracking were observed include RBSC and the α-SiC. Where Hertzian cracking is evident, the increase in scratch width with number of repeat passes in the low load scratch tests is due to the build up of fracture damage. Thus the first pass causes some fracture to the surface which weakens the structure. The second and subsequent repeat passes remove some of this weakened material and cause additional fracture damage. Eventually, for some of the ceramics, films of material and debris from the fracture processes form at the interface.

There is the possibility that reactions with the surrounding atmosphere occur through tribochemical processes. However, there is no specific evidence for these processes which often occur in sliding wear contacts where high temperatures can be generated which accelerate the reactions.

The other fracture process that was observed in the ceramics was the evident intergranular fracture that was seen for the Vitox high purity alumina. This indicates that the strength of the grain boundary is very important in determining the resistance of this material to scratching. Intergranular fracture may also be involved in the scratch testing of the other ceramic materials, but the evidence for this is not clear.

4.2 Ball Cratering

The most puzzling feature in the ball cratering tests was the apparent lack of any dependency of wear on hardness for the hardmetals. In fact, what effect there was seemed to indicate that the wear actually increased as the hardness increased. This type of behaviour is not normally observed.

The mechanisms of damage that were observed in the hardmetals suggest a two-stage process:

- Initially the binder phase was removed from the surface of the hardmetal sample leaving the WC grains unsupported by the binder.
- The WC grains were then fractured and removed; either in fragments or by removal of whole clumps of material. The "pock-marking" that was observed on some of the larger carbide grains was interesting evidence of micro-scale fracture which weakened the structure of the grains.

It was thought that the removal of the binder phase might be due to corrosion by water. It is well known that the cobalt binder phase in hardmetals is corroded by acidic media. However, when different media including strongly alkaline $Ca(OH)_2$ were used for the suspension, there was no correlation with results. This ruled out corrosion as a contributory mechanism, and it is very likely that the removal of the binder phase is a completely mechanical process. This conclusion is also supported by the fact that some Ni binder phase hardmetals were also tested which did not show any dramatic differences in wear from the Co binder materials.
With respect to the removal of the binder phase, it is important to realise that the size of the abrasive that was used in the ball cratering tests is similar in size to the scale of the structure in the hardmetals (4 μm). This increases the likelihood of mechanical removal of the binder phase by abrasion.

A possible mechanism for the removal of the WC particles is by surface fatigue of the WC grains. As the surface fatigue resistance may be expected to have a different dependency on hardness (eg the toughness of the hardmetal will decrease as the hardness increase), this may possibly explain the lack of a strong dependency of wear on hardness in ball cratering of the hardmetals.

Another puzzling feature that was observed in the ball cratering of the hardmetal is the constant wear as the test load is increased. The reason for this behaviour becomes clear when the wear scars for the samples tested at high loads are examined (Figure 45). These show a region where little or no wear has occurred that extends to the trailing edge of the wear scar. In this region, it is suspected that no abrasive suspension has penetrated due to the close contact between the ball and the sample under the increased test loads in these experiments. Thus the wear is limited by starvation of abrasive from the centre of the wear contact. This type of effect has also been observed by other workers for other materials.

By contrast with the hardmetals, with the SiC abrasive, a clear reduction in wear is observed as the hardness of the ceramic is increased. However, when SiO_2 abrasive is used, a maximum wear is observed as the hardness of the sample is increased. This maximum occurs at a sample hardness close to the hardness of the abrasive. This effect is not expected, as it is normally considered that wear should decrease markedly as the hardness of the sample increased above the hardness of the abrasive.

5 CONCLUSIONS AND RECOMMENDATIONS FOR USE OF TESTS

A range of tests and summary procedures for their use has been described, and the results of some preliminary experiments have been given.

The scratch tests are yielding results that give useful information about the response of the ceramics and hardmetals to a variety of different wear conditions.

The high load scratch test gives information of the resistance of materials to deformation under high load single contact conditions whereas the multiple scratch testing is appropriate for the assessment of the damage to materials from abrasion where applied loads are of the order of

a few N and multiple scratching events are likely. The use of both tests should be combined with microscopy of the scratches to determine the mechanisms of how abrasion damage is built up. This will provide information that can be used to improve the selection of materials for a particular application or to suggest how changes in operating conditions might ameliorate abrasion.

By contrast, the ball cratering test does not seem to be giving information which can be easily interpreted; although this test is very relevant to abrasion in conditions where applied loads are low and the size of abrasive slurries is small. The results do not show clear cut trends and further work is needed to correlate the test results to the details of the wear mechanisms.

6 ACKNOWLEDGEMENTS

The work described in this report has been funded by the UK Department of Trade and Industry under the Materials Measurement Programme on Charactersation and Performance of Advanced Materials.

7 REFERENCES

1) M G Gee and S Owen-Jones, Wear Testing Methods and Their Relevance to Industrial Wear Problems, NPL Report CMMT (A)92, December 1997
2) M G Gee, A Gant, W P Byrne and B Roebuck, Abrasion and Reciprocating Wear of Hardmetals and Ceramics, NPL Report CMMT(A)166, May 1999
3) K L Rutherford and I M Hutchings, A micro-abrasive test, with particular application to coated systems, Surf Coat Technol, 79(1996)231-239
4) CSEM Scratch Testing System, CSEM Instruments, Jaquet-Droz 1, CH-2007 Neuchatel, Switzerland
5) R Gahlin, M Larssen, P Hedenquist, S Jacobson & S Hogmark. The Crater Grinder Method as a Means for Coating Wear Evaluation - State of the Art, Surface & Coatings Technology.
6) Plint and Partners TE 66 Test System, Plint and Partners, Wokingham UK
7) H Vetters et al, Development and Validation of Test Methods for Thin Hard Coatings (FASTE), EU Contract, MAT1-CT 940045
8) EU Project, A certified REference MAterial for the Scratch Test – REMAST, EU Contract SMT4-CT98-2238
9) E A Almond, L A Lay, M G Gee. Comparison of Sliding and Abrasive Wear Mechanisms for Cemented Carbides and Ceramics, Proceedings of 2nd International Conference on the Science of Hard Materials, Institute of Physics Conference Series No 75: p919, Adam Hilger, 1986
10) J Larsen-Basse and N Devnani, Science of Hard Materials, Proceedings of 2nd International Conference on the Science of Hard Materials, Institute of Physics Conference Series Number 75, pp 883-895, 1986

8 TABLES

Table 1, Test methods used.

Test Method	Rationale
Ball cratering	Test relevant to abrasion by suspensions of fine abrasive material.
Scratch testing	Test relevant to abrasion; single point simulation of high stress abrasion.
Low load scratch testing: single scratch	Test relevant to abrasion; single point simulation of low stress abrasion.
Low load scratch testing: multiple scratches	Test relevant to abrasion; single point simulation of cumulative build up of abrasion damage.

Table 2, Summary of test conditions

Test	Load, N	Duration	Abrasive Type & Size	Relative Speed	Other
Scratch testing	50	Single pass, 10 mm length	0.2 mm radius diamond indenter	0.01 m s^{-1}	
Low load Scratch testing	4	Single pass, 5 mm length	0.2 mm, 0.05 mm radius diamond indenters	0.002 m s^{-1}	
Multiple pass scratch testing	4	2, 5, 10, 20, 50, 100 passes; 5 mm length	0.2 mm, 0.05 mm, radius diamond indenters	0.002 m s^{-1}	Scratches always in same direction.
Ball cratering	0.25	79m	4 μm silicon carbide, 4 μm silica, 0.25 μm diamond	0.1 m s^{-1}	

Table 3, Hardmetal materials, binder phase is Co unless otherwise specified.

Material	Source	Nominal Binder Content wt%	Arithmetic Mean Linear Intercept µm	Hardness, HV30	Composition, %
A2a		6	1.15	1576	
B1		6	0.29	1925	
B4		6	1.33	1513	
D4		6			
F3		6	0.6	1717	
F4		6		1589	
M4		6	2.94	1221	
M6		6	0.28	1925	
K3		6	0.66	1661	
K5		6	1.31	1487	
L1		6	0.94	1576	
MA6	Marshalls	6	1.56	1265	
MA10	Marshalls	10	1.83	1230	
MA15	Marshalls	15	1.09	1080	
MA20	Marshalls	20	1.22	991	
MA24	Marshalls	24	1.14	860	
MAN6	Marshalls	6*	0.64	1535	5.43 Ni, 0.44 Mo
MAN10	Marshalls	10*	0.80	1280	9.83 Ni
CW15F	CW Carbides	15	1.03	1192	
CW15C	CW Carbides	15	1.94	1043	
CW20C	CW Carbides	20	2.17	890	
CW25C	CW Carbides	25	2.14	804	
CWN8	CW Carbides	8	0.83	1391	7.38 Ni
T	Hydra	10	2.03	1218	
UC9	Hydra	9	4.90	982	
M15	Hydra	15	2.04	1028	

Material	Source	Nominal Binder Content wt%	Arithmetic Mean Linear Intercept µm	Hardness, HV30	Composition, %
T6	Boart Longyear	6	1.24	1494	
G10	Boart Longyear	10	1.76	1238	
G15	Boart Longyear	15	1.93	1100	
N6	Neepsend	6	0.78	1565	
N10	Neepsend	10	0.40	1630	
N15	Neepsend	15	0.56	1255	
TC6	Teco	6	0.86	1589	
T16D	Teco	16	0.94	1227	
T20D	Teco	20	1.02	976	
T25D	Teco	25	1.11	879	
SHM5CN	Sandvik HM	5	0.35	1971	3.35 Co, 1.1 Ni
SHMUF	Sandvik HM	6	0.15	2146	
D10	Dymet	10	1.14	1311	
D15	Dymet	15	0.88	1204	
DN6	Dymet	6*	0.67	1591	5.51 Ni
DN10	Dymet	10*	0.84	1311	9.59 Ni
TC222	Kennametal	6	3.59	1156	0.48 Fe
K3560	Kennametal	10	2.75	1156	0.16 Fe

Table 4, Ceramic materials

Material	Source	Grain Size, µm	Hardness, HV0.1	Density	Composition
RBSN	Tenmat	1-2	750	2.53	Si_3N_4
RBSC	Tenmat	10-30	2000	2.96	SiC, 10 % Si
SSN	Tenmat	3	1600	3.11	
α-SiC	Carborundum	10	2300	2.87	SiC
Vitox	Morgan Matroc	1-2	1900	3.96	99.99 % alumina
Sintox	Morgan Matroc	3-8	1600	3.72	95 % alumina

Table 5, Results of high load (50 N) scratch tests

Sample	Scratch Width, µm	Friction Coefficient
M4	0.095	0.35
K5	0.078	0.26
B4	0.083	0.23
A2a	0.091	0.23
L1	0.081	0.19
F4	0.080	0.24
F3	0.079	0.23
M6	0.066	0.16
SHMUF	0.072	0.27
TC222	0.125	0.34
N6	0.089	0.29
MA10	0.105	0.29
N10	0.089	0.27
CWC15C	0.124	0.29
D15	0.109	0.29
N15	0.097	0.28
CWC20C	0.132	0.30
MAN10	0.104	0.33
CWN8	0.107	0.33
RSBC	0.092	0.26
α-SiC	0.091	0.28
Sintox	0.129	0.35
SSN	0.094	0.29
Vitox	0.109	0.27

Table 6, Results of low load (4 N) scratch tests on hardmetal samples with 200 μm indenter. Results given are scratch widths in μm.

Materials	Repeats						
	1	2	5	10	20	50	100
MAN10	22.3		26.0		26.4		35.6
D15	30.9				45.4	45.3	46.9
N15	30.6		40.7		42.6	38.3	40.2
N10	32.7		33.5	43.2	47.3		47.6
MA10	24.8	27.4	27.9	29.2	29.9	31.7	32.1
TC222	29.3		34.1	37.6	37.8	38.7	40.7
N6	22.1	26.9	30.0	31.1	27.9	29.9	34.2
CWN8	31.7	35.9	42.2	34.3	47.2	37.4	52.8
CWC15C	28.8	38.1	32.0	34.4	39.6	39.5	45.9
CWC20C	34.6	42.5	43.5	44.1	45.9	45.5	64.7
SHMUF	30.3	35.2	35.3	42.0	38.2	41.4	39.7

Table 7, Results of low load (4 N) scratch tests on ceramic samples with 200 μm indenter. Results given are scratch widths in μm.

Materials	Repeats						
	1	2	5	10	20	50	100
RBSC	27.8	35.4	42.0	42.3	39.0	48.3	48.7
Vitox	15.5		16.9	18.0	25.0	47.3	80.1
Sintox	12.8	14.0	19.6	20.1	25.2	32.4	30.2
SSN	10.0	14.2	17.5			27.1	34.0
α-SiC	20.3	28.8	28.8	34.6	49.7	81.9	92.6

Table 8, Results of low load (4 N) scratch tests on hardmetal samples with 50 μm indenter. Results given are scratch widths in μm.

Materials	Repeats						
	1	2	5	10	20	50	100
MAN10	28.8	32.6	34.7	39.7		50.2	60.3
D15	32.8	35.1	39.0	42.1	44.8	51.0	57.5
N15	30.0	31.2	36.4	39.2	41.1	46.3	48.4
N10	24.4	25.7	26.9	28.8	28.6	32.9	39.0
MA10	28.1	30.9	36.3	37.4		47.1	53.5
TC222	36.0	37.7	43.0	48.1	54.9	69.7	77.6
N6	25.5	27.7	30.2	33.3	37.6	44.9	52.6
CWN8	28.9	30.8	34.6	36.7	41.8	51.5	59.7
CWC15C	34.0	40.1	42.3	44.6	48.1	51.9	63.9
CWC20C	30.5	33.4	35.5	38.5	38.7	47.1	64.2
SHMUF	28.4	28.4	32.3	34.5	44.0	39.6	46.3

Table 9, Results of low load (4 N) scratch tests on ceramic samples with 200 μm indenter. Results given are scratch widths in μm.

Materials	Repeats						
	1	2	5	10	20	50	100
RBSC	35.5	47.0	53.8	70.8	81.3	88.5	102.8
Vitox	26.7	47.1	67.9	83.9	102.9	128.4	134.0
Sintox	29.6	27.9	60.4	68.4	81.9	108.9	107.6
SiN	21.6	26.4	29.4	32.2	37.9	37.6	29.1
SSN	28.2	32.6	35.1	43.6	45.3	51.1	52.3

Table 10, Results of low load (4 N) scratch tests on hardmetal samples with 200 μm indenter. Results given are values of friction coefficient for final repeat of given scratch.

Materials	Repeats						
	1	2	5	10	20	50	100
MA10	0.61	0.51	0.53	0.57		0.66	0.72
D15	0.53	0.40	0.40	0.46	0.48	0.52	0.56
N15	0.57	0.44	0.45	0.45	0.48	0.51	0.55
N10	0.41	0.44	0.45	0.46	0.47	0.51	0.57
MA10	0.55	0.46	0.44	0.48	0.54	0.63	0.65
TC222	0.66	0.54	0.59	0.61	0.64	0.66	0.67
N6	0.53	0.44	0.46	0.50	0.53	0.59	0.65
CWN8	0.53	0.49	0.48	0.54	0.60	0.62	0.68
CWC15	0.58	0.41	0.41	0.51	0.55	0.59	0.61
CWC20	0.54	0.52	0.47	0.51	0.56	0.60	0.61
SHMUF	0.35	0.38	0.41	0.47	0.52		0.54

Table 11, Results of low load (4 N) scratch tests on ceramic samples with 200 μm indenter. Results given are values of friction coefficient for final repeat of given scratch.

Materials	Repeats						
	1	2	5	10	20	50	100
RBSC	0.45	0.58	0.74	0.78	0.82	0.87	0.94
Vitox	0.49	0.56	0.65	0.54	0.40	0.33	0.30
Sintox	0.40	0.41	0.50	0.44	0.37	0.31	0.30
SSN	0.21	0.19	0.17	0.20	0.20	0.16	0.17

Table 12, Results of low load (4 N) scratch tests on hardmetal samples with 50 μm indenter. Results given are values of friction coefficient for final repeat of given scratch.

Materials	Repeats						
	1	2	5	10	20	50	100
MA10	0.28	0.30	0.33		0.34		0.36
D15	0.19				0.29	0.33	0.37
N15	0.27		0.29	0.31	0.34	0.35	0.29
N10	0.29		0.30	0.27	0.25		0.25
MA10	0.22	0.23	0.25	0.30	0.30	0.29	0.29
TC222	0.28		0.32	0.36	0.38	0.43	0.54
N6	0.33	0.30	0.27	0.27	0.26	0.24	0.24
CWN8	0.36	0.36	0.40	0.43	0.43	0.47	0.55
CWC15	0.22	0.23	0.23	0.26	0.33	0.38	0.42
CWC20	0.34	0.34	0.36	0.38	0.39	0.40	0.45
SHMUF	0.12	0.24	0.21	0.20		0.14	0.13

Table 13, Results of low load (4 N) scratch tests on ceramic samples with 50 μm indenter. Results given are values of friction coefficient for final repeat of given scratch.

Materials	Repeats						
	1	2	5	10	20	50	100
RBSC	0.41	0.45	0.39	0.36	0.34	0.13	0.13
Vitox	0.10		0.16	0.16	0.16	0.16	0.18
Sintox	0.17	0.18	0.16	0.16	0.17	0.17	0.18
SSN	0.15	0.14	0.15	0.15	0.15	0.16	0.16
AsiC	0.42	0.44	0.45	0.44	0.37	0.20	0.19

Table 14, Ball cratering results for hardmetals. Results are quoted as diameter of craters in mm.

Material	1000 rev, 0.25 N, water	2000 rev, 0.25 N, water	500 rev, 0.25 N, water	1000 rev, 0.25 N, water	1000 rev, 0.25 N, IMS	1000 rev, 0.25 N, $Ca(OH)_2$	1000 rev, 0.25 N, paraffin	1000 rev, 5 N, water
L1	1.06	1.06	1.00					
M6	1.10	1.27	1.04	1.18	1.15	1.24		
A2a	0.31	0.47	0.36	1.07	1.05	1.17		
F4	0.81	0.88	0.57	1.12	0.90	1.09		
L1	0.83	0.88	0.62	1.15	1.18	1.21		
K5	0.75	0.94	0.70	0.99	0.97	1.09		
M4	0.60	0.52	0.49	0.75	0.93	0.76		
M4	0.78	0.96	0.68					
B4	0.83	0.99	0.73	1.36	1.26	1.26		
K3	0.73	0.73	0.57	0.99	1.01	1.07		
D1	1.13	1.22	0.93		1.07		1.16	
M4	0.82	0.88	0.79		0.88		0.84	
M6	1.16	1.37	1.05		1.12		1.17	
D4	1.07	1.24	0.62		1.08		0.97	
MA20	1.03	1.30	0.84		1.33		1.11	
MA10	0.78	0.95	0.74		1.05		1.01	
MA24	1.15	1.25	1.04		1.41		1.21	
MA15	1.13	1.42	0.97		1.22		1.32	
MAN6	1.01	1.26	0.83		1.12		1.18	
UC9	0.76	0.80	0.63		0.74		0.76	
T	0.92	1.03	0.74		0.88		0.97	
M15	0.95	1.09	0.83		1.00		0.90	
CWC15F	1.33							1.15
CWC15C	1.14							0.97
CWC20C	1.11							1.06
CWC25C	1.09							1.10

Table 15, Ball cratering results on ceramics. Results are given as crater diameters in mm.

Material	SiC, 1000 rev, 0.25 N, water	SiC, 1000 rev, 5 N, water	SiO_2, 1000 rev, 0.25 N, water	SiO_2, 1000 rev, 5N, water	0.25 μm diamond, 0.25 N
SINTOX	1.8	1.69	0.43	0.66	1.12
VITOX	1.3	1.18	0.59	0.71	1.13
RBSN	2.35	2.59	0	0.53	0.96
RBSC	0.86	0.98	0.43	0.49	0.98
SIN	1.65	1.74	0.34	1	0.87
α-SiC	0.84	0.89	0.25	0.44	1.06
SSN	1.99	2.11	0.34	0.91	0.94

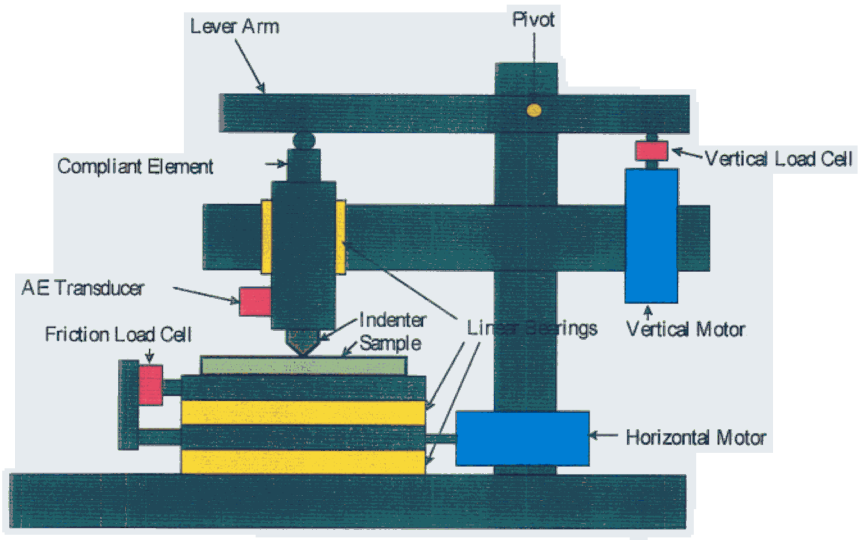

Figure 1, Schematic diagram of high load scratch testing system

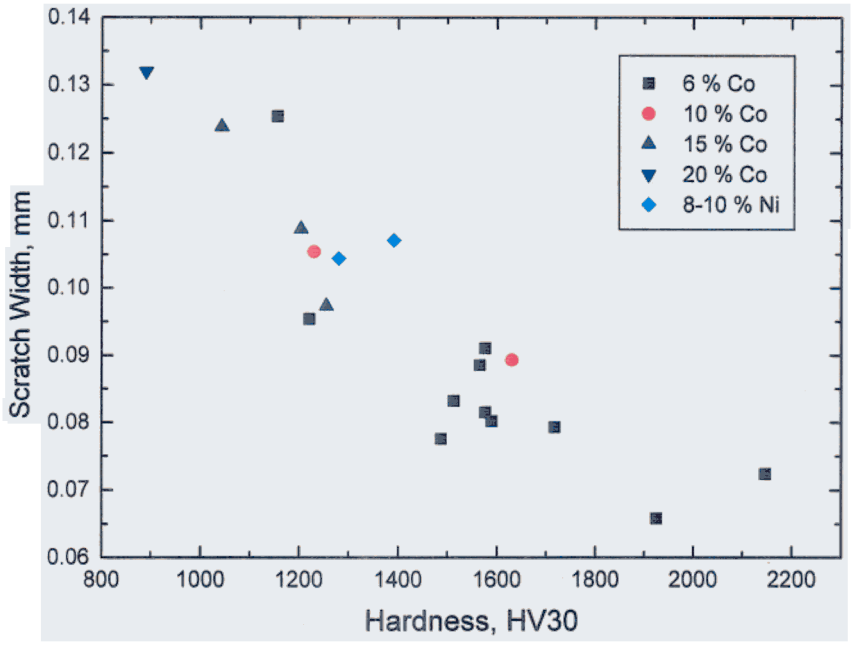

Figure 2, Decrease in scratch width with increase in high load scratch tests on hardmetals

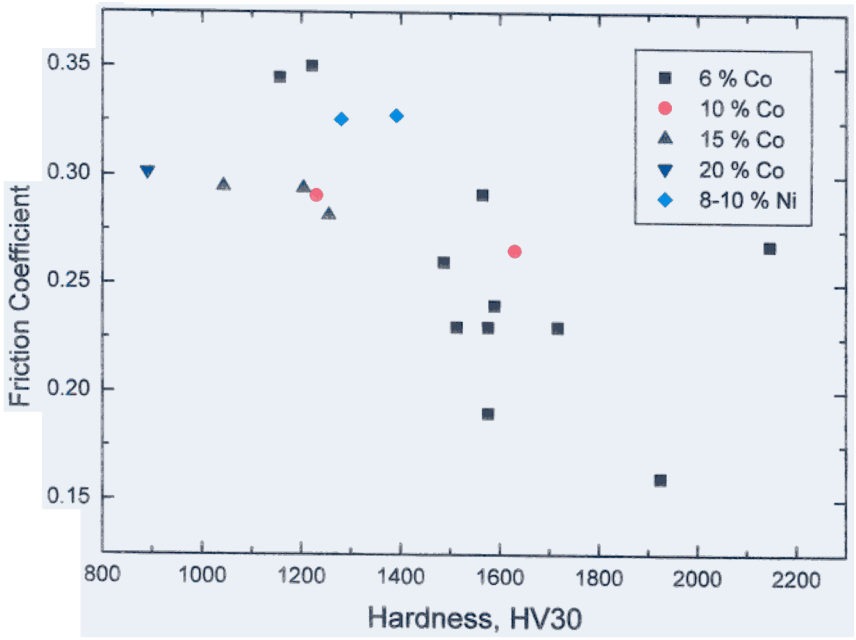

Figure 3, Variation in friction coefficient with hardness for high load scratch tests on hardmetals.

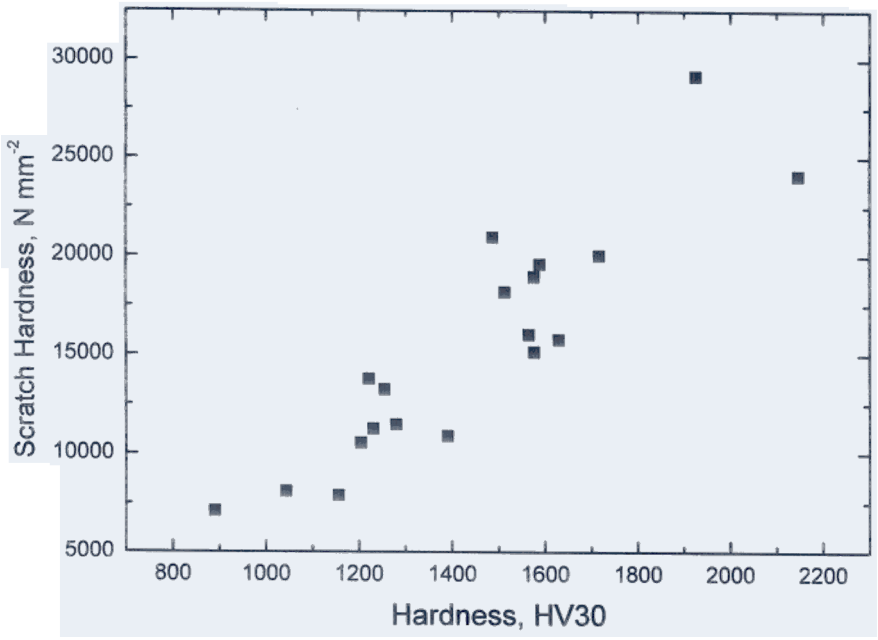

Figure 4, Variation of scratch hardness with conventional Vickers hardness for high load scratch tests on hardmetals.

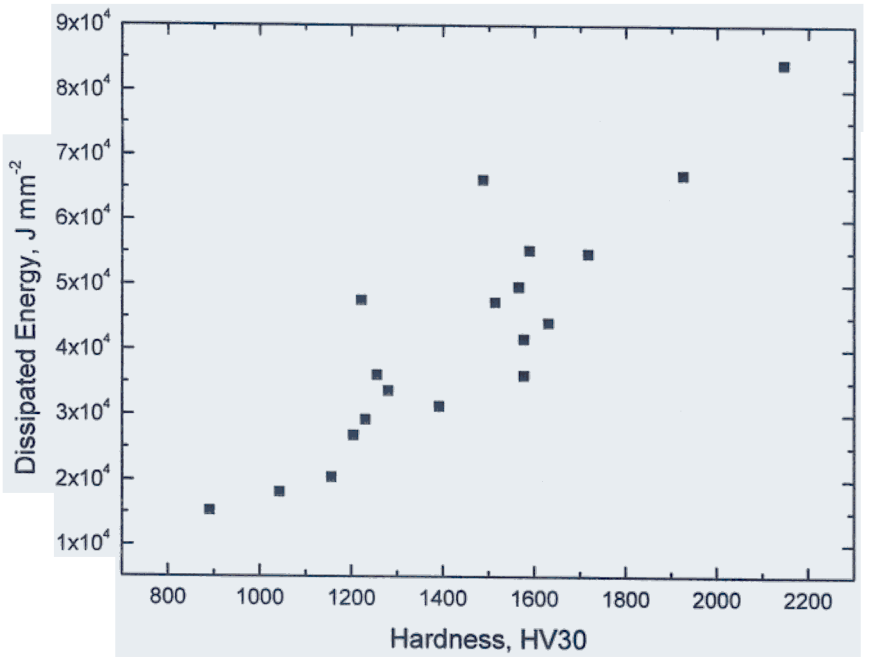

Figure 5, Variation of dissipated energy with hardness for high load scratch tests on hardmetals

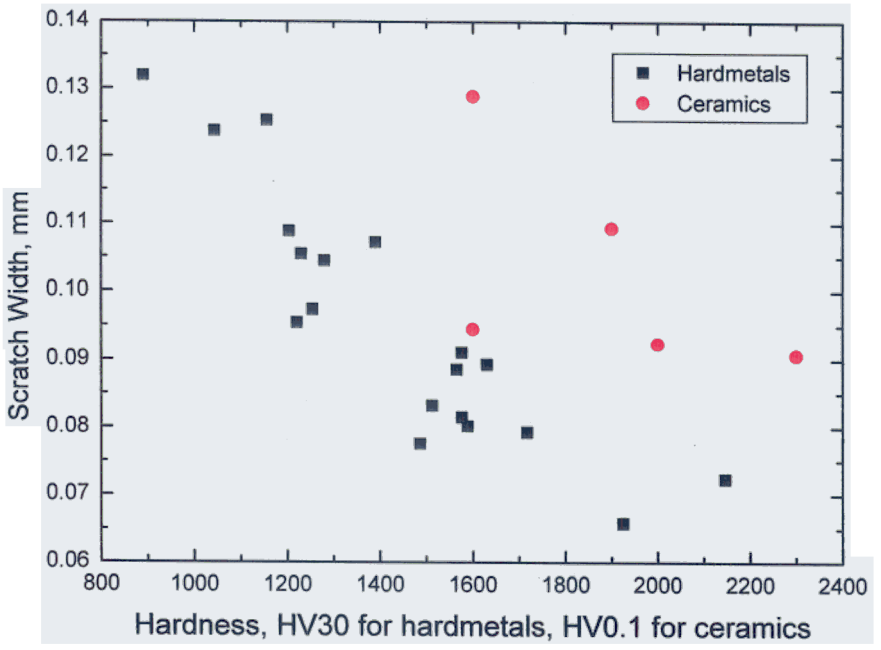

Figure 6, Variation of scratch width with hardness for high load scratches on hardmetals and ceramics.

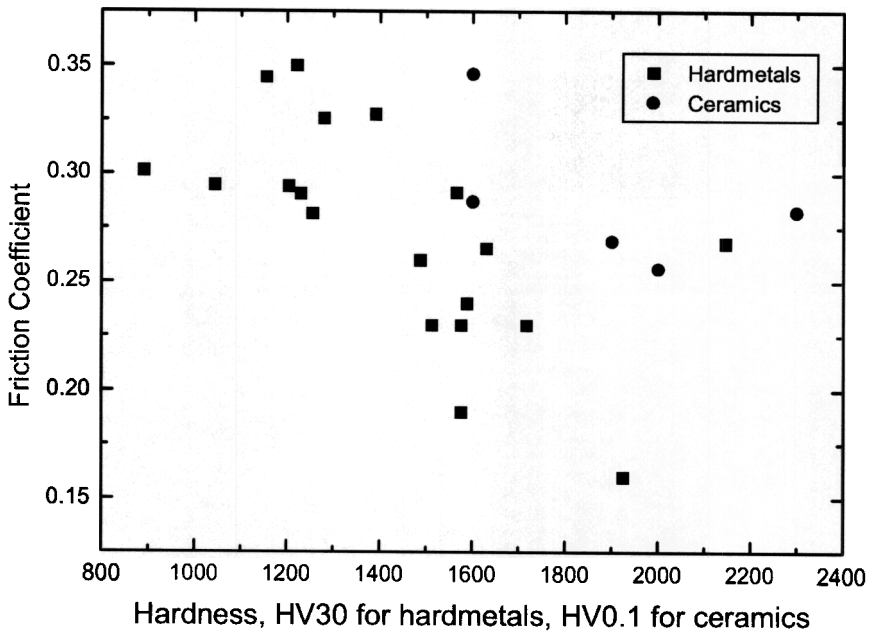

Figure 7, Variation of friction coefficient with hardness for high load scratches on hardmetals and ceramics.

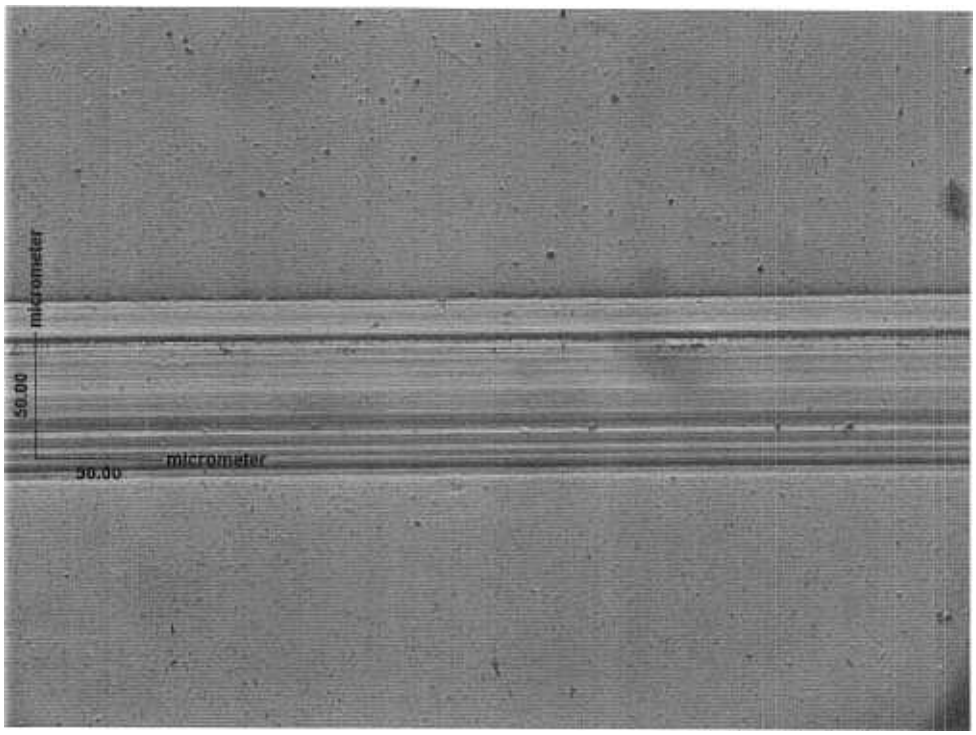

a)

Figure 8, Optical micrographs of high load scratches on hardmetals, a) SHMUF ultra-fine hardmetal, b) TC222, c) MA10.

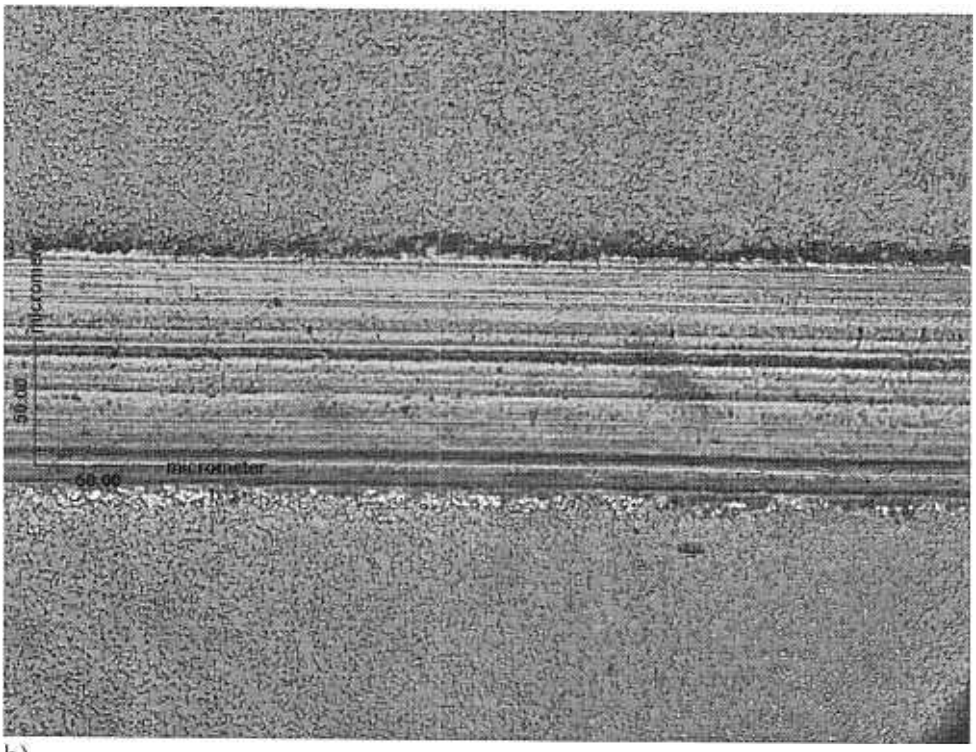

b)

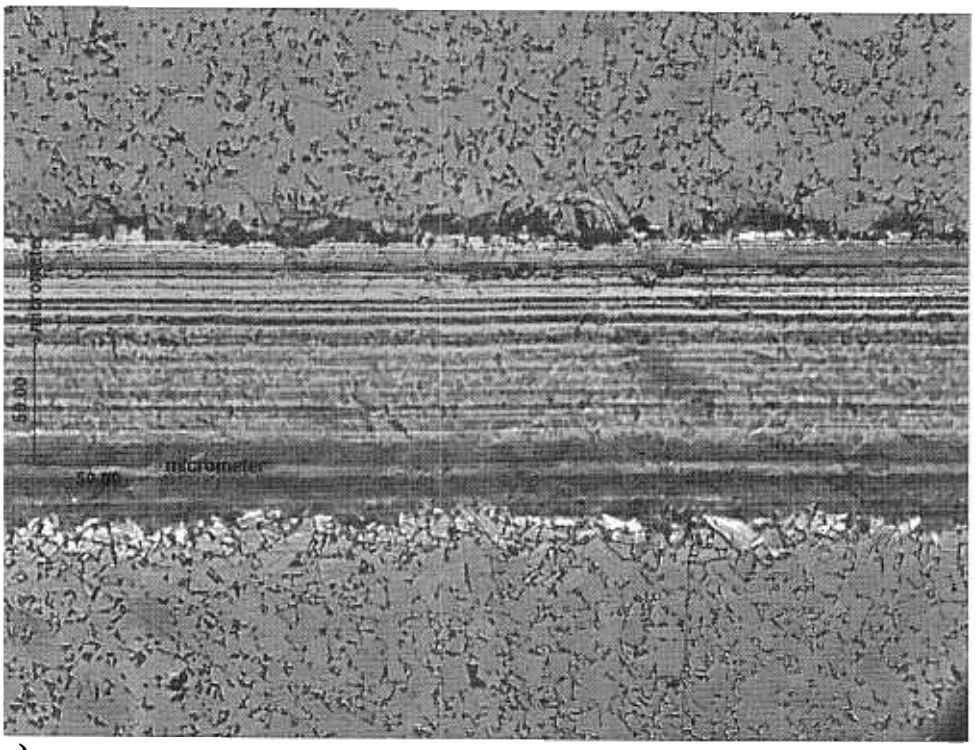

c)

Figure 8, Optical micrographs of high load scratches on hardmetals, a) SHMUF ultra-fine hardmetal, b) TC222, c) MA10.

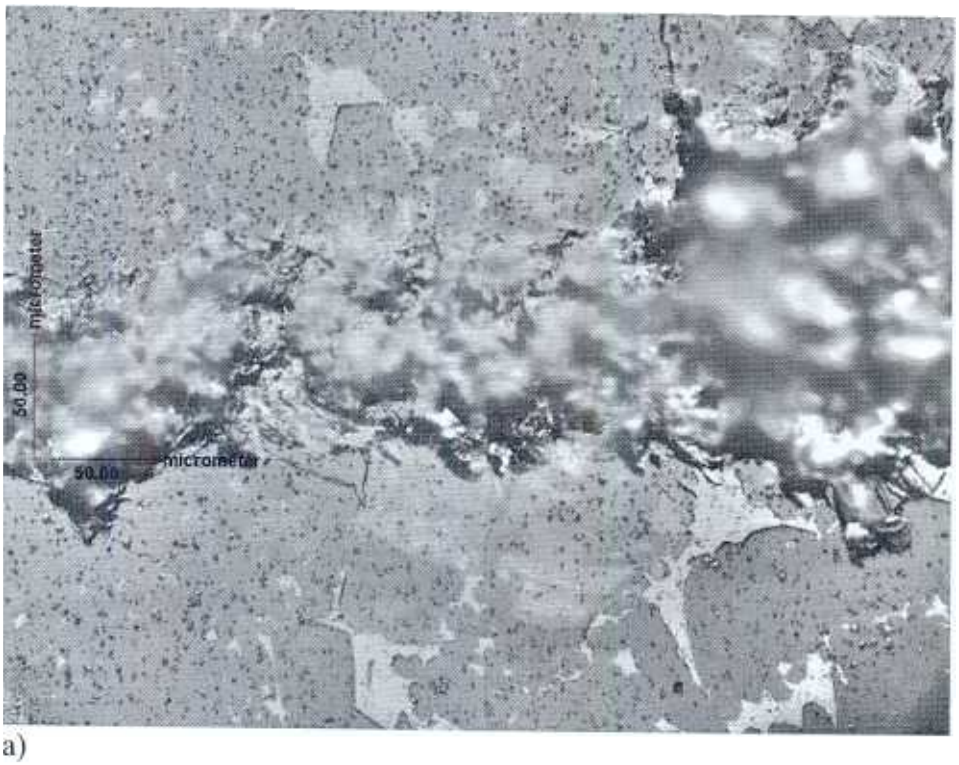

a)

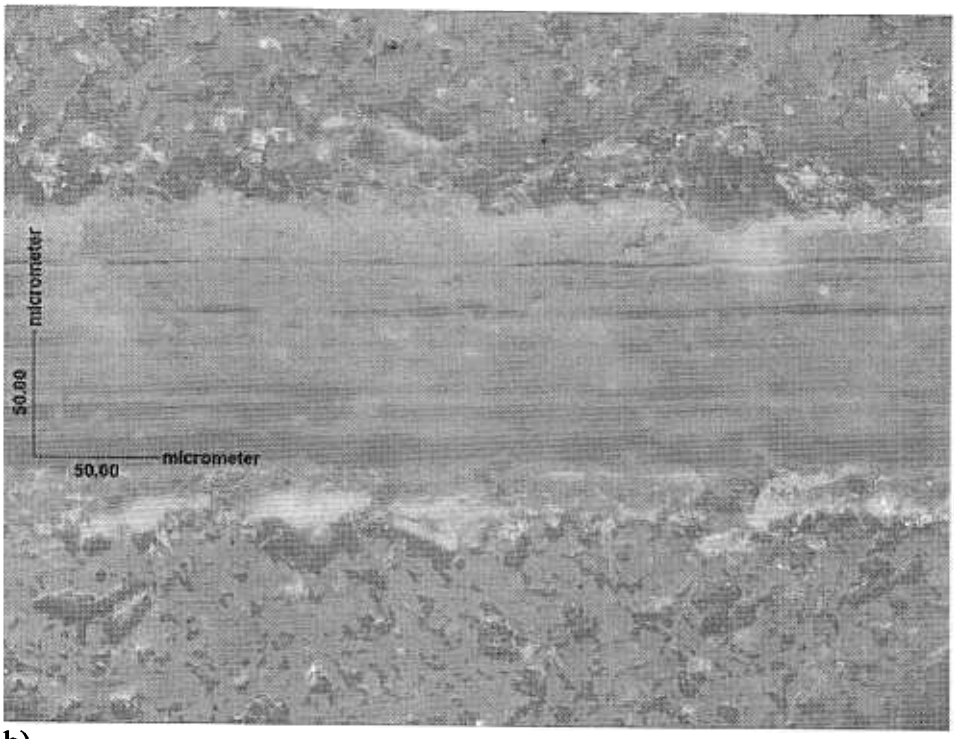

b)

Figure 9, Optical microgrphs of high load scratches on ceramics, a) RBSC, b) Sintox alumina, c) SSN and d) α-SiC.

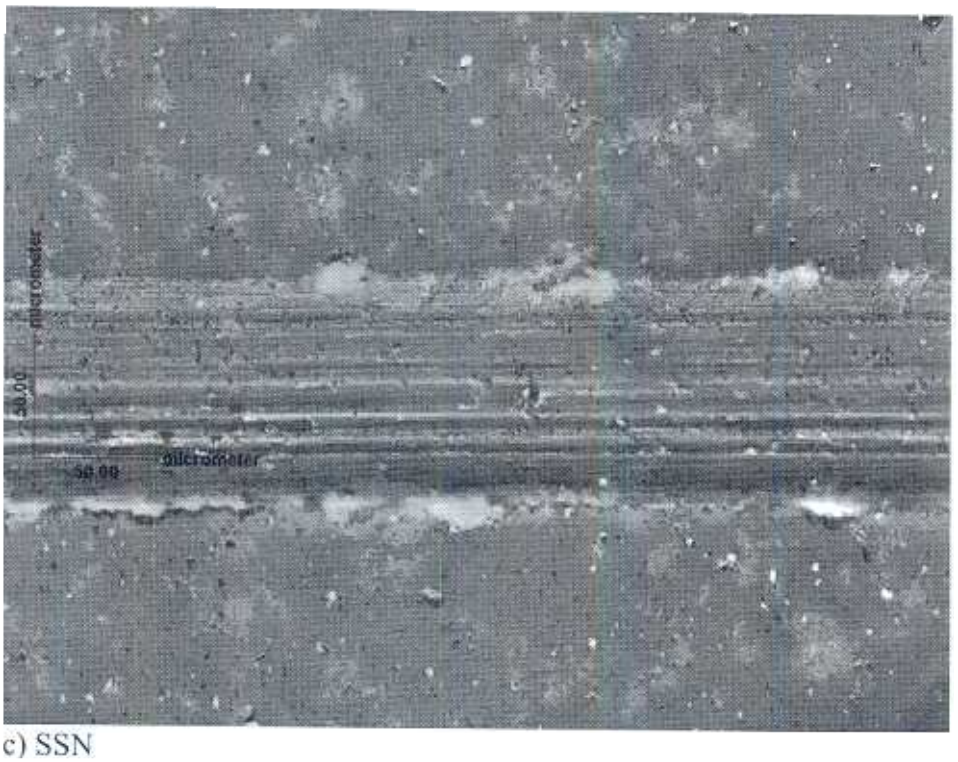

c) SSN

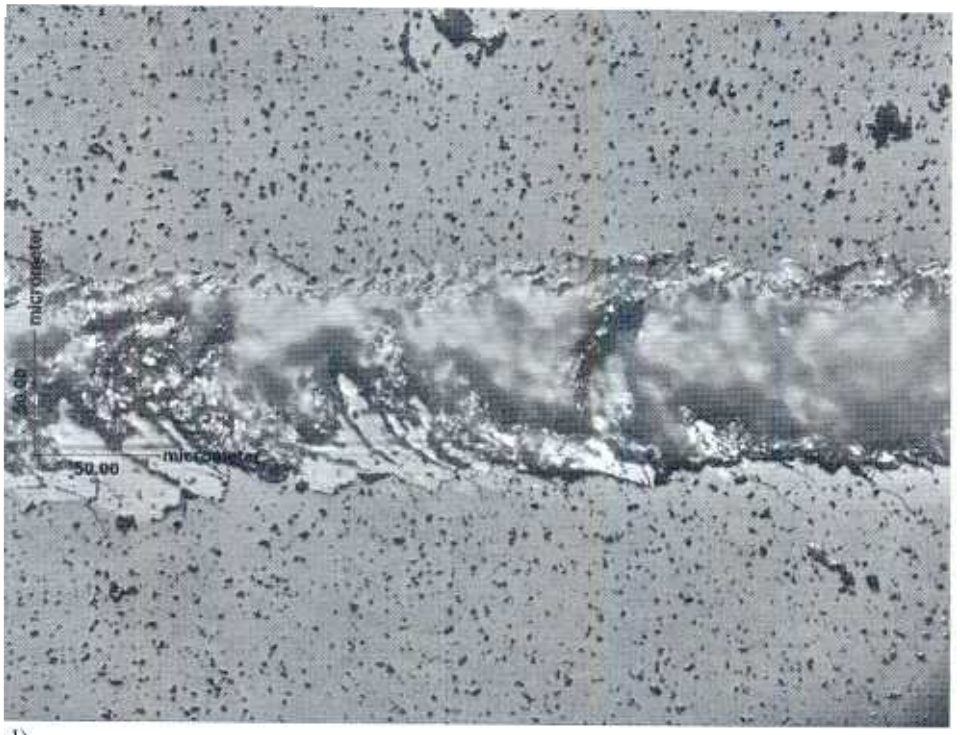

d)

Figure 9, Optical micrograph of high load scratches on ceramics, a) RBSC, b) Sintox alumina, c) SSN and d) α-SiC.

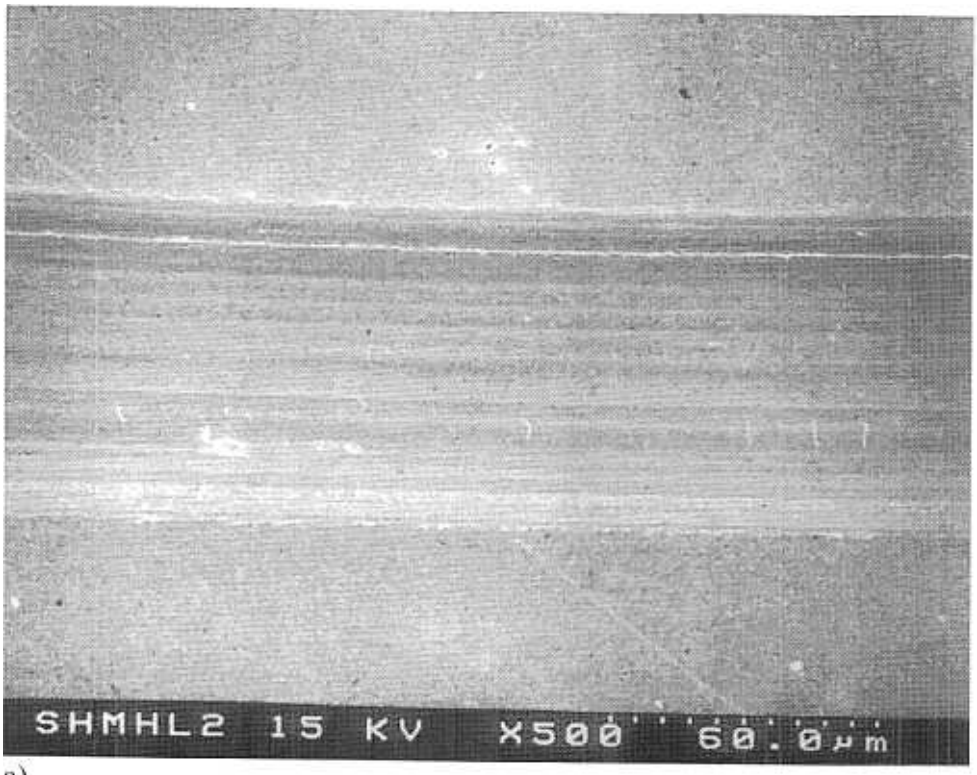

a)

b)

Figure 10, Scanning electron micrographs on hardmetals scratched in high load tests, a) SHMUF, b) SHMUF, c) CW20C, d) CWC20C.

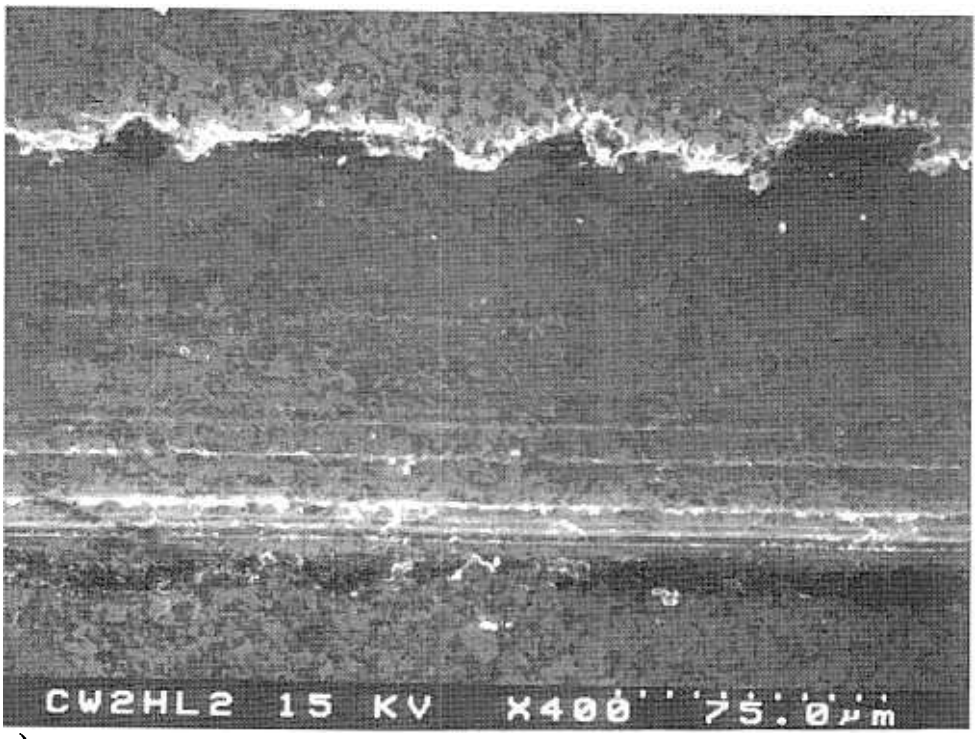

c)

d)

Figure 10, Scanning electron micrographs on hardmetals scratched in high load tests, a) SHMUF, b) SHMUF, c) CW20C, d) CWC20C.

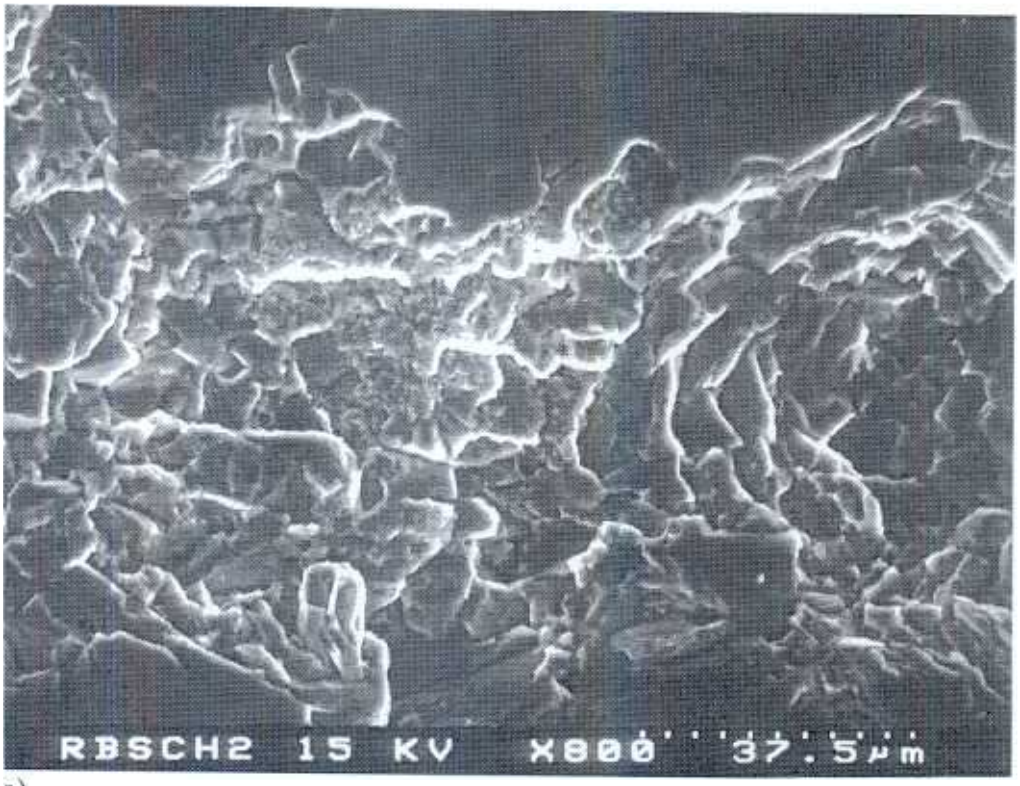

a)

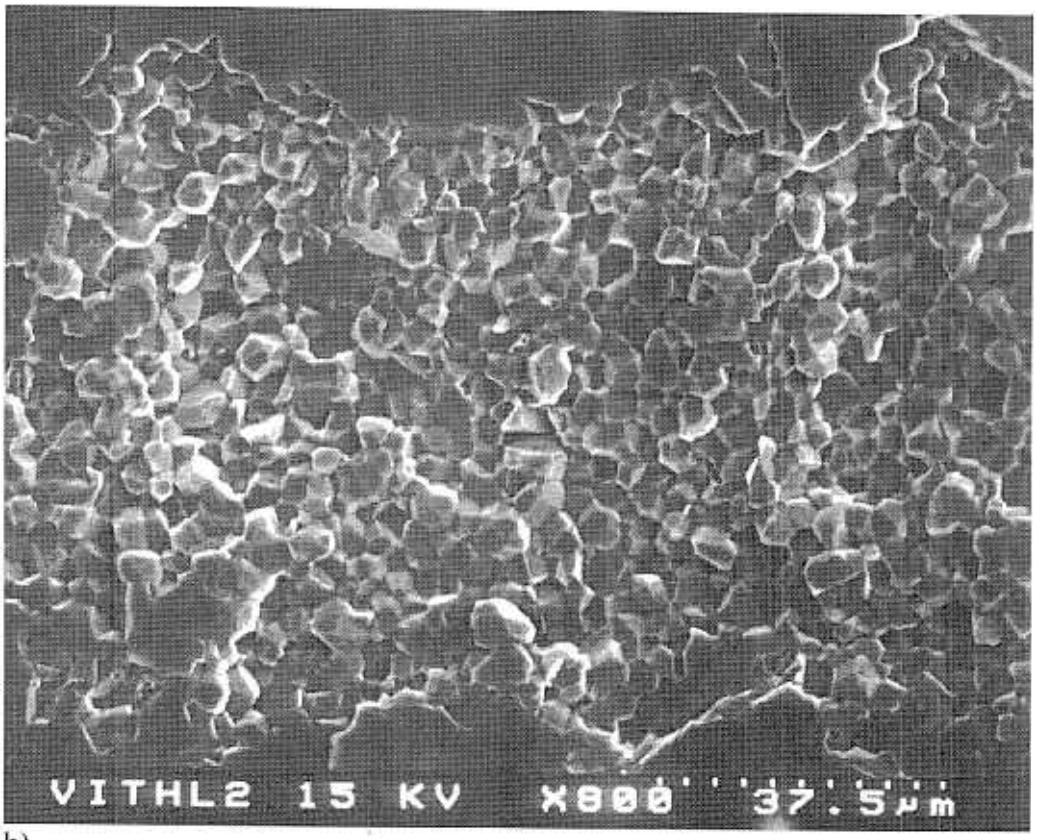

b)

Figure 11, Scanning electron micrographs of high load scratches on ceramic samples, a) RBSC, b) Vitox, c) Vitox, d) α-SiC, e) α-SiC

c)

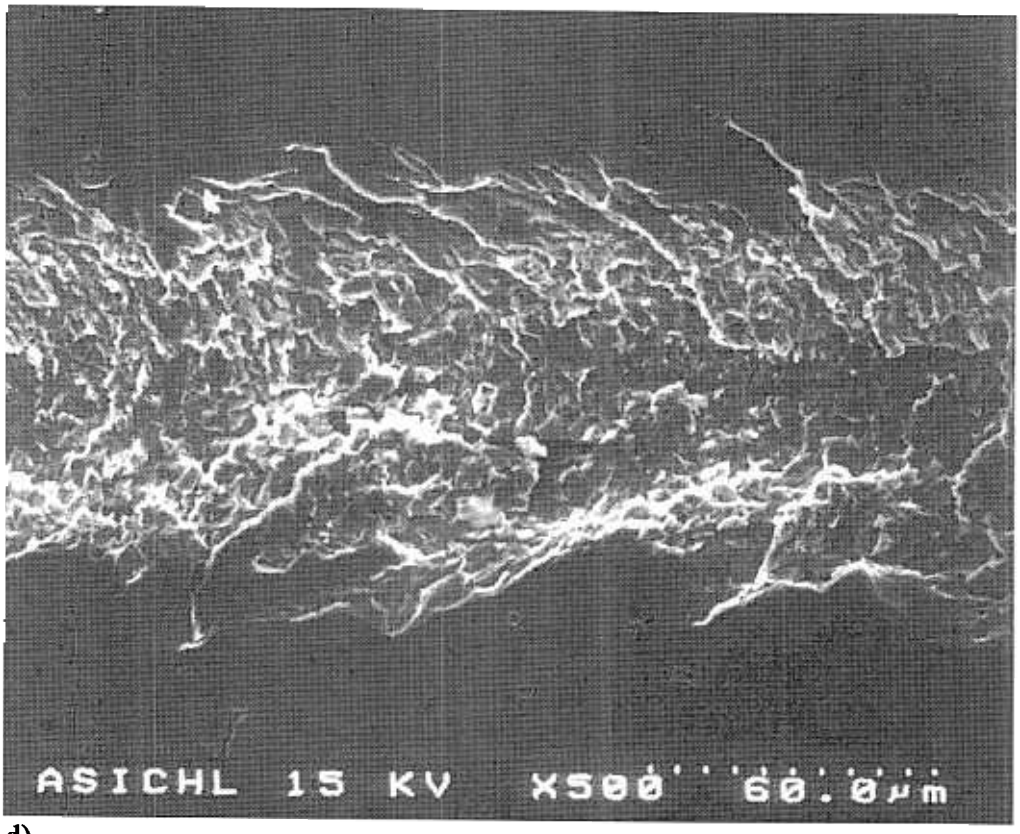

d)

Figure 11, Scanning electron micrographs of high load scratches on ceramic samples, a) RBSC, b) Vitox, c) Vitox, d) α-SiC, e) α-SiC

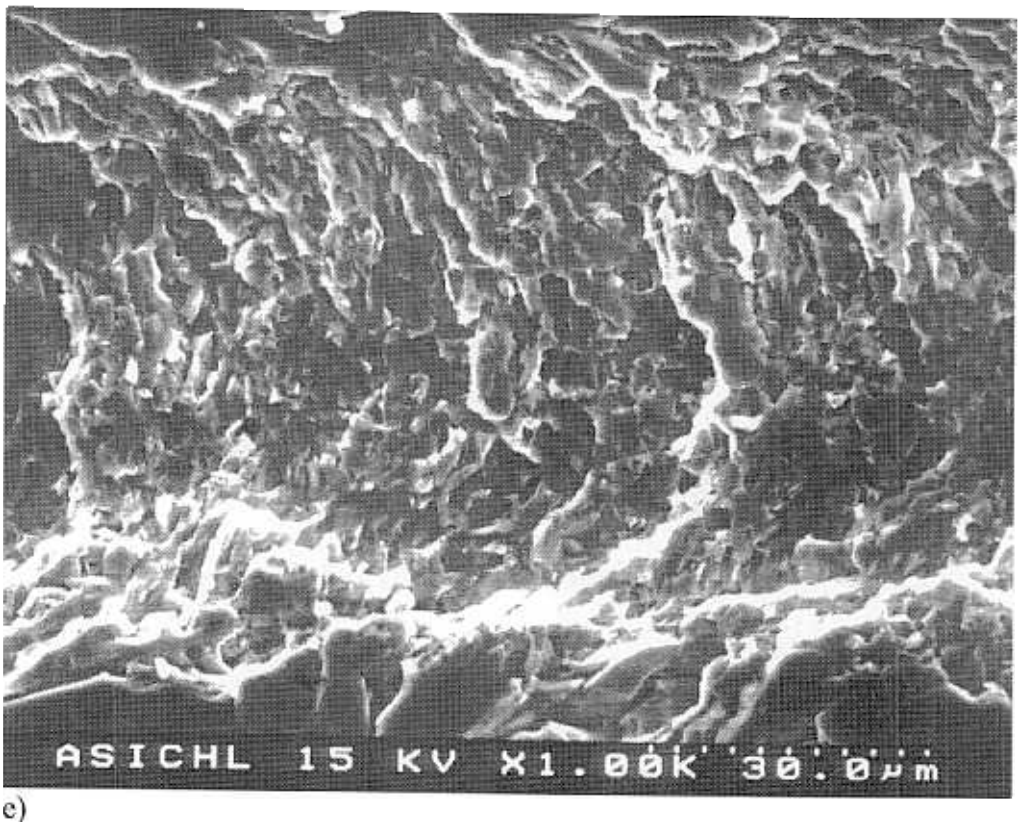

c)

Figure 11, Scanning electron micrographs of high load scratches on ceramic samples, a) RBSC, b) Vitox, c) Vitox, d) α-SiC, e) α-SiC

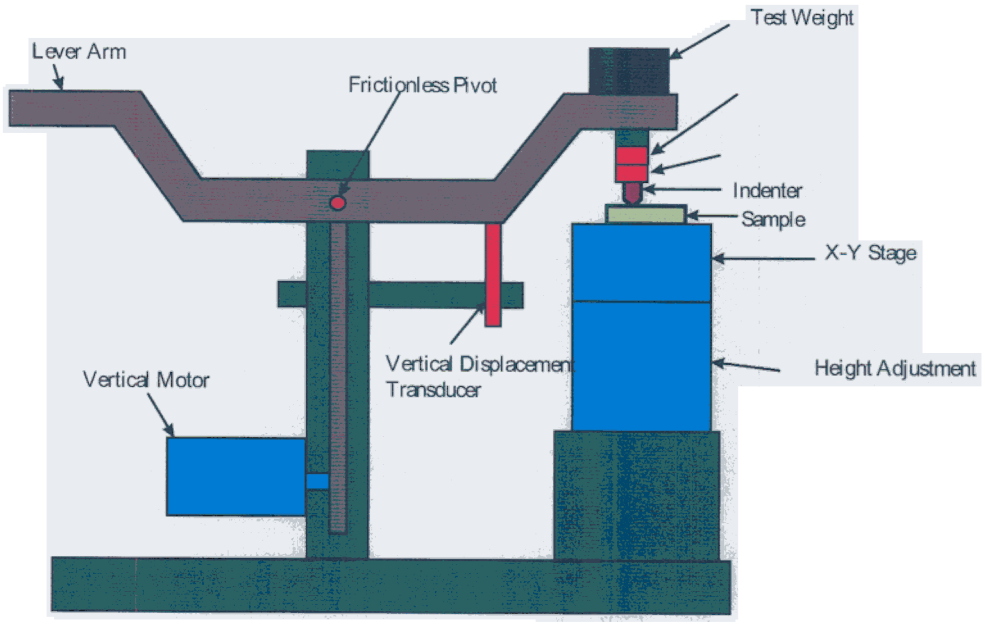

Figure 12, Schematic diagram of low load scratch testing system.

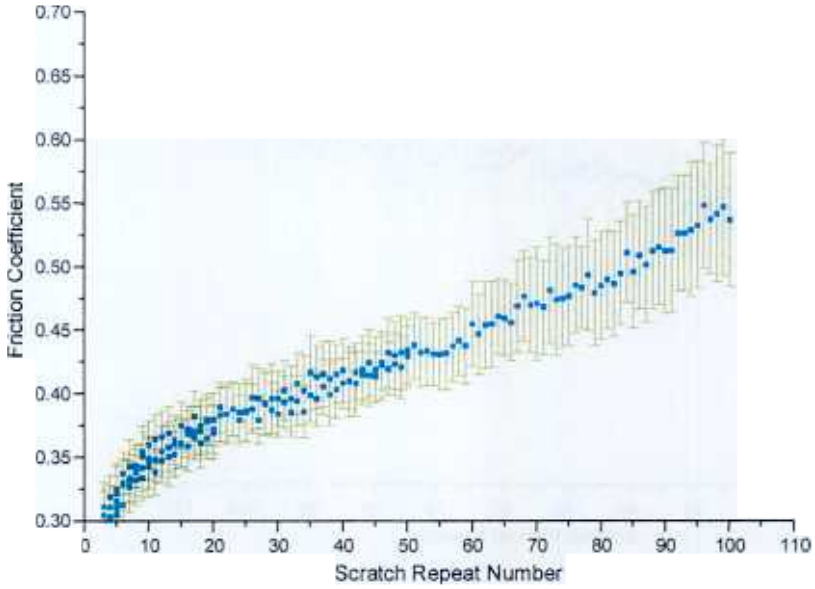

a)

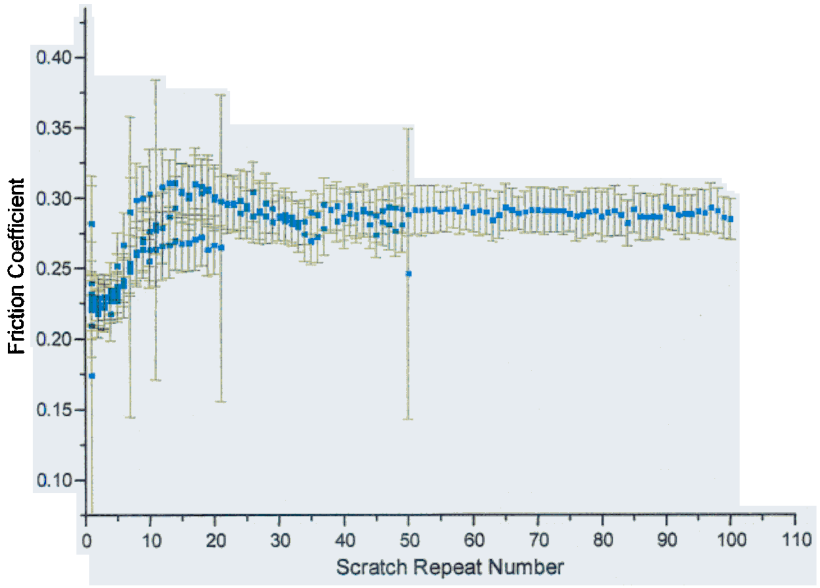

b)

Figure 13, Variation in average friction coefficient with scratch repeat number for selected hardmetals samples, a) TC222 with 200 µm indenter, b) MA10 with 200 µm indenter, c) CWC20C with 50 µm indenter, d) CWC15C with 200 µm indenter, e) SHMUF with 50 µm indenter, f) SHMUF with 200 µm indenter.

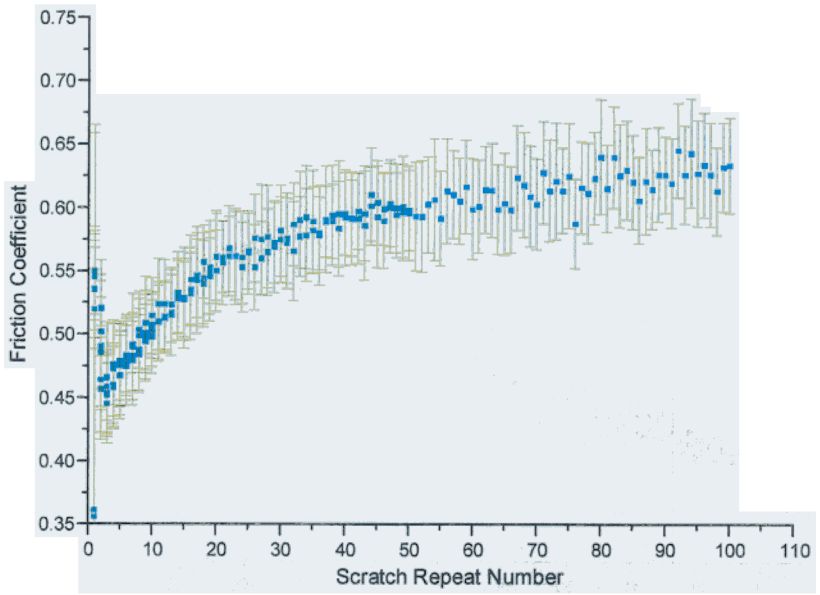

c)

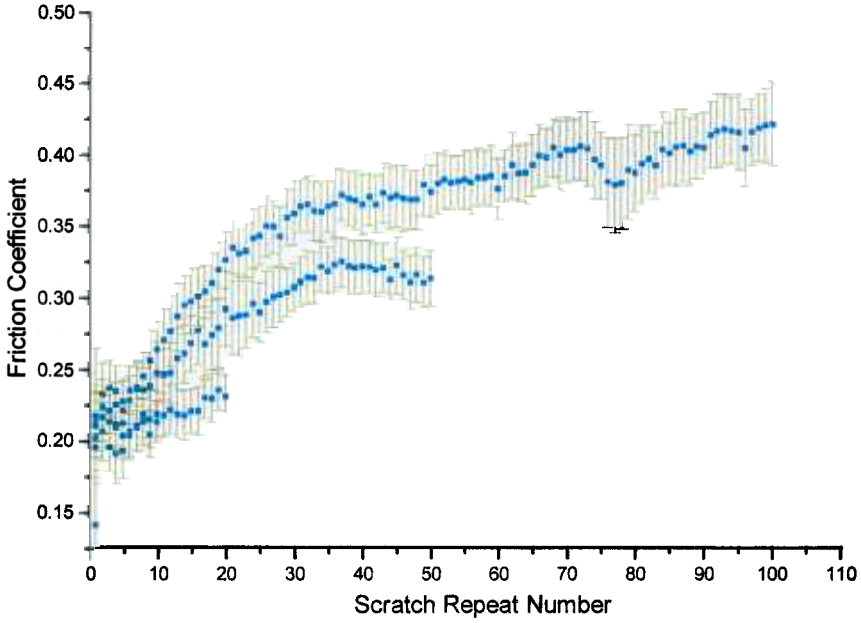

d)

Figure 13, Variation in average friction coefficient with scratch repeat number for selected hardmetals samples, a) TC222 with 200 µm indenter, b) MA10 with 200 µm indenter, c) CWC20C with 50 µm indenter, d) CWC15C with 200 µm indenter, e) SHMUF with 50 µm indenter, f) SHMUF with 200 µm indenter.

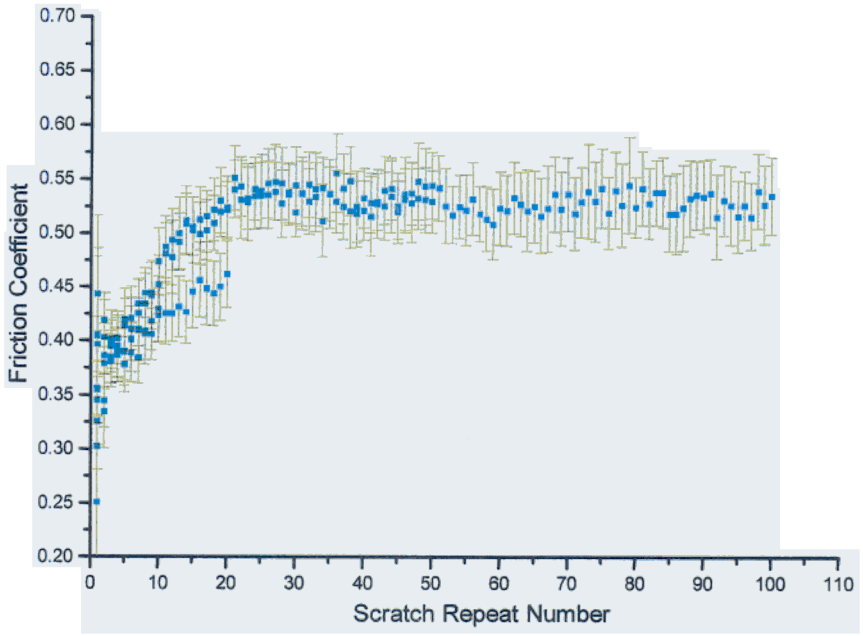

e)

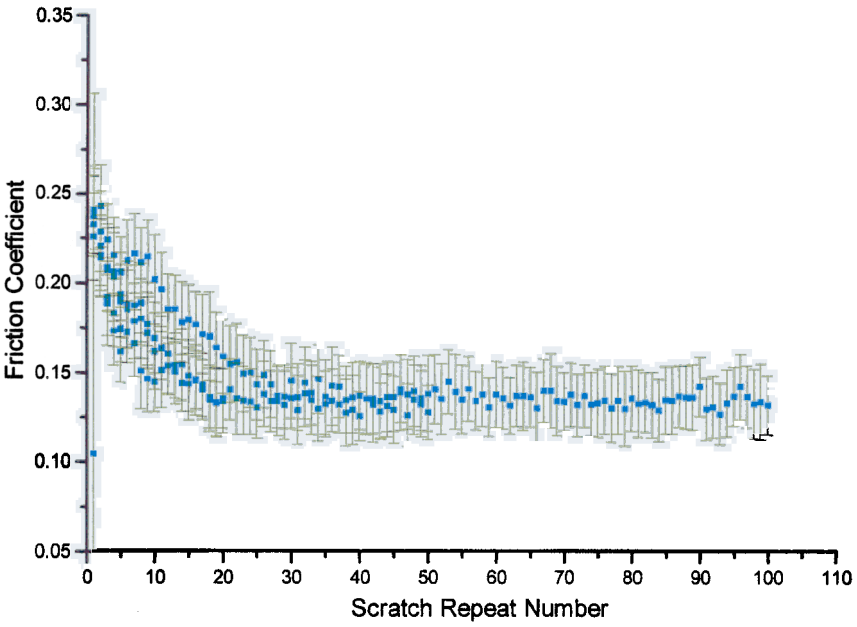

f)

Figure 13, Variation in average friction coefficient with scratch repeat number for selected hardmetals samples, a) TC222 with 200 μm indenter, b) MA10 with 200 μm indenter, c) CWC20C with 50 μm indenter, d) CWC15C with 200 μm indenter, e) SHMUF with 50 μm indenter, f) SHMUF with 200 μm indenter.

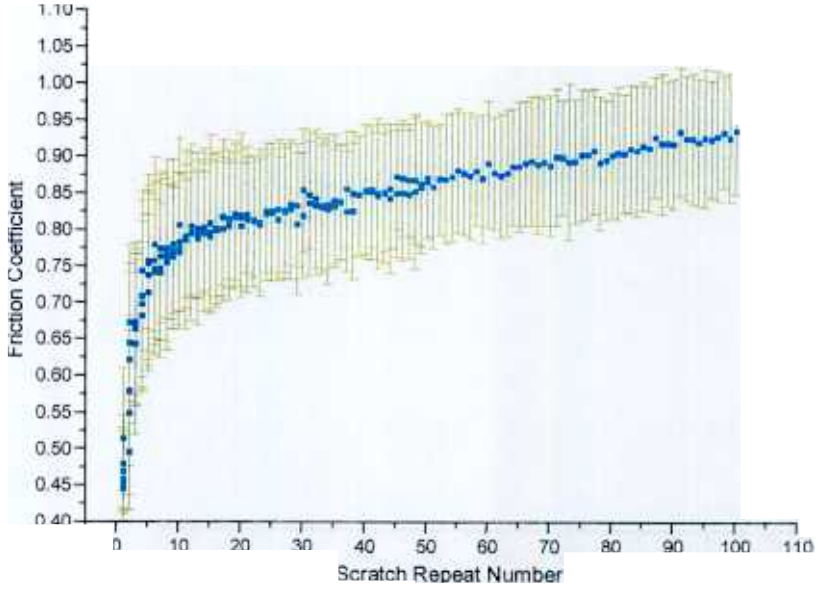

a)

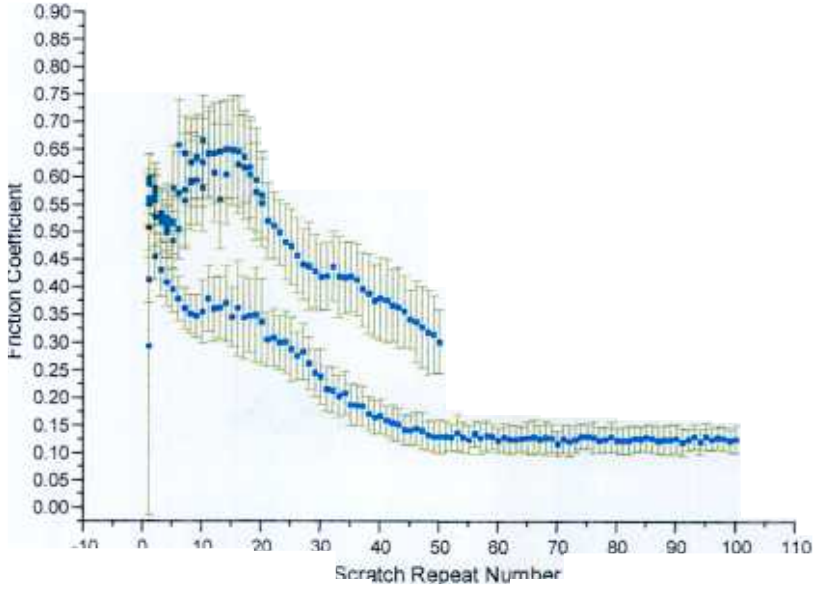

b)

Figure 14, Variation in average friction coefficient with scratch repeat number for selected ceramic samples, a) RBSC with 50 μm indenter, b) RBSC with 200 μm indenter, c) Vitox with 50 μm indenter, d) Vitox with 200 μm indenter, e) Sintox with 50 μm indenter, f) SSN with 200 μm indenter, g) α-SiC with 50 μm indenter, h) α-SiC with 200 μm indenter

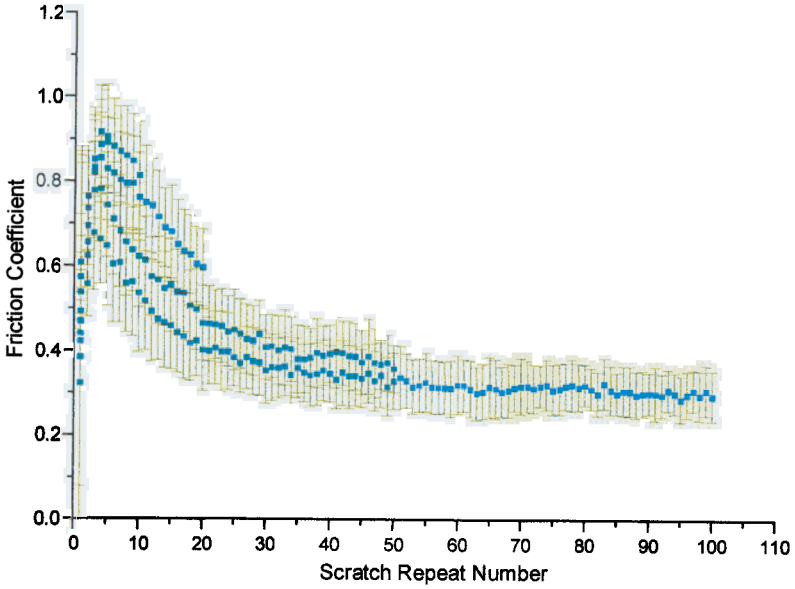

c)

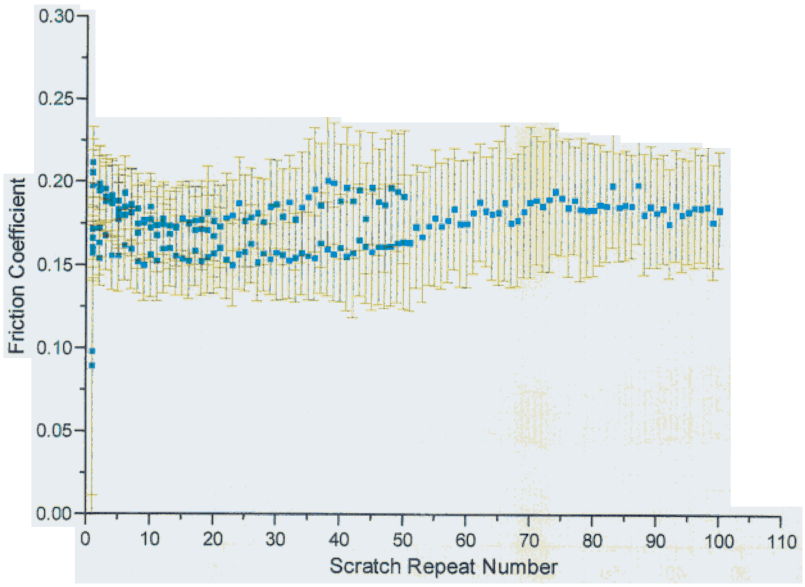

d)

Figure 14, Variation in average friction coefficient with scratch repeat number for selected ceramic samples, a) RBSC with 50 μm indenter, b) RBSC with 200 μm indenter, c) Vitox with 50 μm indenter, d) Vitox with 200 μm indenter, e) Sintox with 50 μm indenter, f) SSN with 200 μm indenter, g) α-SiC with 50 μm indenter, h) α-SiC with 200 μm indenter.

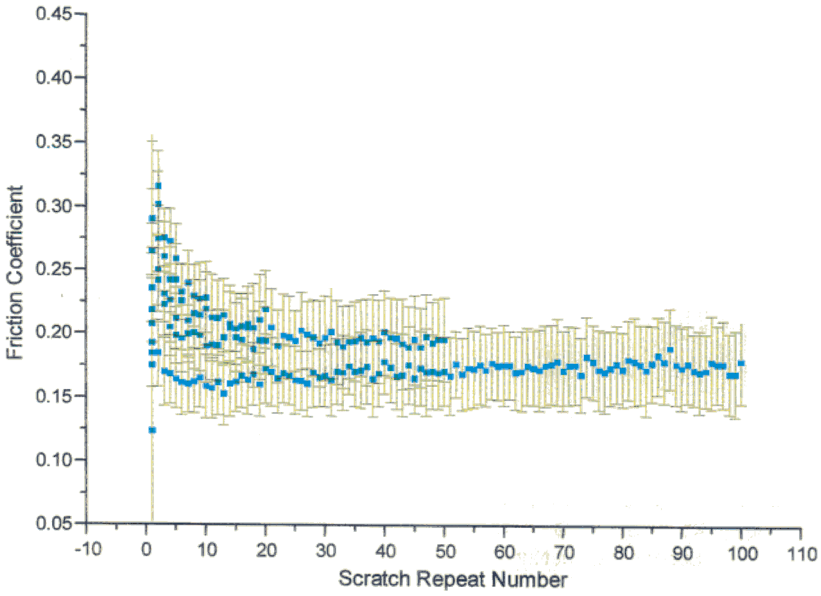

e)

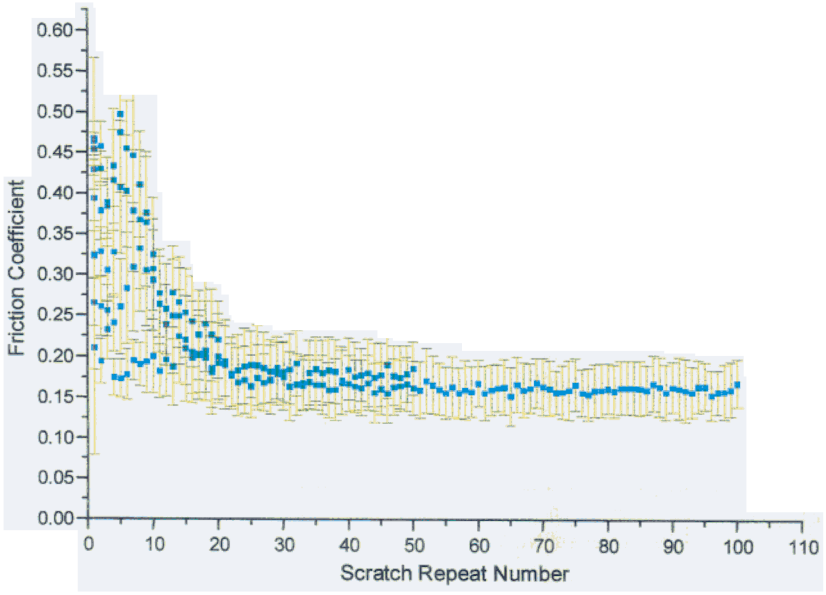

f)

Figure 14, Variation in average friction coefficient with scratch repeat number for selected ceramic samples, a) RBSC with 50 μm indenter, b) RBSC with 200 μm indenter, c) Vitox with 50 μm indenter, d) Vitox with 200 μm indenter, e) Sintox with 50 μm indenter, f) SSN with 200 μm indenter, g) α-SiC with 50 μm indenter, h) α-SiC with 200 μm indenter.

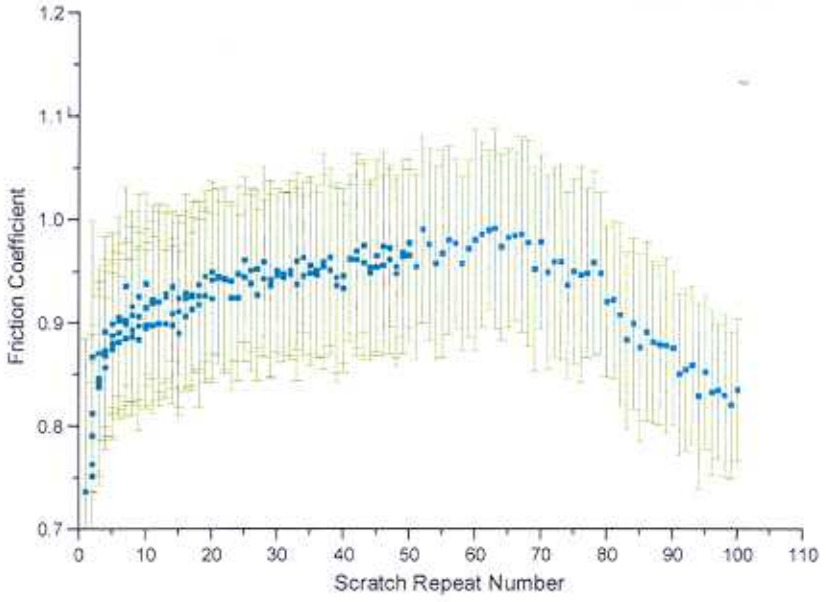

g)

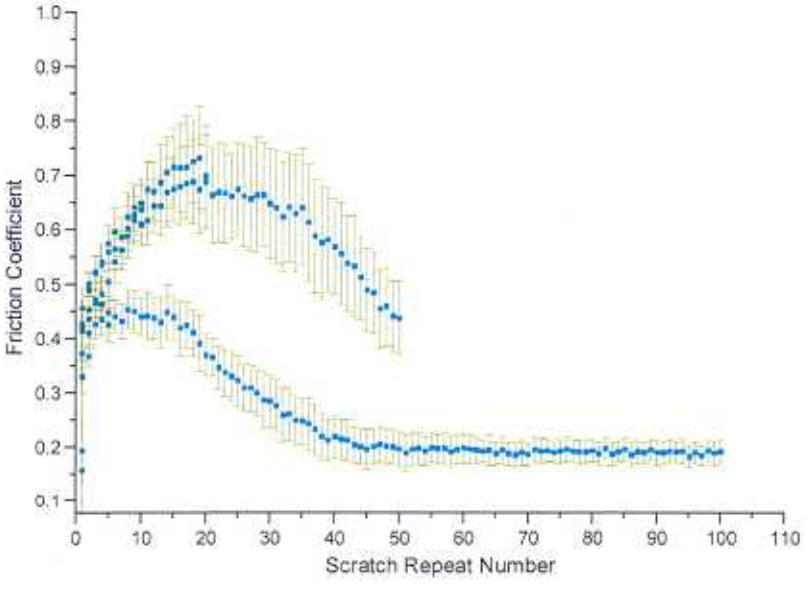

h)

Figure 14, Variation in average friction coefficient with scratch repeat number for selected ceramic samples, a) RBSC with 50 μm indenter, b) RBSC with 200 μm indenter, c) Vitox with 50 μm indenter, d) Vitox with 200 μm indenter, e) Sintox with 50 μm indenter, f) SSN with 200 μm indenter, g) α-SiC with 50 μm indenter, h) α-SiC with 200 μm indenter.

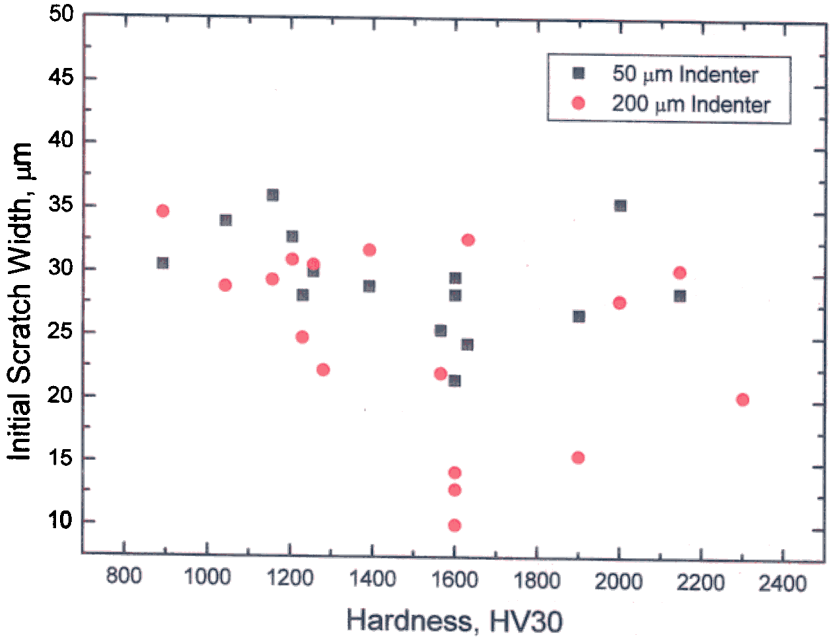

Figure 15, Variation of initial (first repeat scratch) scratch width with hardness of hardmetal samples for low load scratch tests.

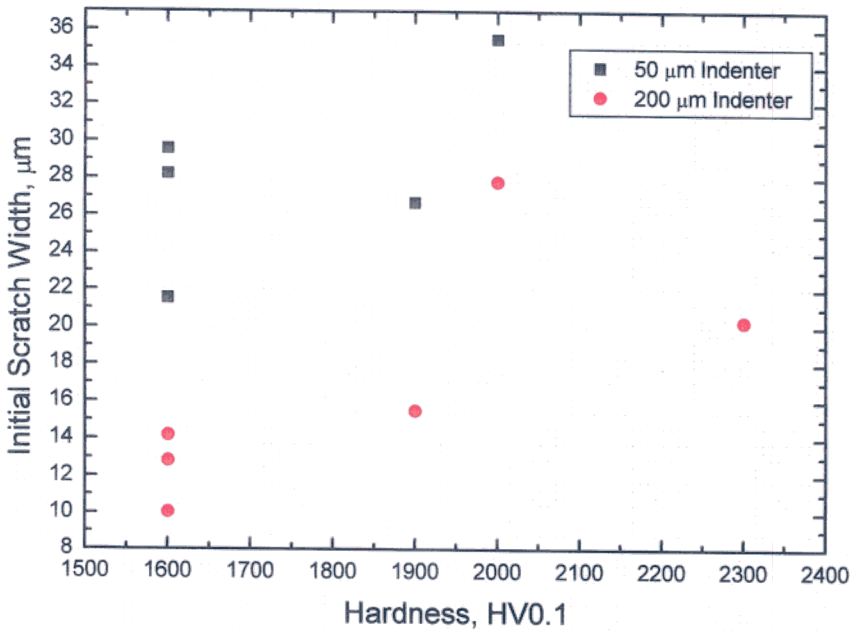

Figure 16, Variation in initial (first repeat) scratch width with hardness of ceramic samples in low load scratch tests.

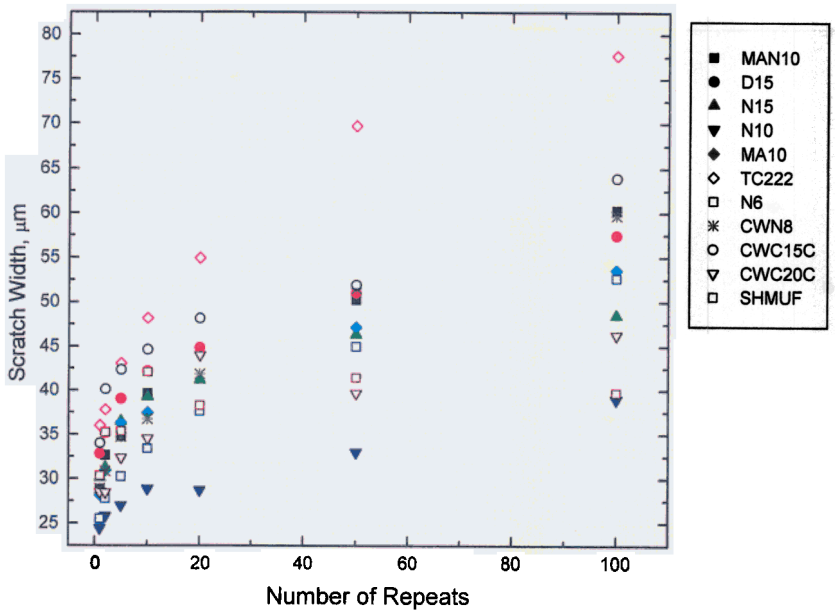

a)

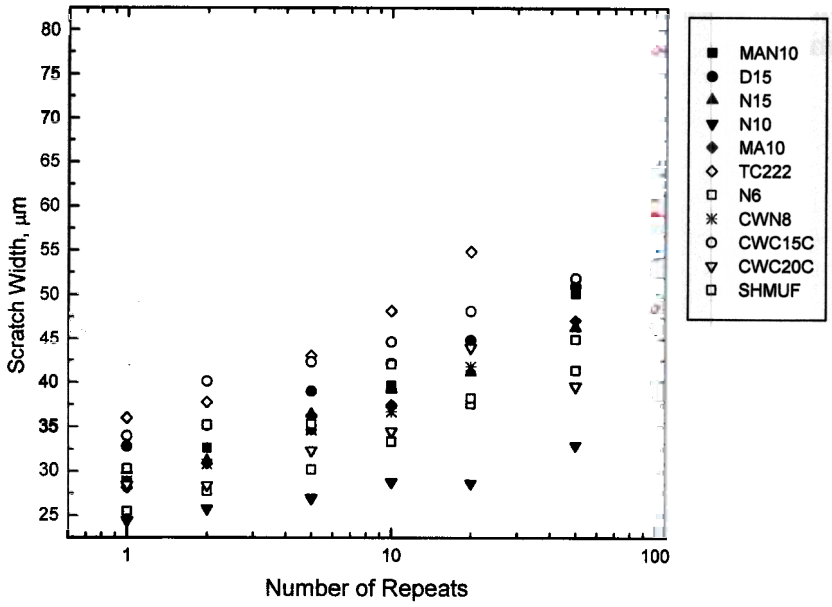

b)

Figure 17, Change in width of scratch with number of repeat scratches in low load scratch tests with 50 µm indenter, a) hardmetals, b) hardmetals (logarithmic number of repeats), c) ceramics.

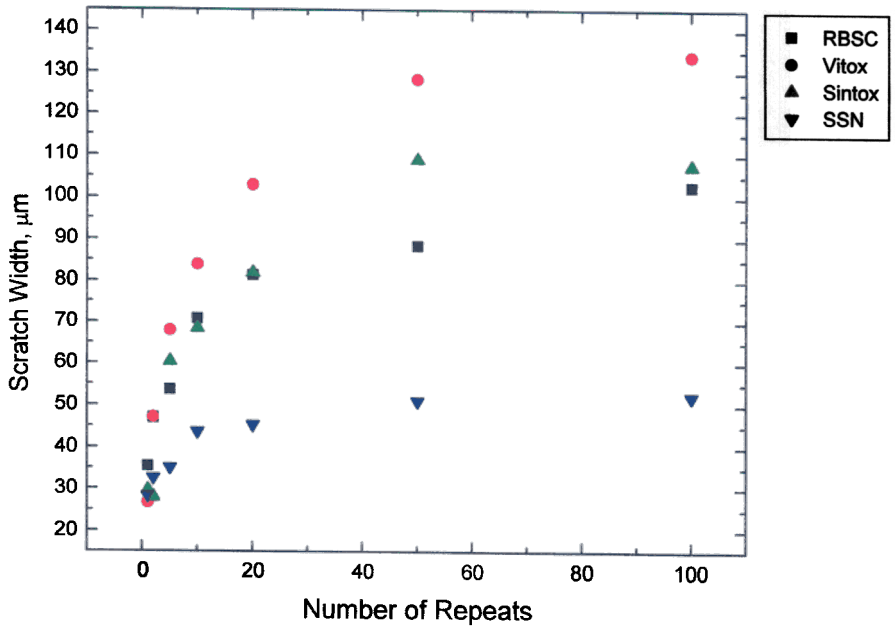

c)

Figure 17, Change in width of scratch with number of repeat scratches in low load scratch tests with 50 µm indenter, a) hardmetals, b) hardmetals (logarithmic number of repeats), c) ceramics.

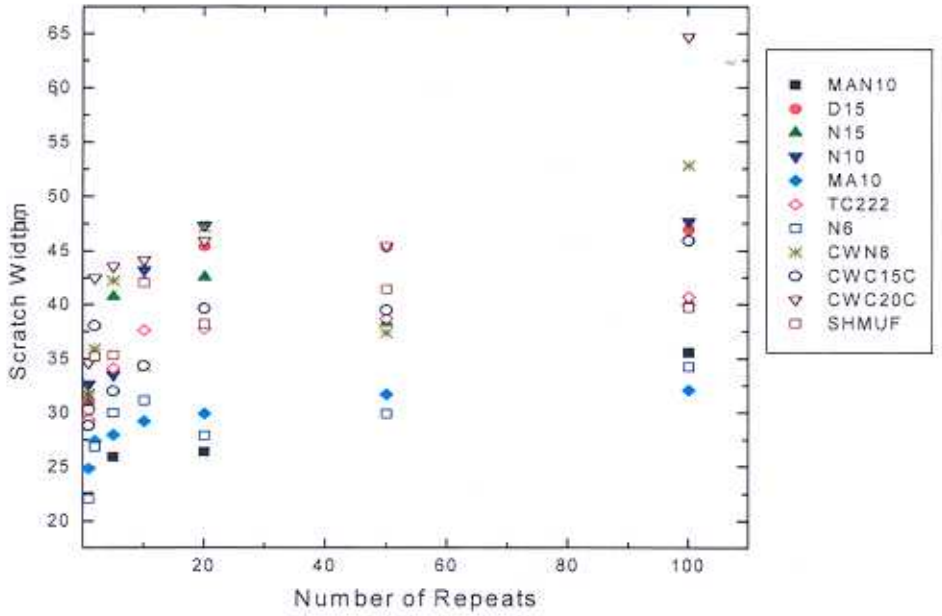

a)

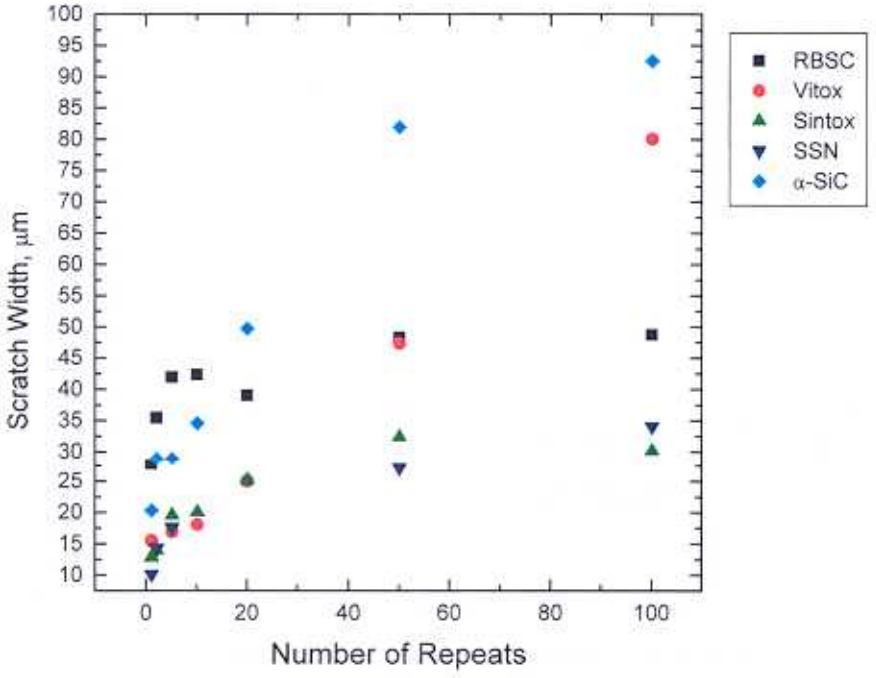

b)

Figure 18, Change in width of scratch with number of repeat scratches in low load scratch tests with 200 µm indenter, a) hardmetals, b) ceramics.

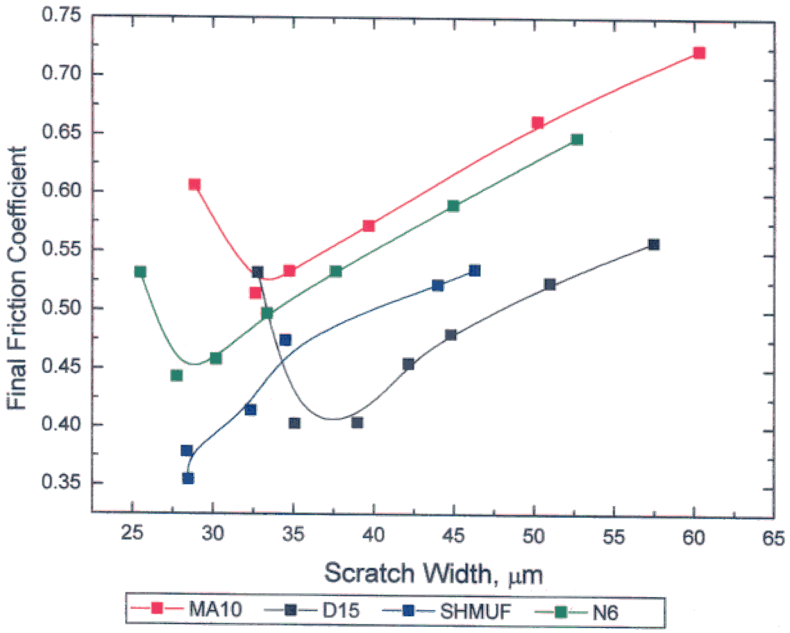

a)

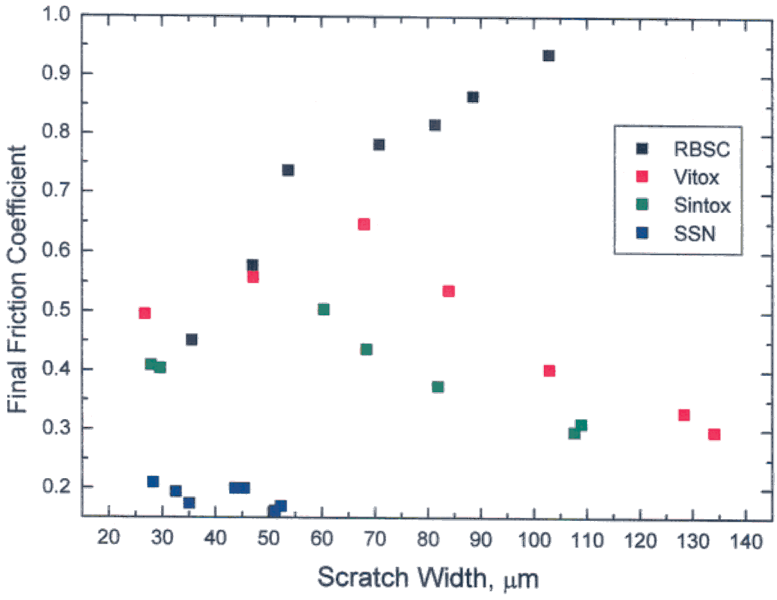

b)

Figure 19, Variation of final friction coefficient with final scratch width for low load scratch tests (final is after 100 repeat scratches), a) hardmetal with 50 μm indenter, b) ceramics with 50 μm indenter, c) hardmetals with 200 μm indenter, d) ceramics with 200 μm indenter.

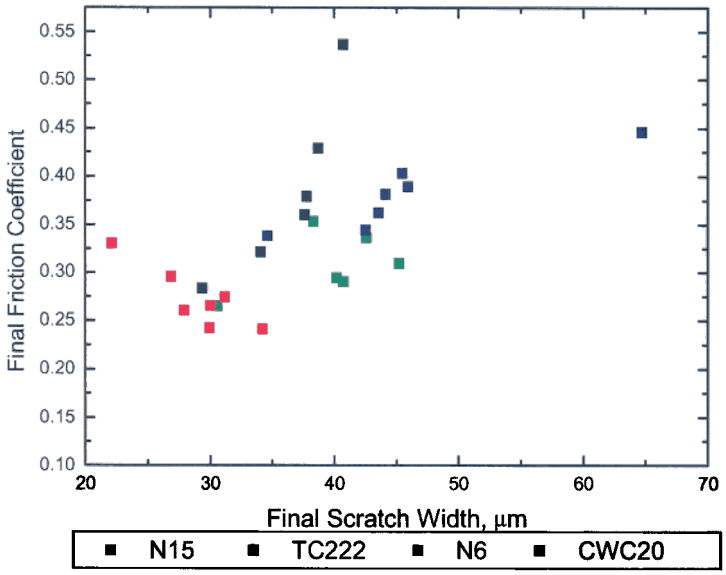

c)

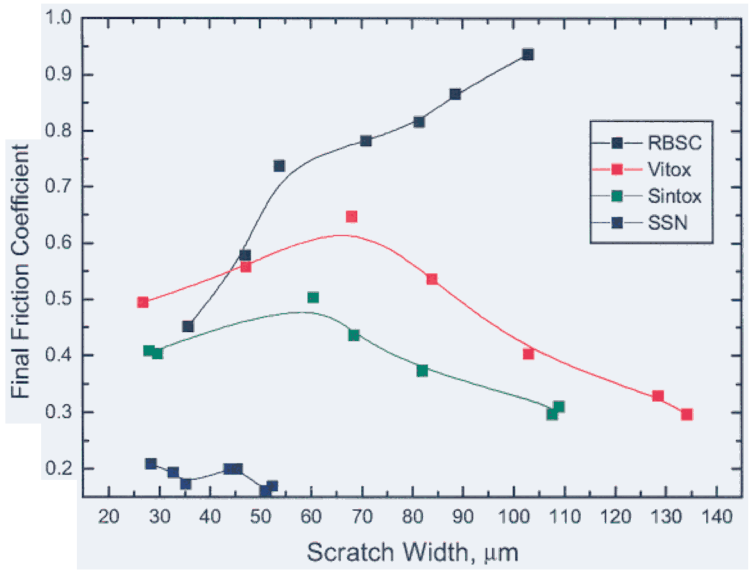

d)

Figure 19, Variation of final friction coefficient with final scratch width for low load scratch tests (final is after 100 repeat scratches), a) hardmetal with 50 µm indenter, b) ceramics with 50 µm indenter, c) hardmetals with 200 µm indenter, d) ceramics with 200 µm indenter.

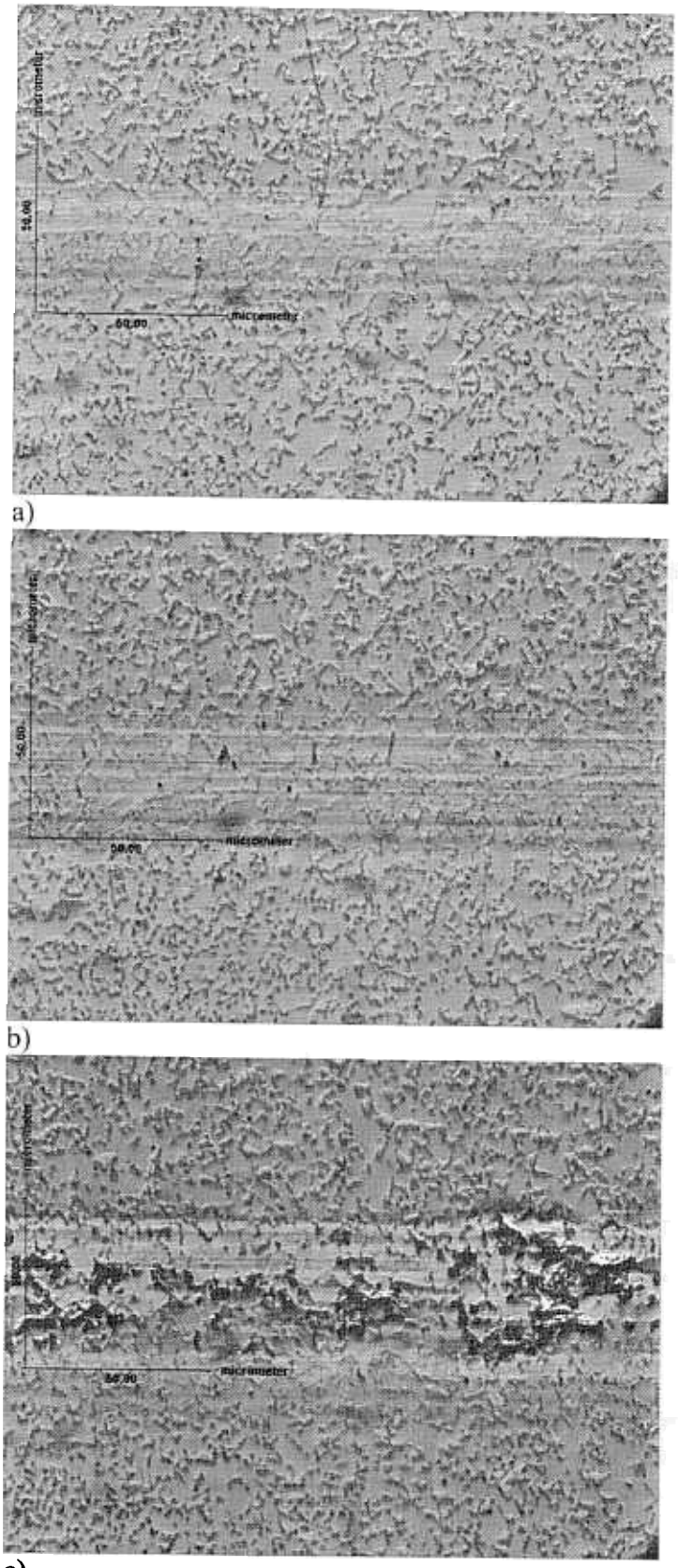

Figure 20, Low Load Scratches for CWC15C hardmetal with 200 µm indenter, a) single pass, b) two passes, c) 100 passes

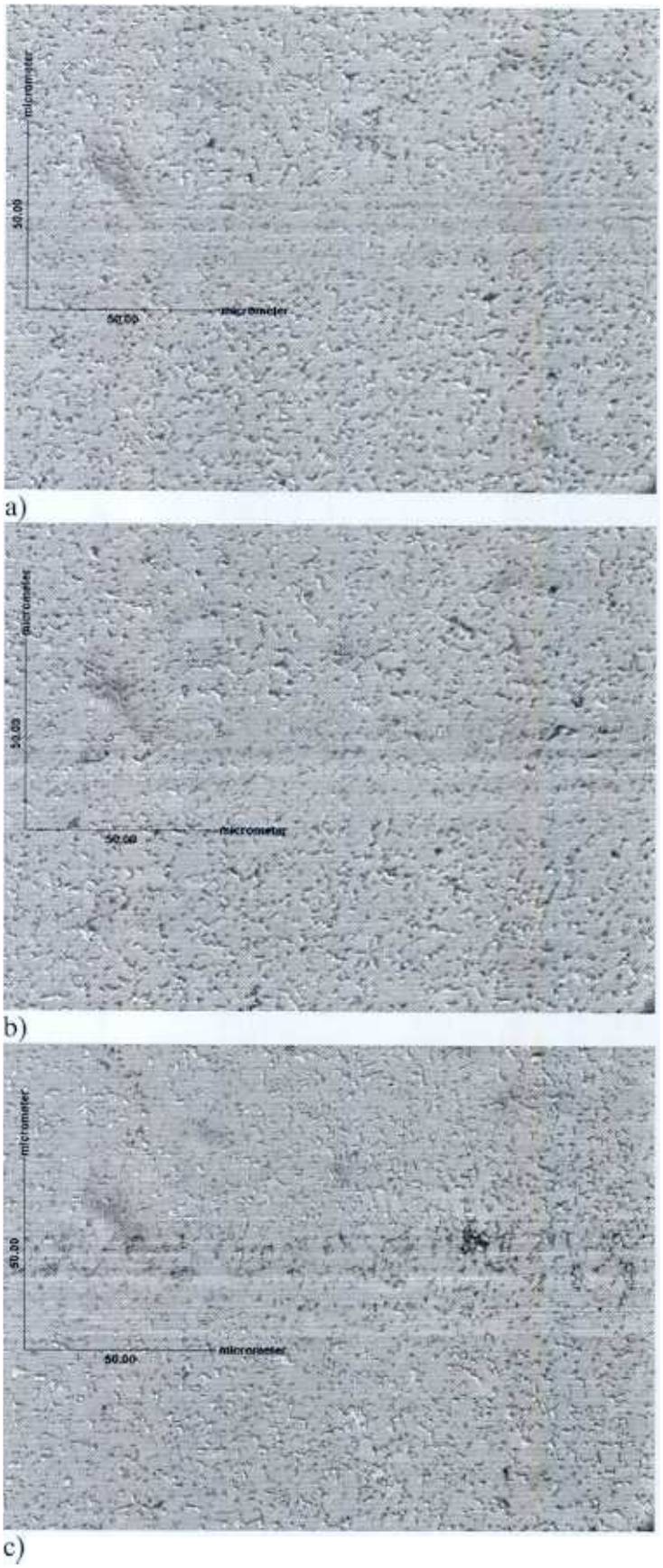

Figure 21, Low Load Scratches for MA10 hardmetal with 200 µm indenter, a) single pass, b) two passes, c) 100 passes

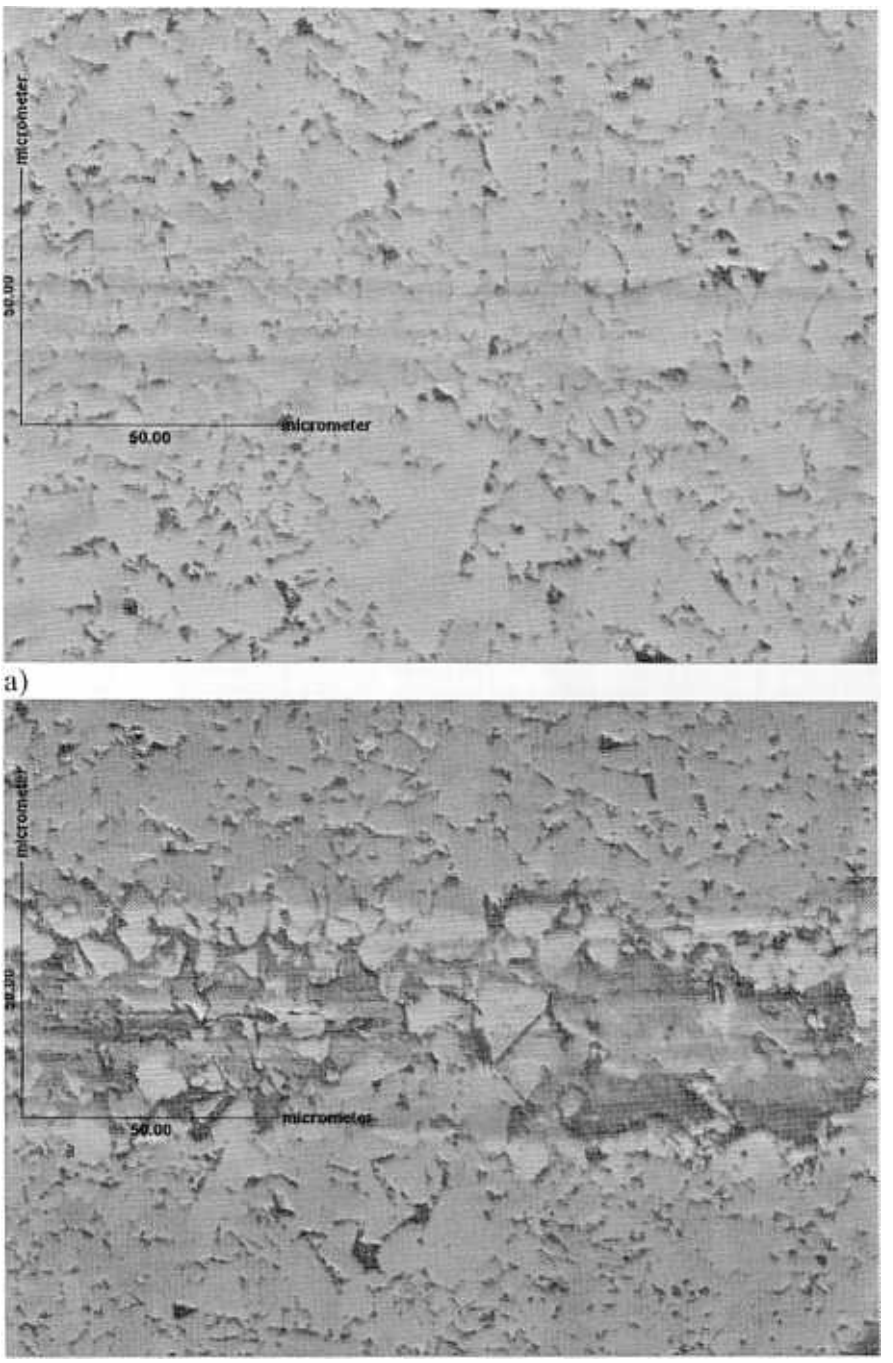

a)

b)

Figure 22, Low Load Scratches for a) TC222 hardmetal with a 200 µm indenter and a single pass, b) TC222 hardmetal with a 200 µm indenter and 100 passes, c) SHMUF hardmetal with 200 µm indenter and a single pass, d) SHMUF hardmetal with a 200 µm indenter and two passes, e) SHMUF hardmetal with a 200 µm indenter and 100 passes.

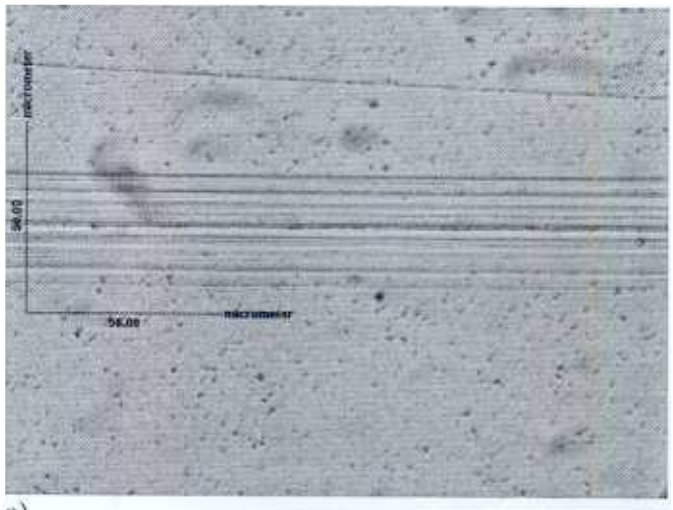

c)

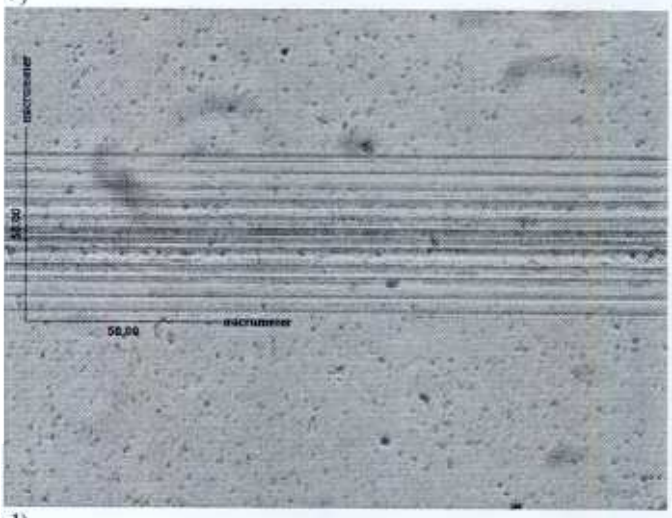

d)

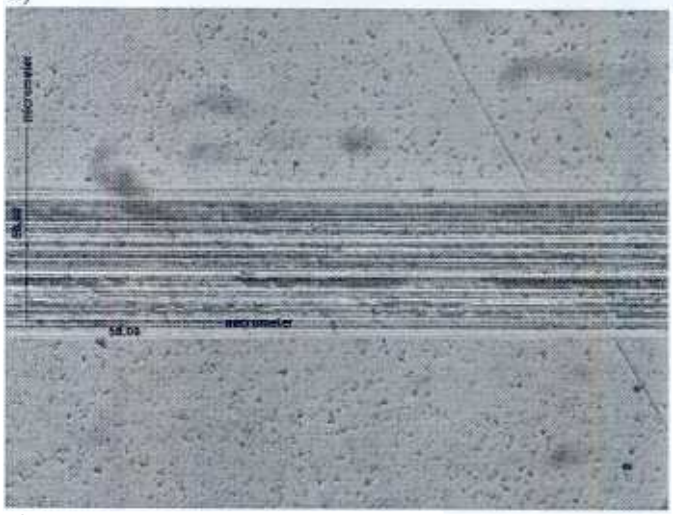

e)

Figure 22, Low Load Scratches for a) TC222 hardmetal with a 200 µm indenter and a single pass, b) TC222 hardmetal with a 200 µm indenter and 100 passes, c) SHMUF hardmetal with 200 µm indenter and a single pass, d) SHMUF hardmetal with a 200 µm indenter and two passes, e) SHMUF hardmetal with a 200 µm indenter and 100 passes.

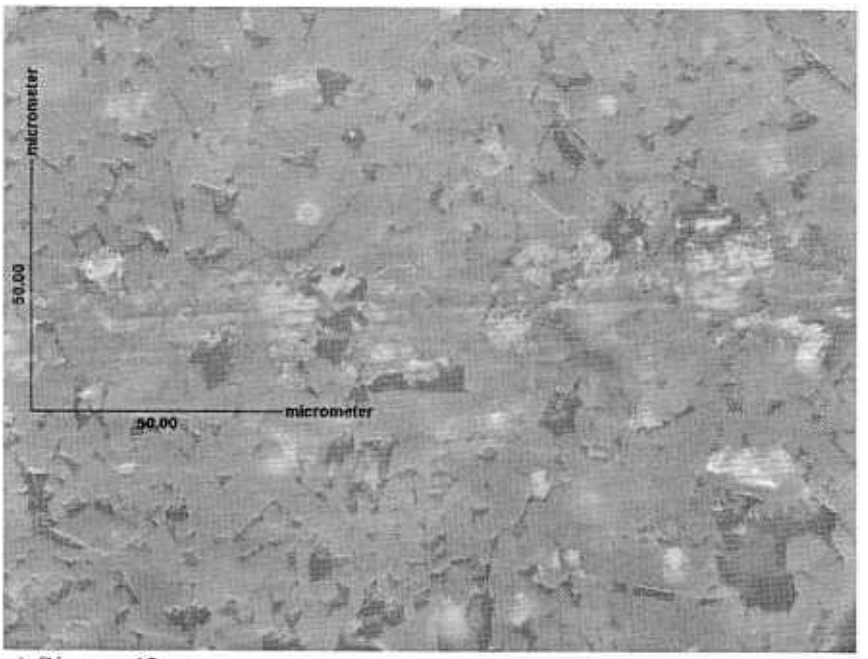

a) Sintox 42

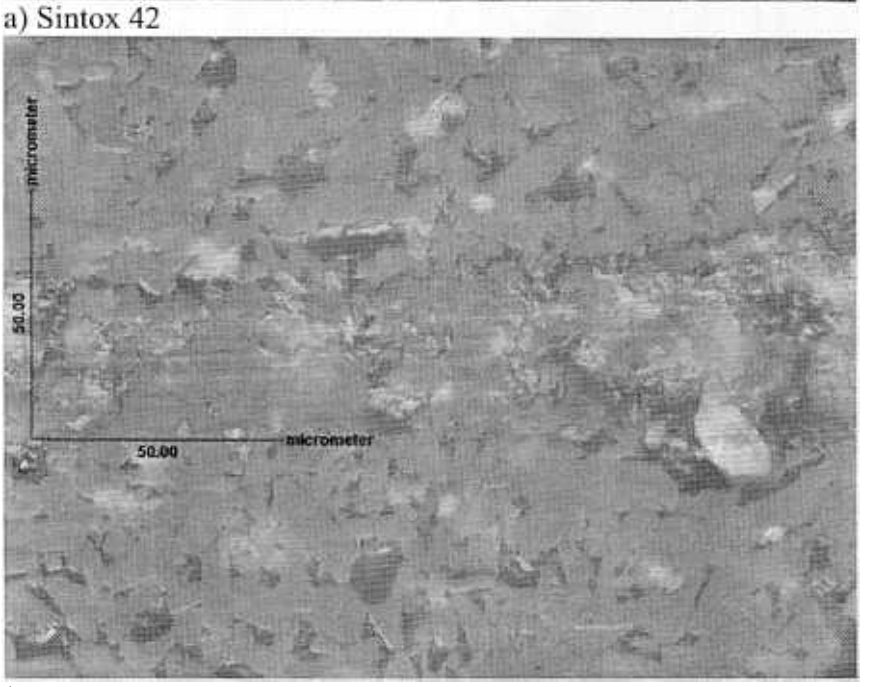

b) Sintox72

Figure 23, Optical micrographs of low load scratches on Sintox with 200 μm indenter, a) 10 repeat passes, b) 100 repeat passes.

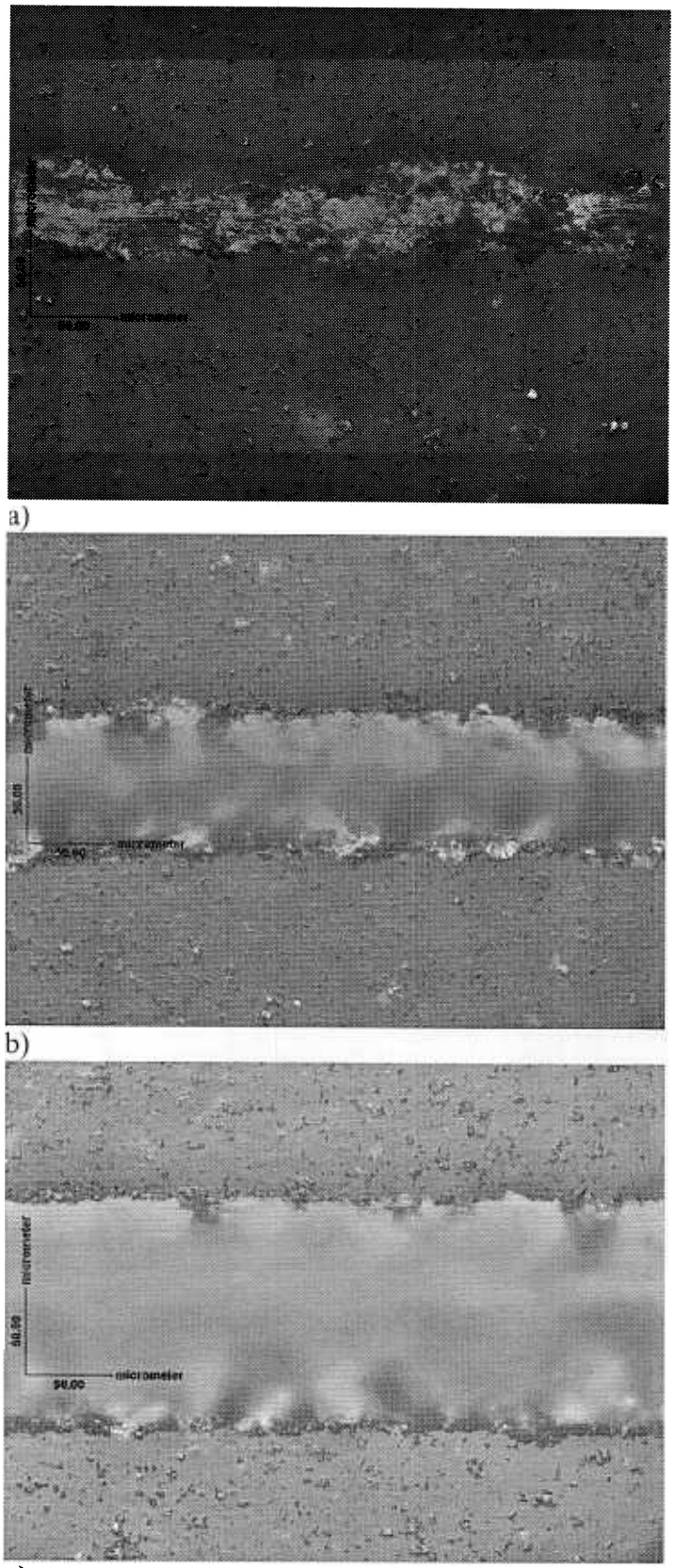

Figure 24, Optical micrographs of low load scratches on Vitox with 50 μm indenter, a) single repeat pass, b) 10 repeat passes, c) 100 repeat passes

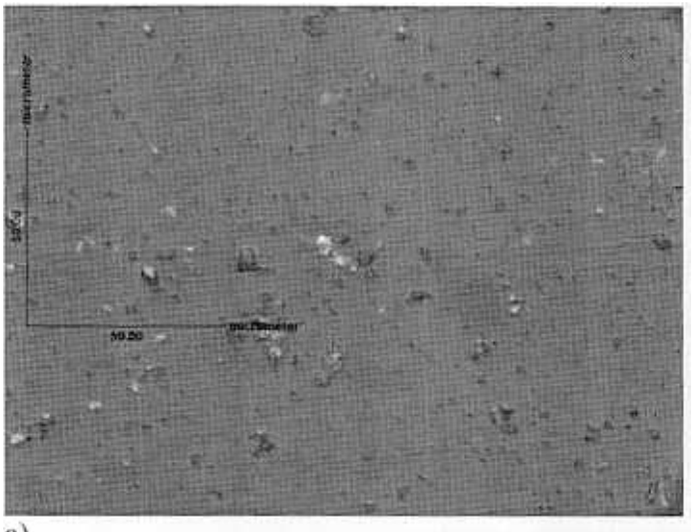

a)

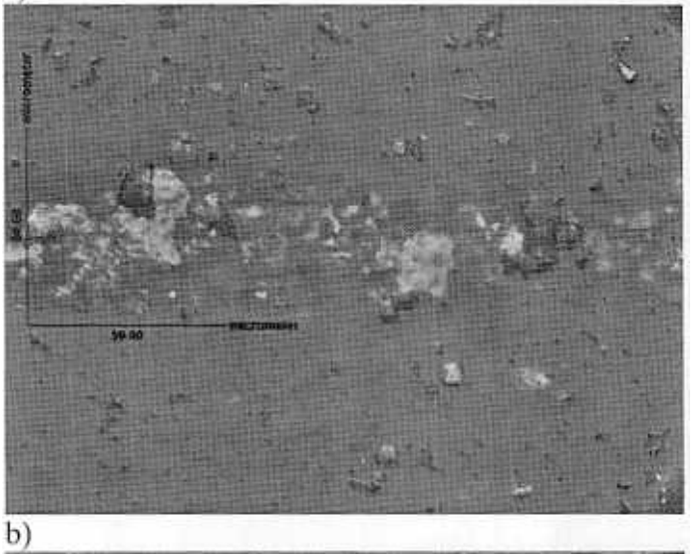

b)

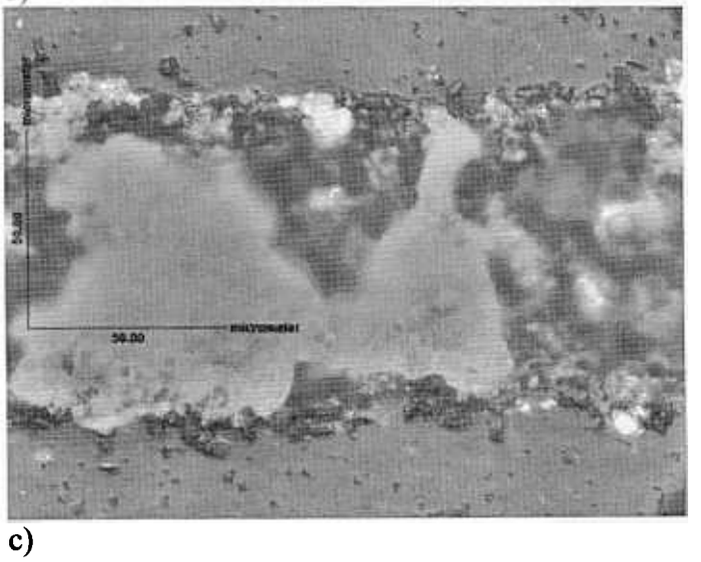

c)

Figure 25, Optical micrographs of low load scratches on Vitox with 200 µm indenter, a) single repeat pass, b) 10 repeat passes, c) 100 repeat passes

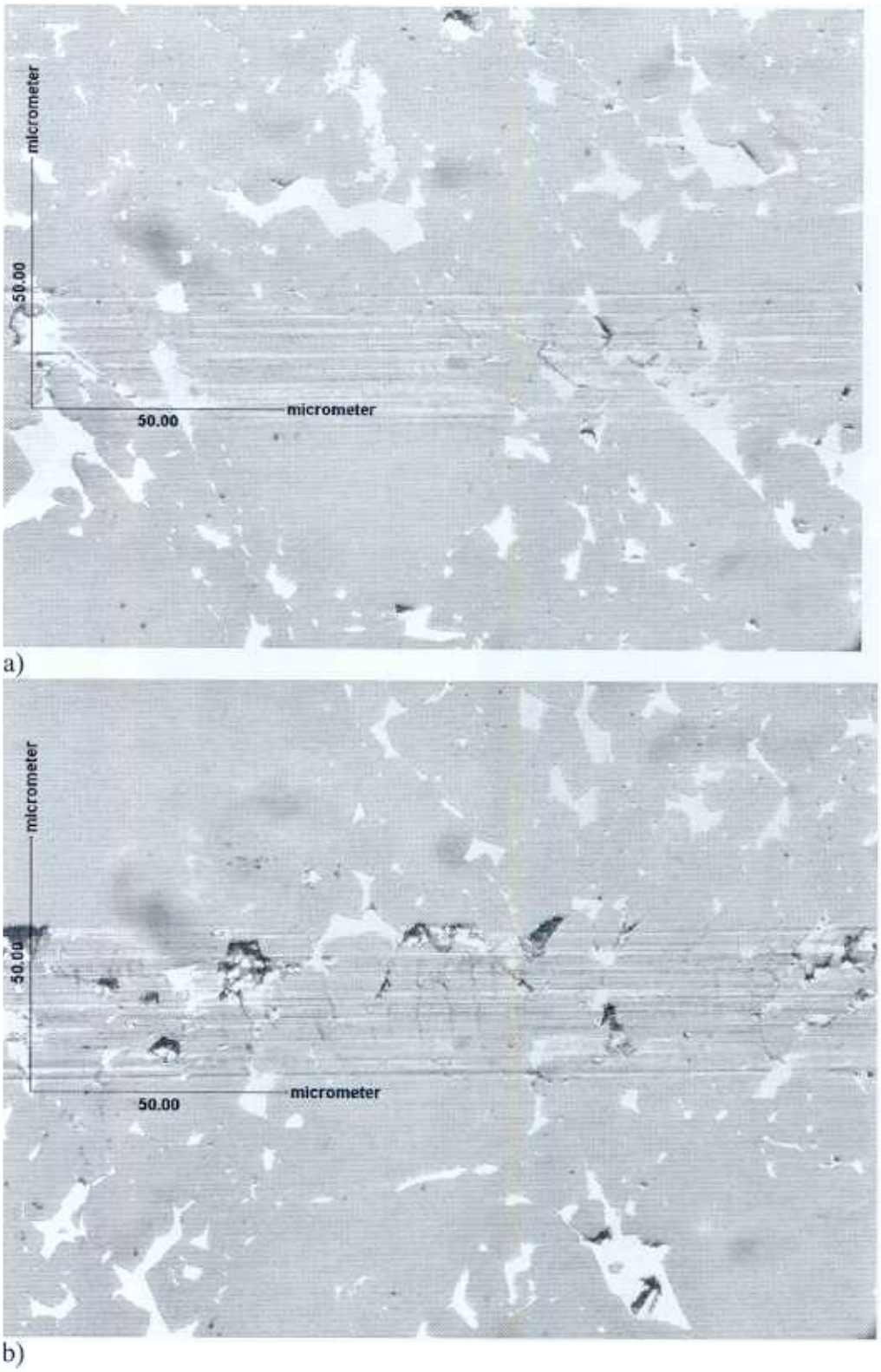

Figure 26, Optical micrographs of low load scratches on RBSC with 200 μm indenter, a) single repeat pass, b) 2 repeat passes, c) 10 repeat passes, d) 100 repeat passes.

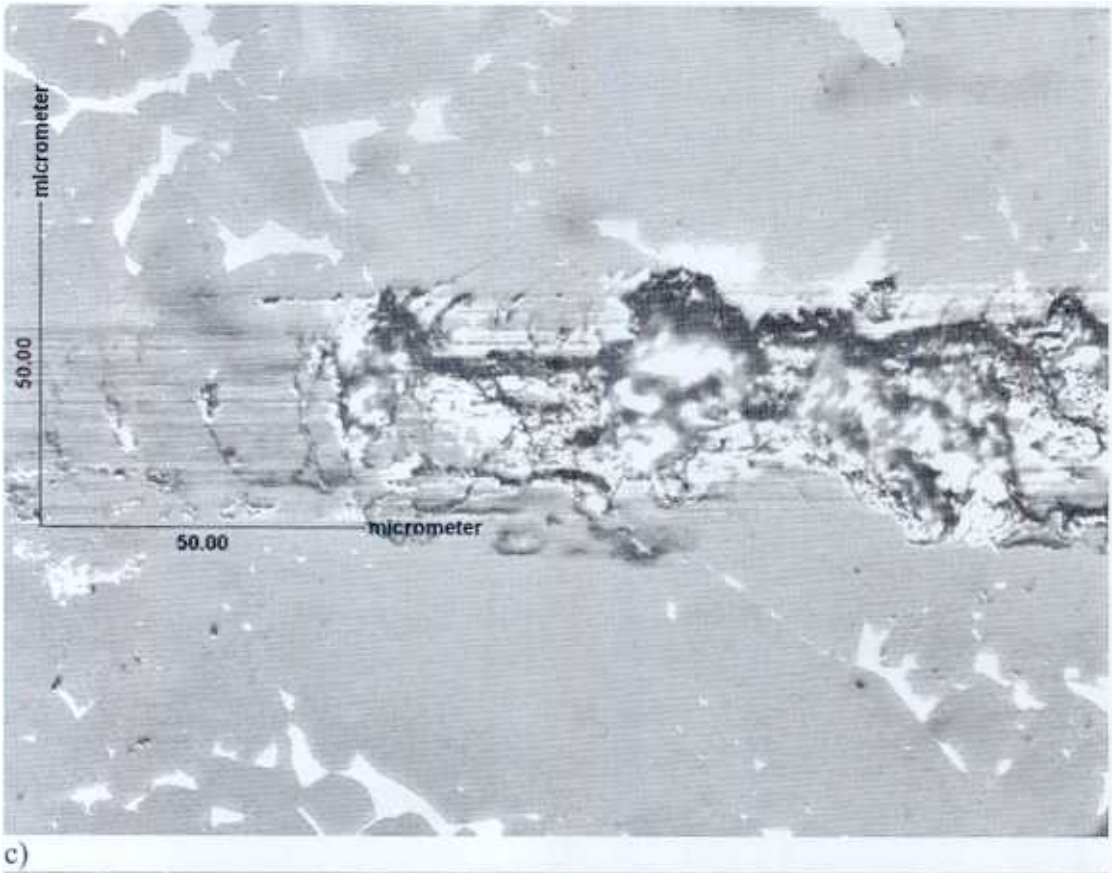

c)

d)

Figure 26, Optical micrographs of low load scratches on RBSC with 200 μm indenter, a) single repeat pass, b) 2 repeat passes, c) 10 repeat passes, d) 100 repeat passes.

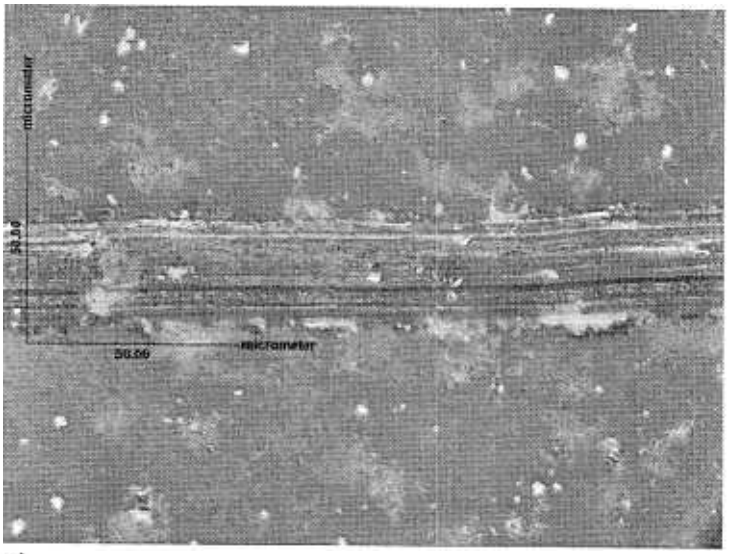

a)

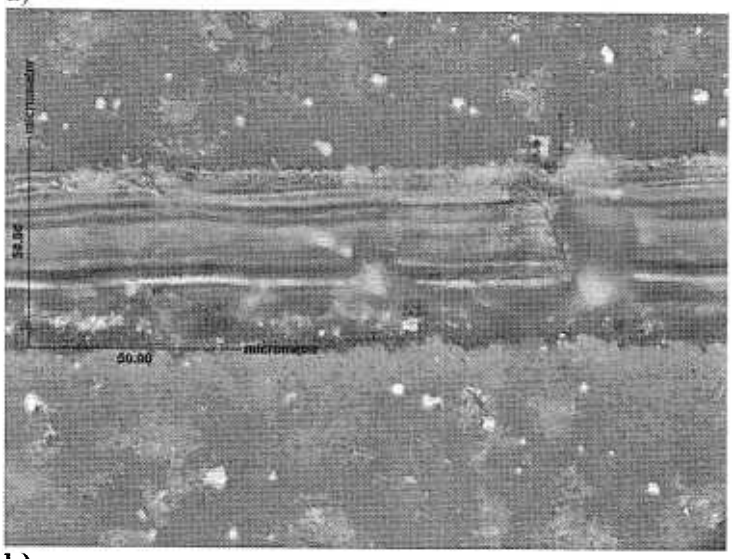

b)

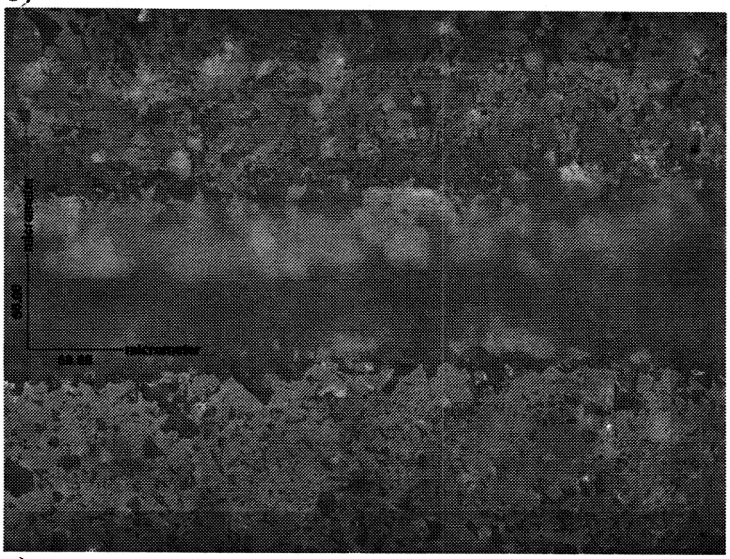

c)

Figure 27, Optical micrographs of low load scratches on SSN sample with50 μm indenter, a) single pass, b) 10 passes, c) 100 passes.

Figure 27, Scanning electron micrographs of low load scratch tests on N15 hardmetal, a) 100 passes with 200 µm indenter, b) 10 passes with 50 µm indenter, c) 100 passes with 50 µm indnter.

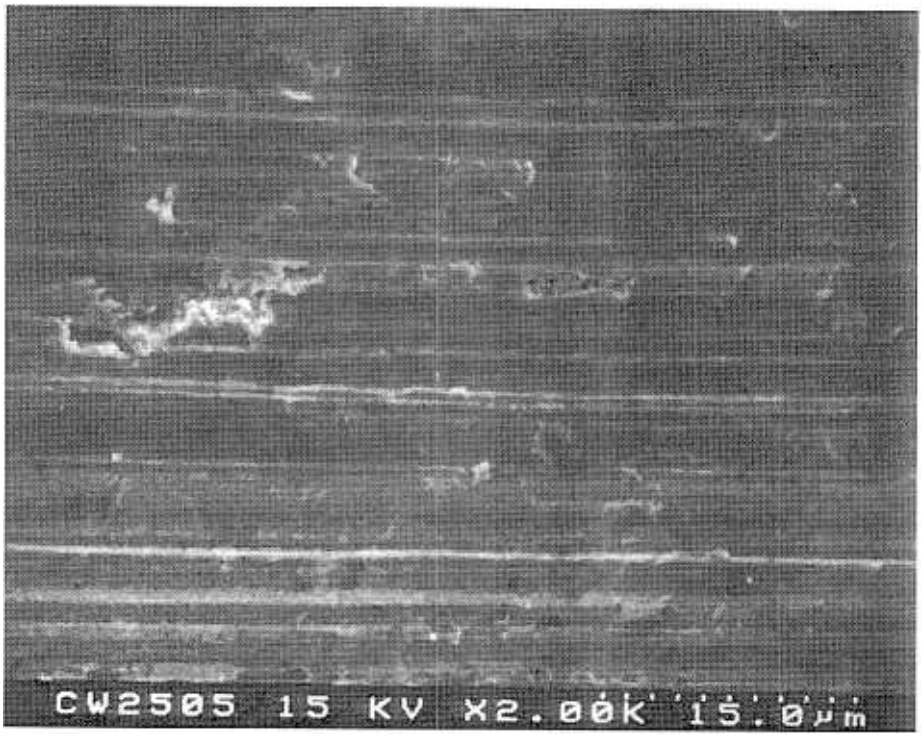

Figure 28, Scanning electron micrograph of 100 passes in low load scratch test on CWC25C hardmetal.

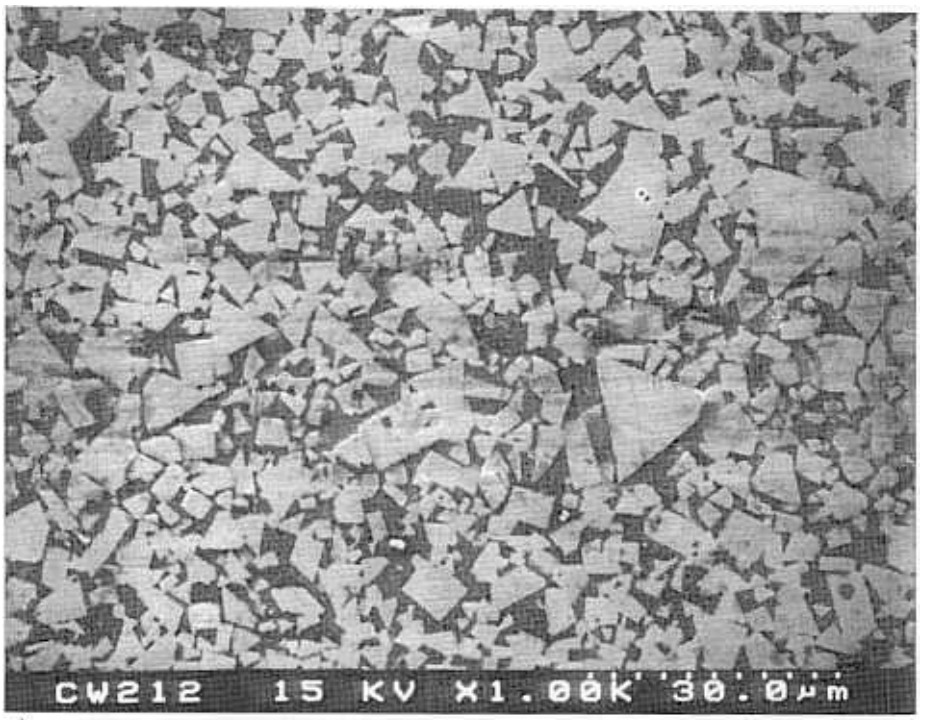

a)

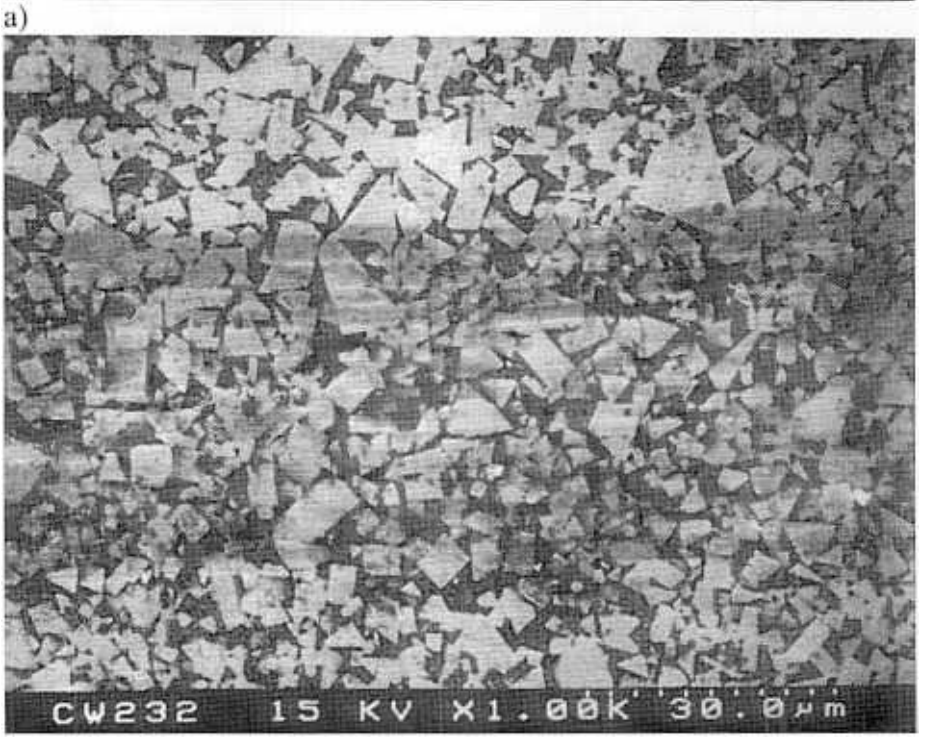

b)

Figure 29 Scanning electron micrographs of low load scratch tests on CWC20C hardmetal, a) single pass with 200 µm indenter, b) 5 passes with 200 µm indenter, c) 50 passes with 200 µm indnter, d) 100 passes with 200 µm indenter, e) 100 passes with 200 µm indenter, f) 100 passes with 200 µm indenter, g) 100 passes with 200 µm indenter.

c)

d)

Figure 29 Scanning electron micrographs of low load scratch tests on CWC20C hardmetal, a) single pass with 200 µm indenter, b) 5 passes with 200 µm indenter, c) 50 passes with 200 µm indnter, d) 100 passes with 200 µm indenter, e) 100 passes with 200 µm indenter, f) 100 passes with 200 µm indenter, g) 100 passes with 200 µm indenter.

e)

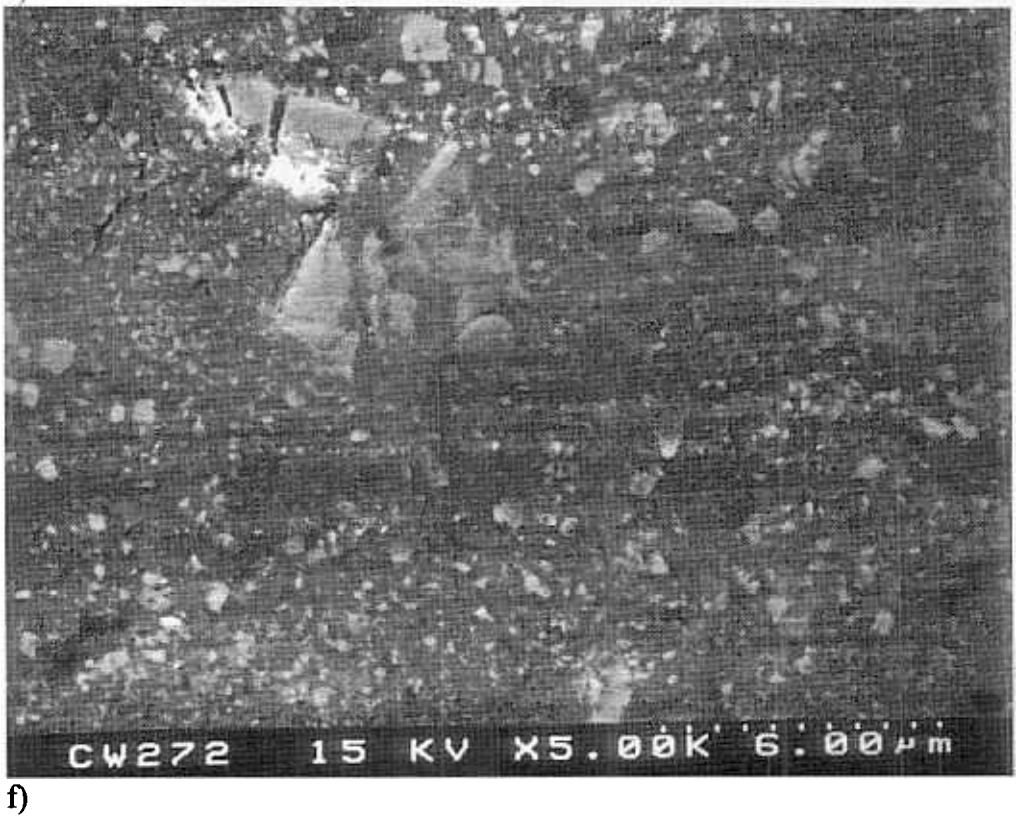

f)

Figure 29 Scanning electron micrographs of low load scratch tests on CWC20C hardmetal, a) single pass with 200 µm indenter, b) 5 passes with 200 µm indenter, c) 50 passes with 200 µm indnter, d) 100 passes with 200 µm indenter, e) 100 passes with 200 µm indenter, f) 100 passes with 200 µm indenter, g) 100 passes with 200 µm indenter.

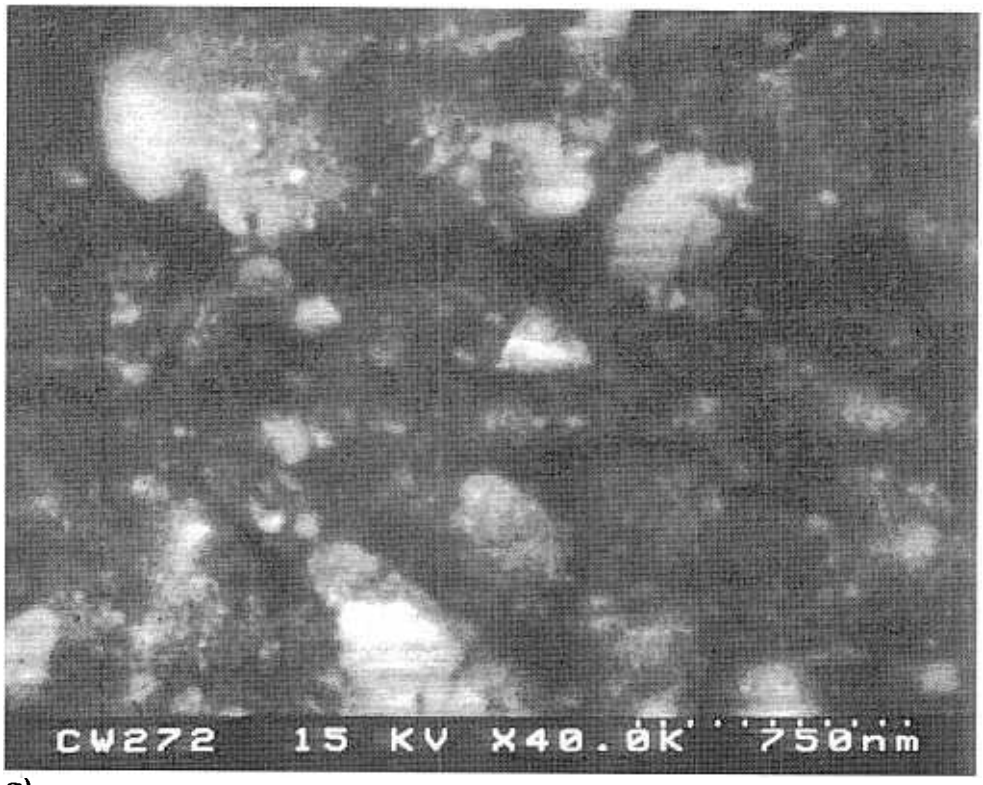

g)

Figure 29 Scanning electron micrographs of low load scratch tests on CWC20C hardmetal, a) single pass with 200 μm indenter, b) 5 passes with 200 μm indenter, c) 50 passes with 200 μm indnter, d) 100 passes with 200 μm indenter, e) 100 passes with 200 μm indenter, f) 100 passes with 200 μm indenter, g) 100 passes with 200 μm indenter.

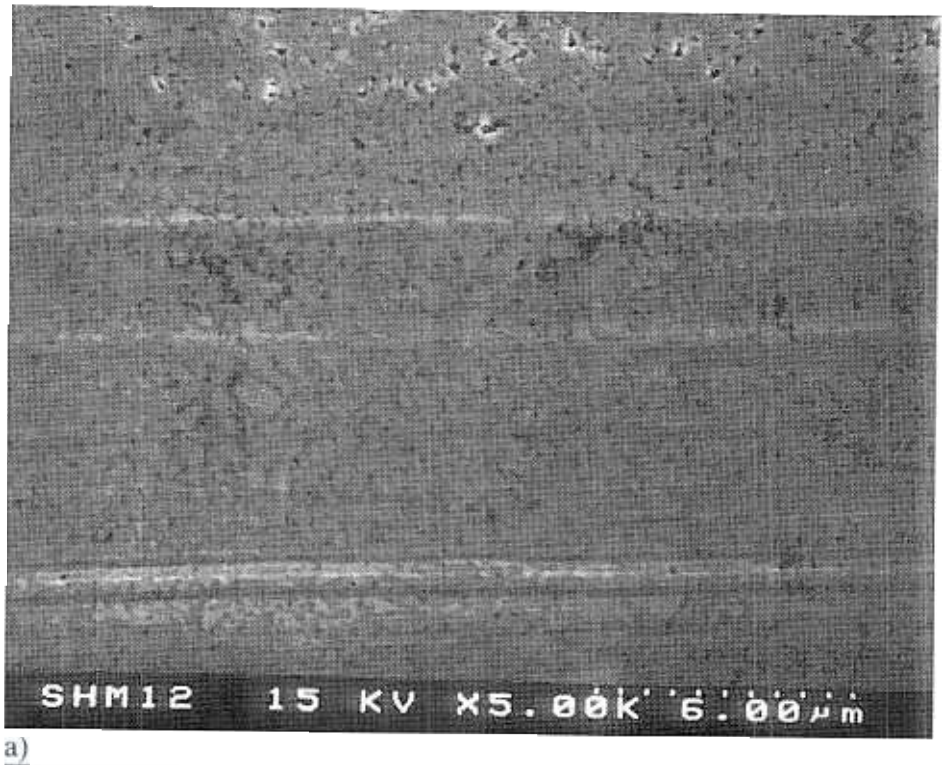

a)

b)

Figure 30, Scanning electron micrographs of low load scratch tests on SHMUF hardmetal, a) single pass with 200 µm indenter, b) 10 passes with 200 µm indenter, c) 50 passes with 200 µm indenter, d) 10 passes with 50 µm indenter, e) 50 passes with 200 µm indenter, f) 100 passes with 200 µm indenter.

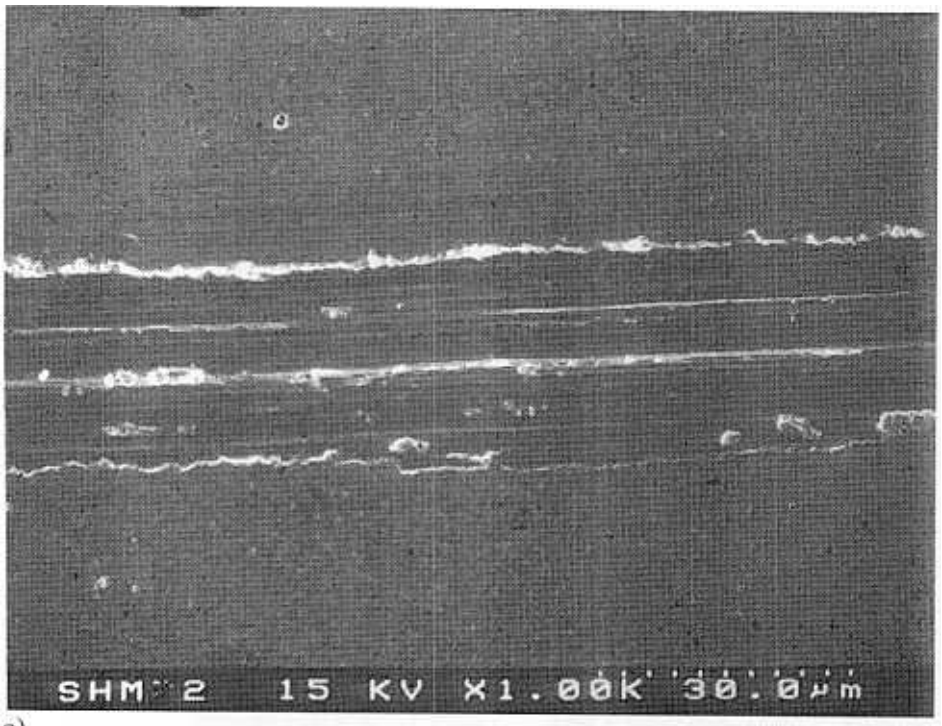

c)

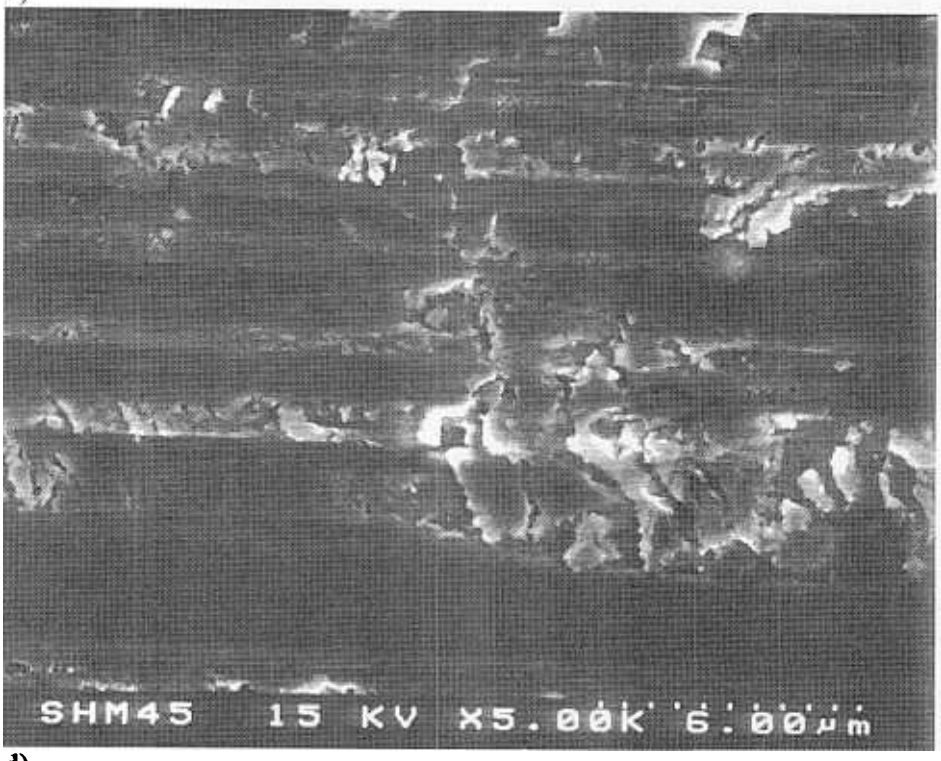

d)

Figure 30, Scanning electron micrographs of low load scratch tests on SHMUF hardmetal, a) single pass with 200 µm indenter, b) 10 passes with 200 µm indenter, c) 50 passes with 200 µm indenter, d) 10 passes with 50 µm indenter, e) 50 passes with 200 µm indenter, f) 100 passes with 200 µm indenter..

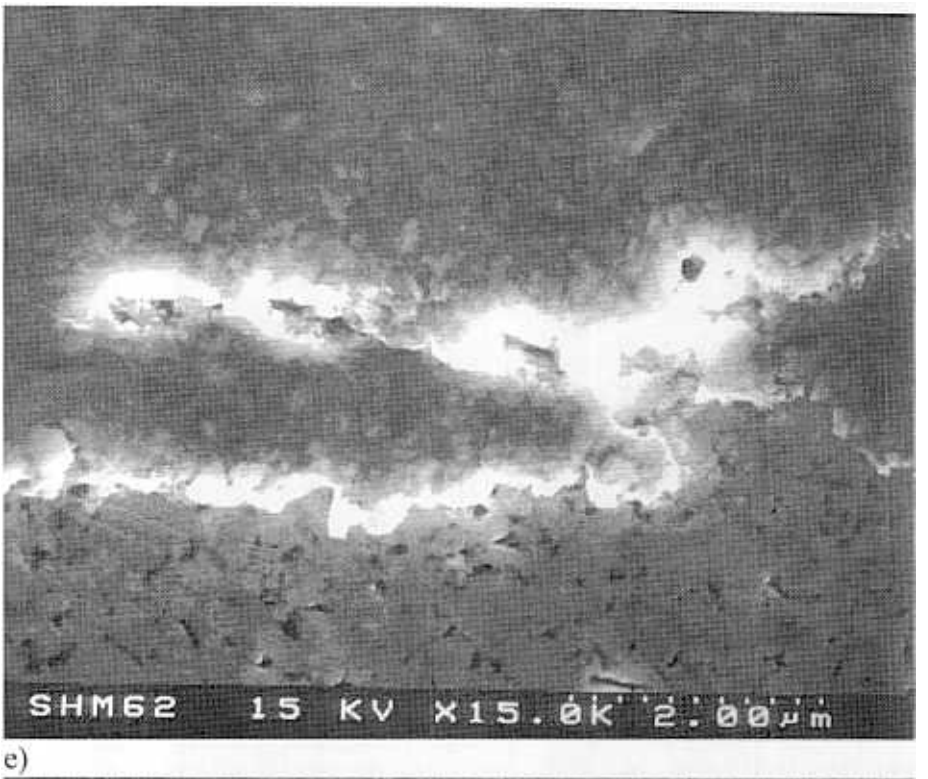

e)

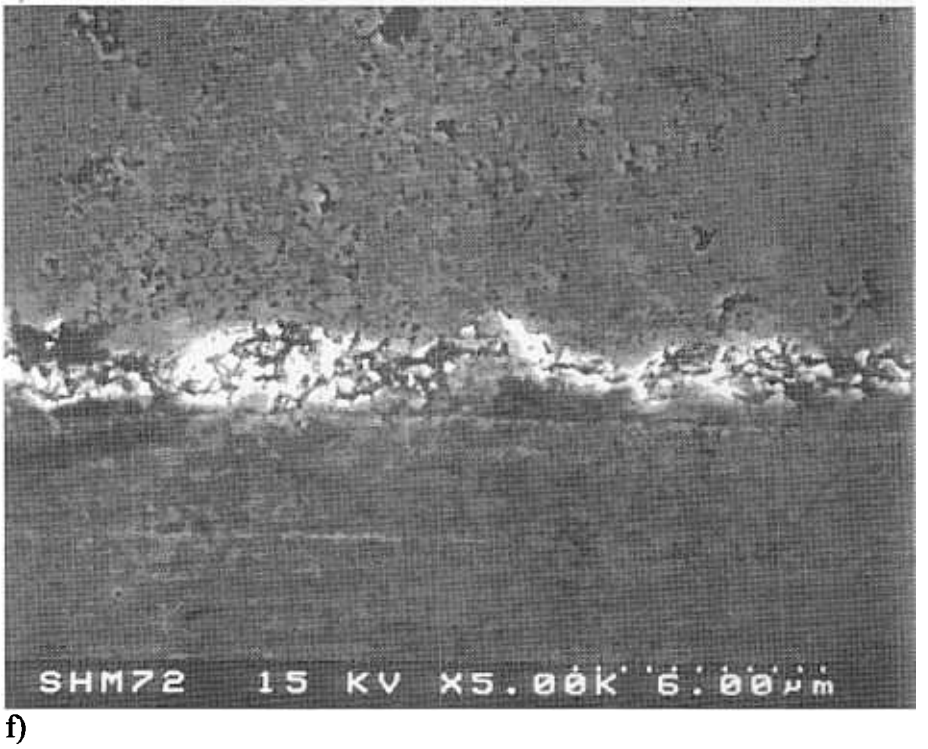

f)

Figure 30, Scanning electron micrographs of low load scratch tests on SHMUF hardmetal, a) single pass with 200 µm indenter, b) 10 passes with 200 µm indenter, c) 50 passes with 200 µm indenter, d) 10 passes with 50 µm indenter, e) 50 passes with 200 µm indenter, f) 100 passes with 200 µm indenter.

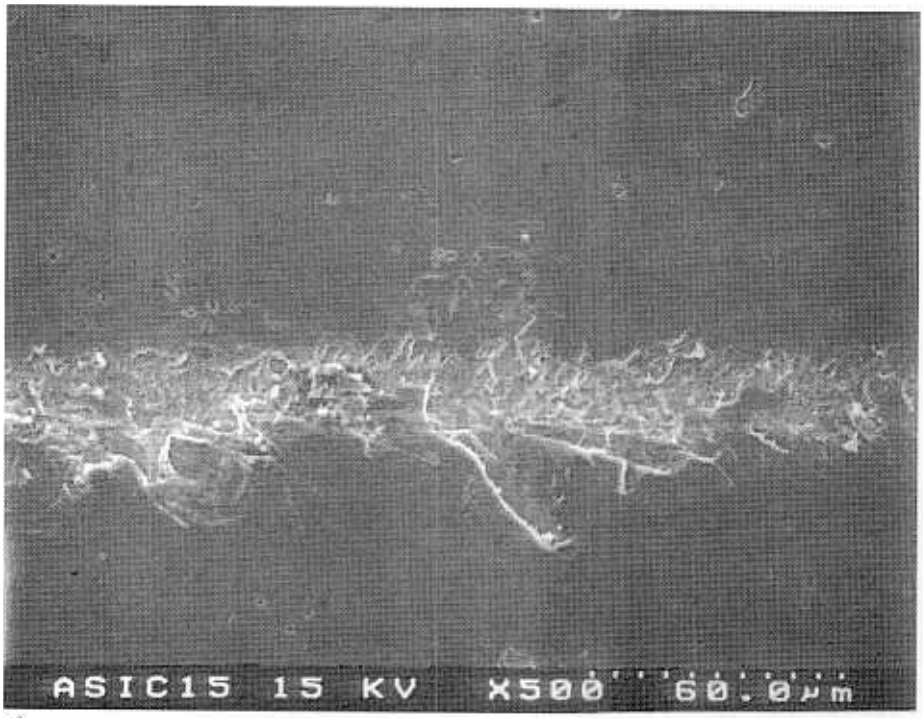

a)

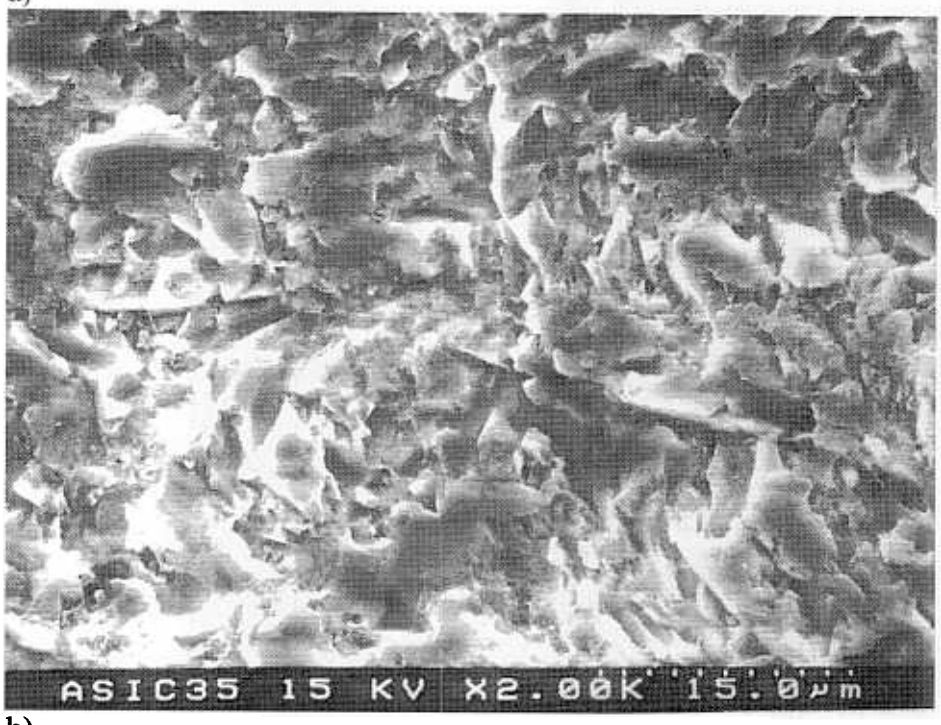

b)

Figure 31, Scanning electron micrographs of low load scratch tests on α-SiC ceramic, a) single pass with 50 µm indenter, b) 5 passes with 50 µm indenter, c) 10 passes with 50 µm indenter, d) 5 passes with 200 µm indenter, e) 20 passes with 200 µm indenter, f) 50 passes with 200 µm indenter, g) 100 passes with 200 µm indenter, h) 100 passes with 200 µm indenter, i) 100 passes with 200 µm indenter.

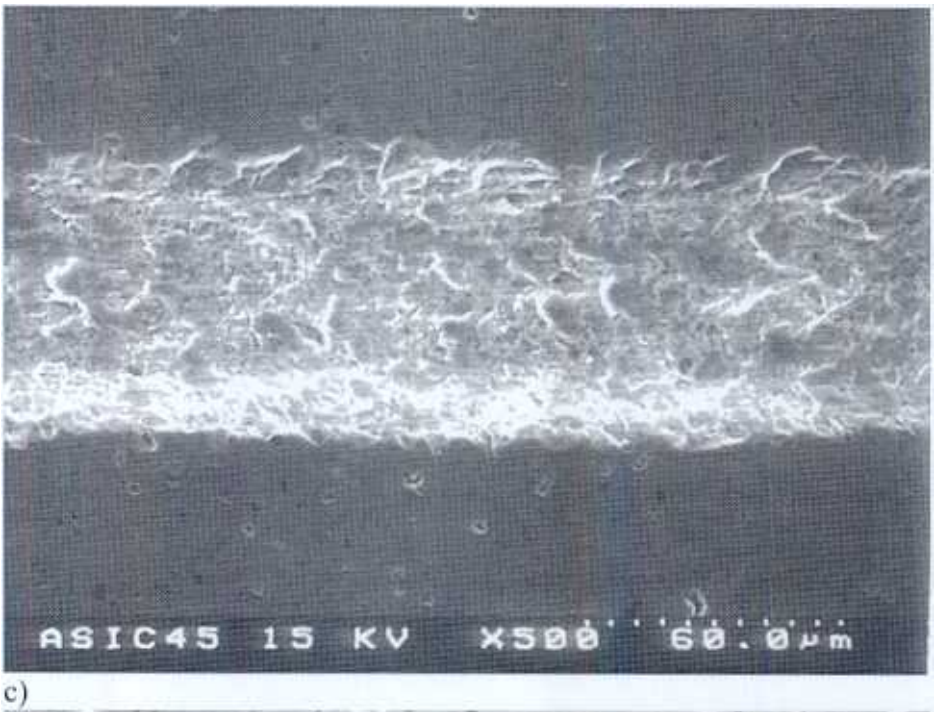

c)

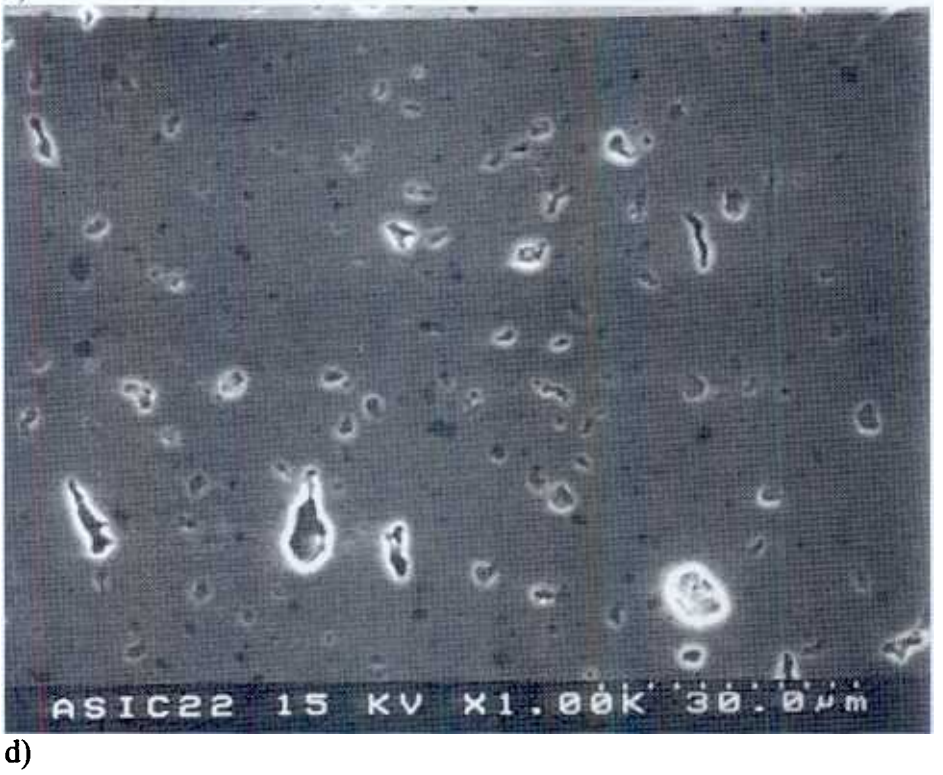

d)

Figure 31, Scanning electron micrographs of low load scratch tests on α-SiC ceramic, a) single pass with 50 µm indenter, b) 5 passes with 50 µm indenter, c) 10 passes with 50 µm indenter, d) 5 passes with 200 µm indenter, e) 20 passes with 200 µm indenter, f) 50 passes with 200 µm indenter, g) 100 passes with 200 µm indenter, h) 100 passes with 200 µm indenter, i) 100 passes with 200 µm indenter.

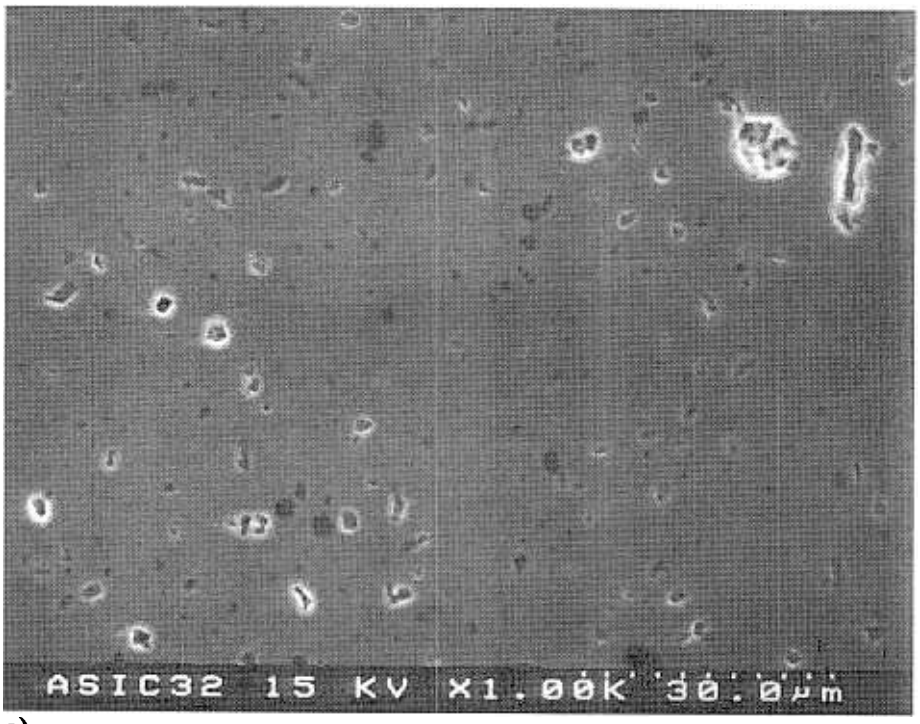

e)

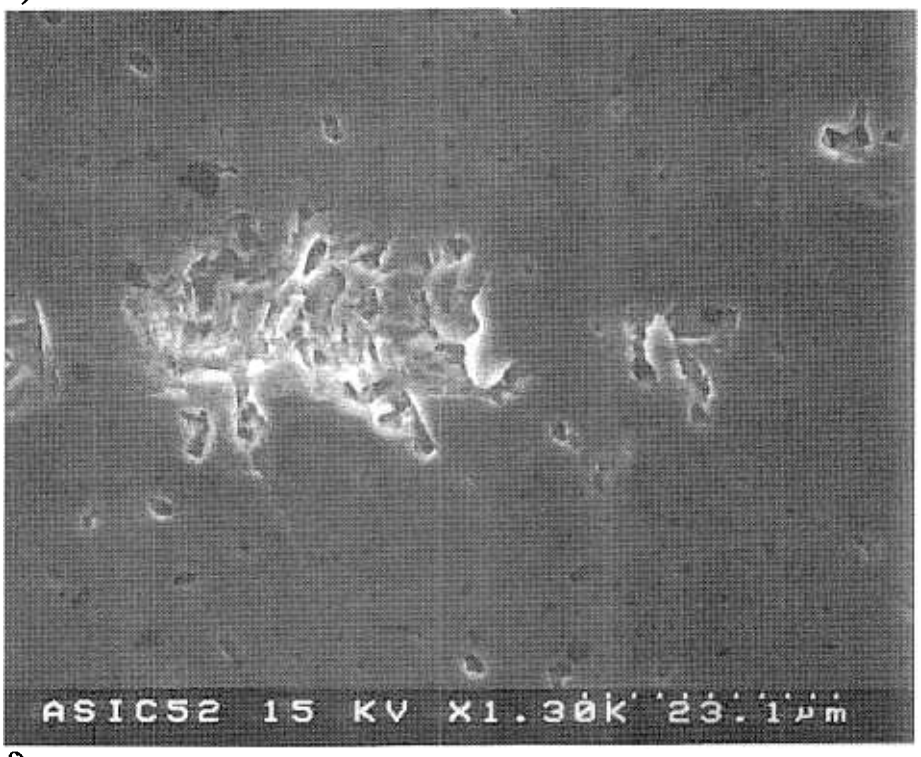

f)

Figure 31, Scanning electron micrographs of low load scratch tests on α-SiC ceramic, a) single pass with 50 µm indenter, b) 5 passes with 50 µm indenter, c) 10 passes with 50 µm indenter, d) 5 passes with 200 µm indenter, e) 20 passes with 200 µm indenter, f) 50 passes with 200 µm indenter, g) 100 passes with 200 µm indenter, h) 100 passes with 200 µm indenter, i) 100 passes with 200 µm indenter.

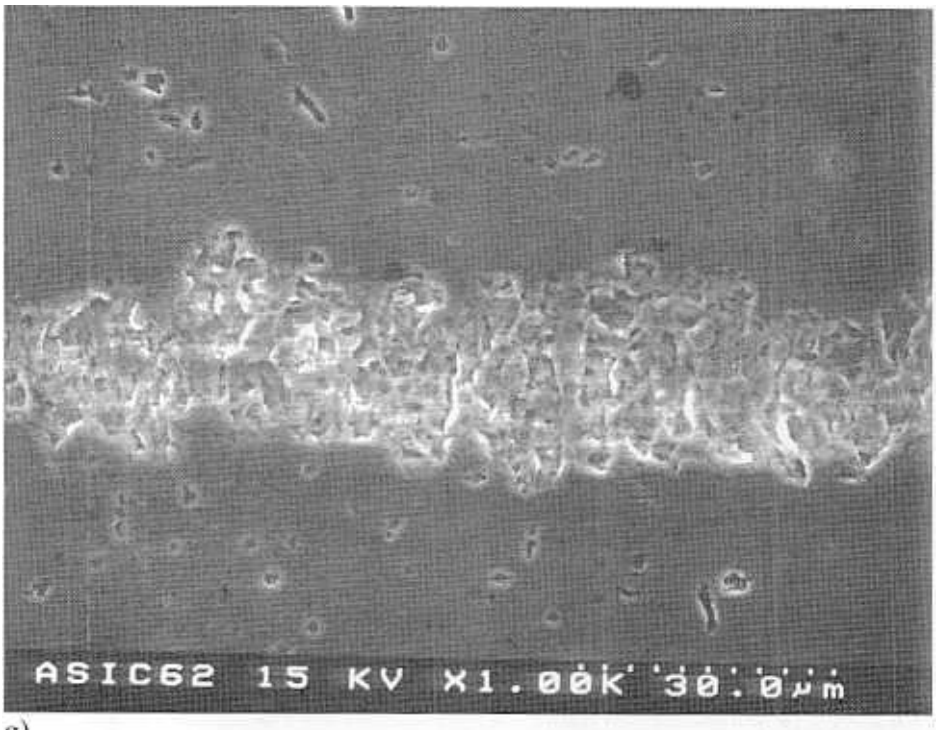

g)

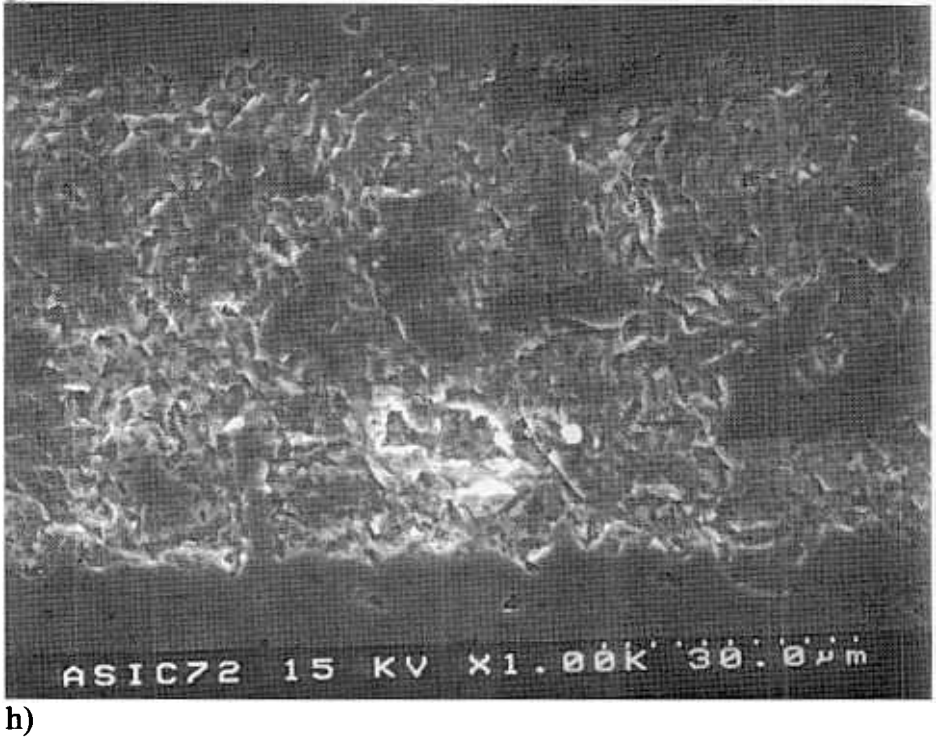

h)

Figure 31, Scanning electron micrographs of low load scratch tests on α-SiC ceramic, a) single pass with 50 µm indenter, b) 5 passes with 50 µm indenter, c) 10 passes with 50 µm indenter, d) 5 passes with 200 µm indenter, e) 20 passes with 200 µm indenter, f) 50 passes with 200 µm indenter, g) 100 passes with 200 µm indenter, h) 100 passes with 200 µm indenter, i) 100 passes with 200 µm indenter.

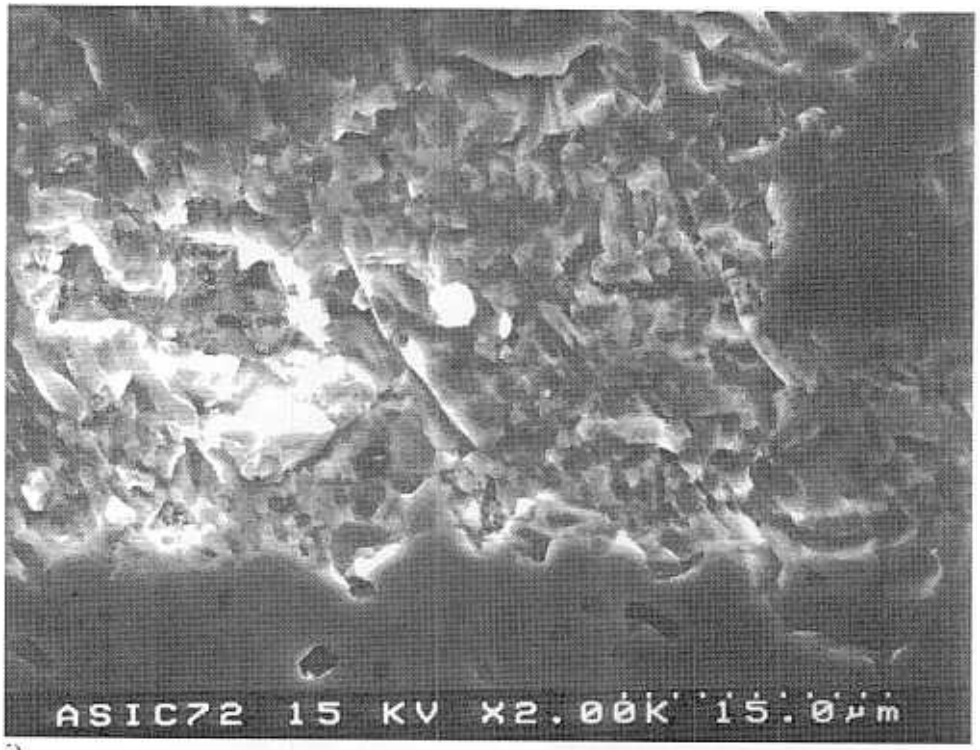

i)

Figure 31, Scanning electron micrographs of low load scratch tests on α-SiC ceramic, a) single pass with 50 µm indenter, b) 5 passes with 50 µm indenter, c) 10 passes with 50 µm indenter, d) 5 passes with 200 µm indenter, e) 20 passes with 200 µm indenter, f) 50 passes with 200 µm indenter, g) 100 passes with 200 µm indenter, h) 100 passes with 200 µm indenter, i) 100 passes with 200 µm indenter.

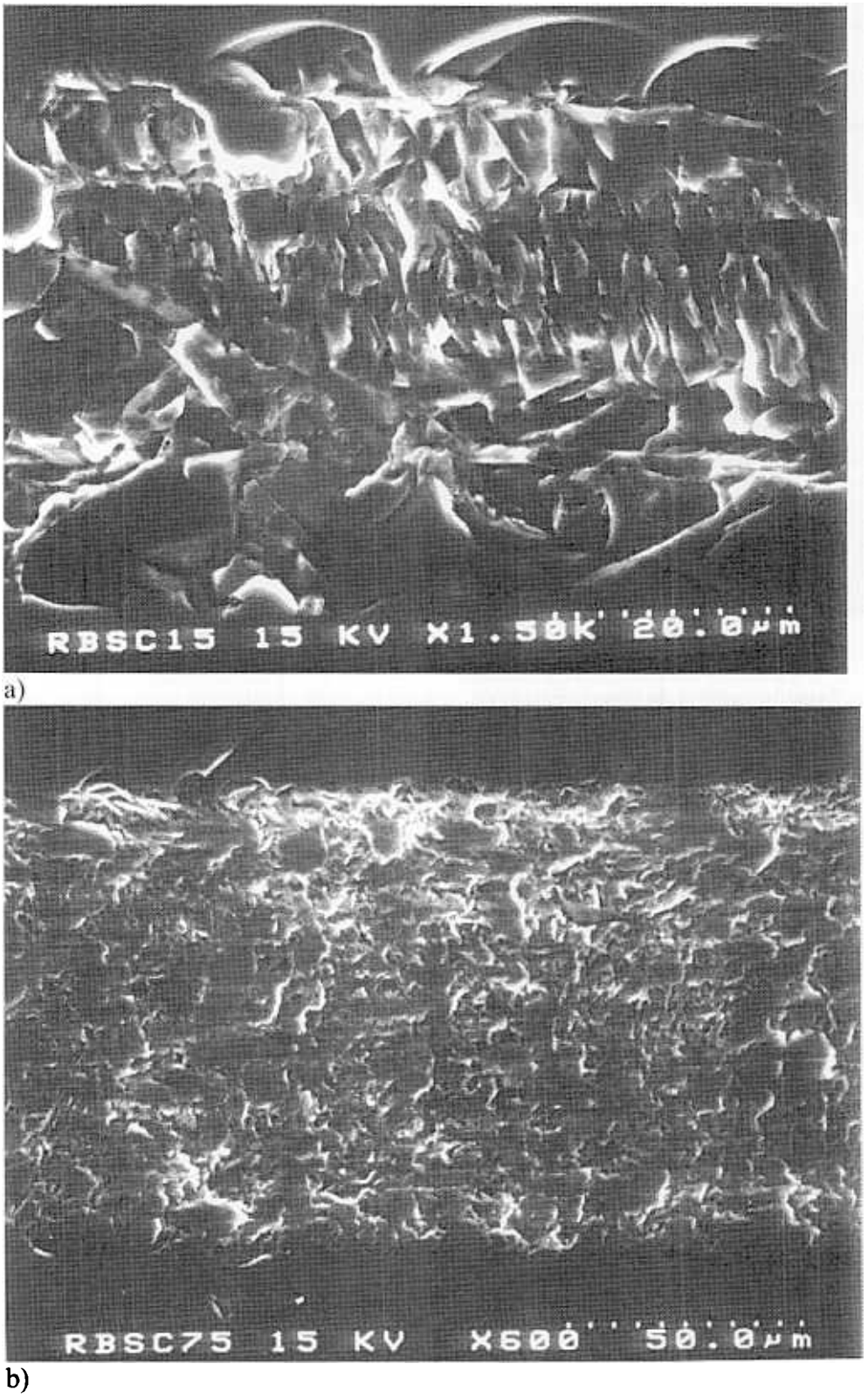

Figure 32, Scanning electron micrographs of low load scratch tests on RBSC ceramic, a) single pass with 50 µm indenter, b) 100 passes with 50 µm indenter, c) 2 passes with 50 µm indenter, d) 20 passes with 200 µm indenter, e) 200 passes with 200 µm indenter, f) 200 passes with 200 µm indenter.

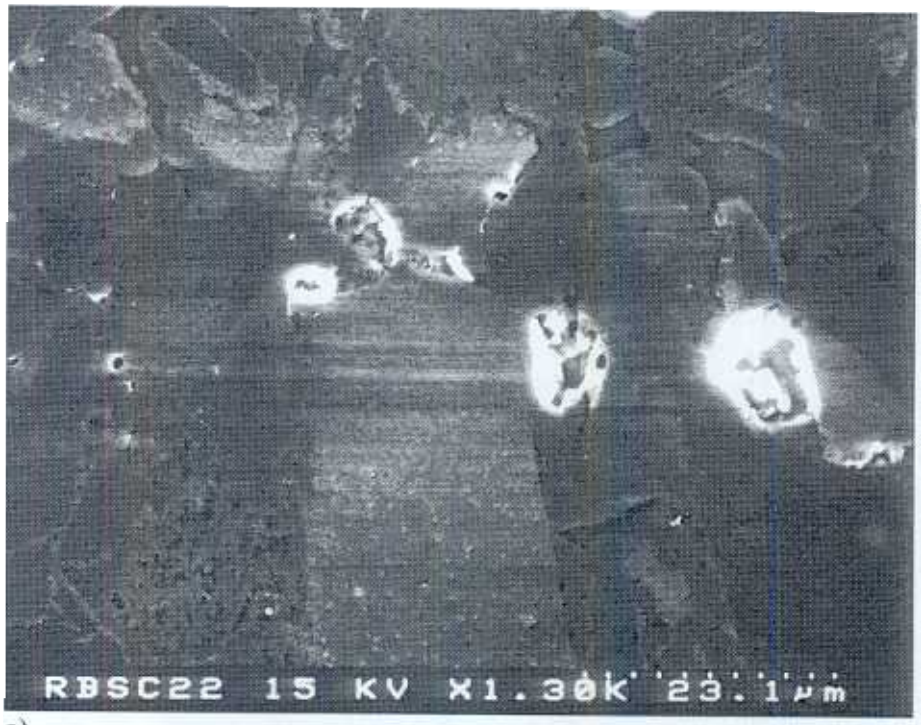

c)

d)

Figure 32, Scanning electron micrographs of low load scratch tests on RBSC ceramic, a) single pass with 50 µm indenter, b) 100 passes with 50 µm indenter, c) 2 passes with 50 µm indenter, d) 20 passes with 200 µm indenter, e) 200 passes with 200 µm indenter, f) 200 passes with 200 µm indenter.

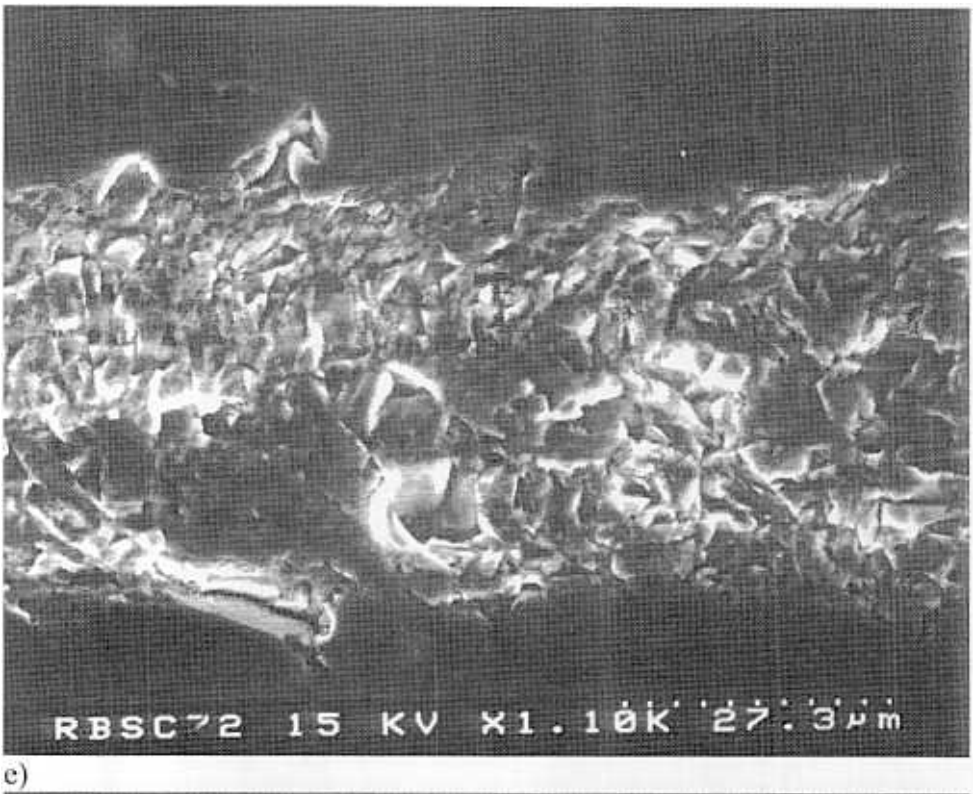

c)

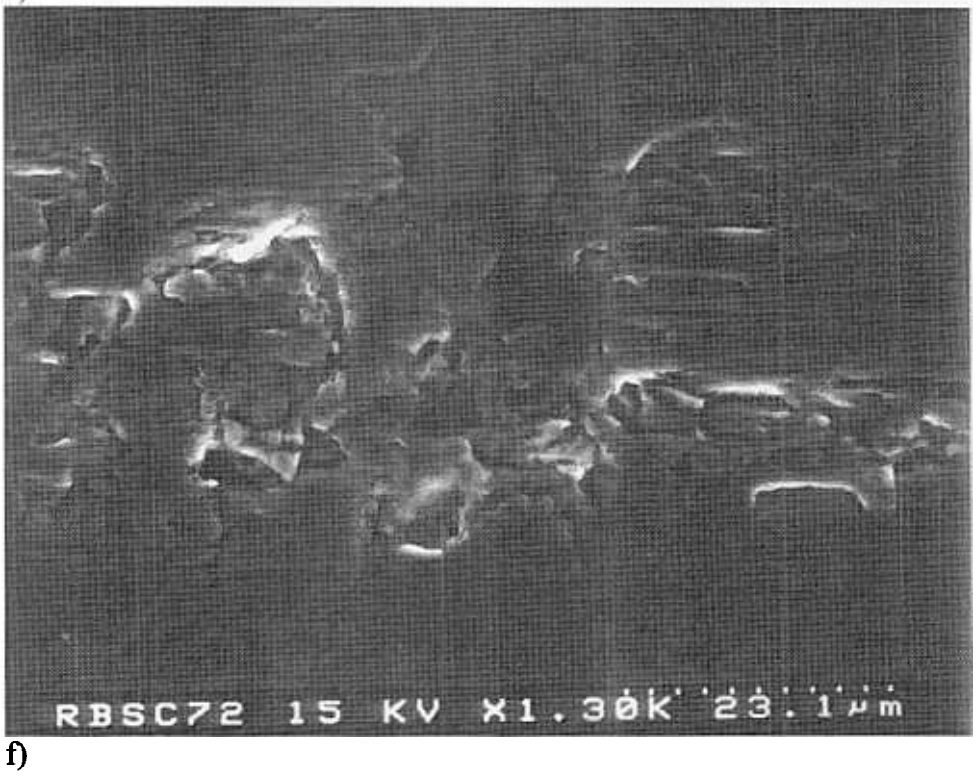

f)

Figure 32, Scanning electron micrographs of low load scratch tests on RBSC ceramic, a) single pass with 50 µm indenter, b) 100 passes with 50 µm indenter, c) 2 passes with 50 µm indenter, d) 20 passes with 200 µm indenter, e) 200 passes with 200 µm indenter, f) 200 passes with 200 µm indenter.

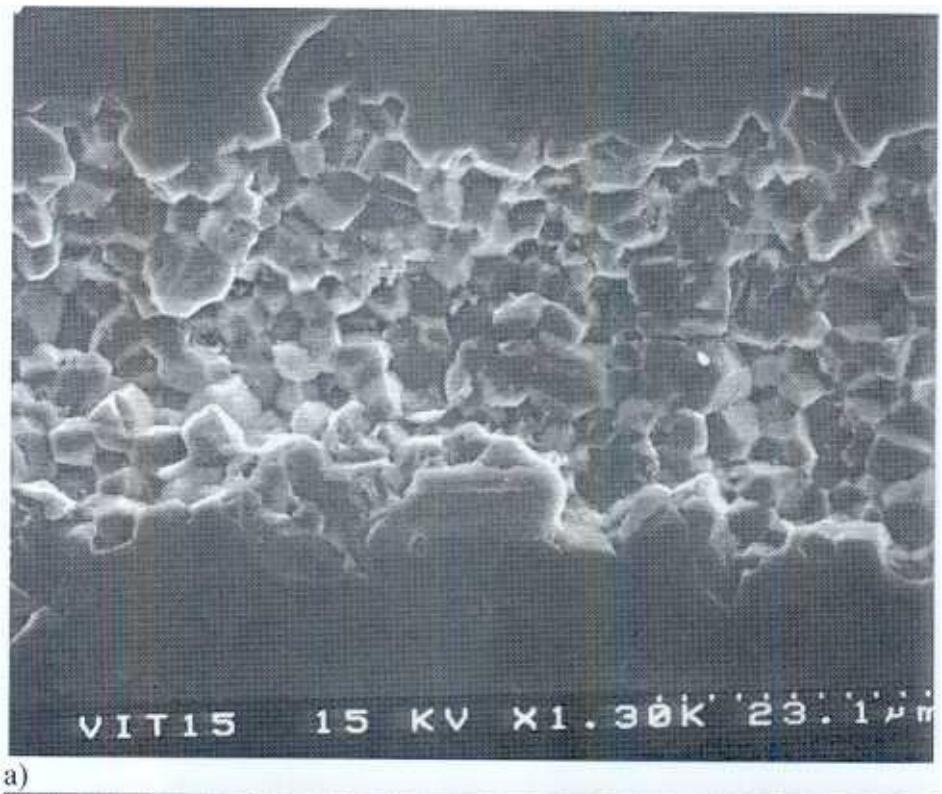

a)

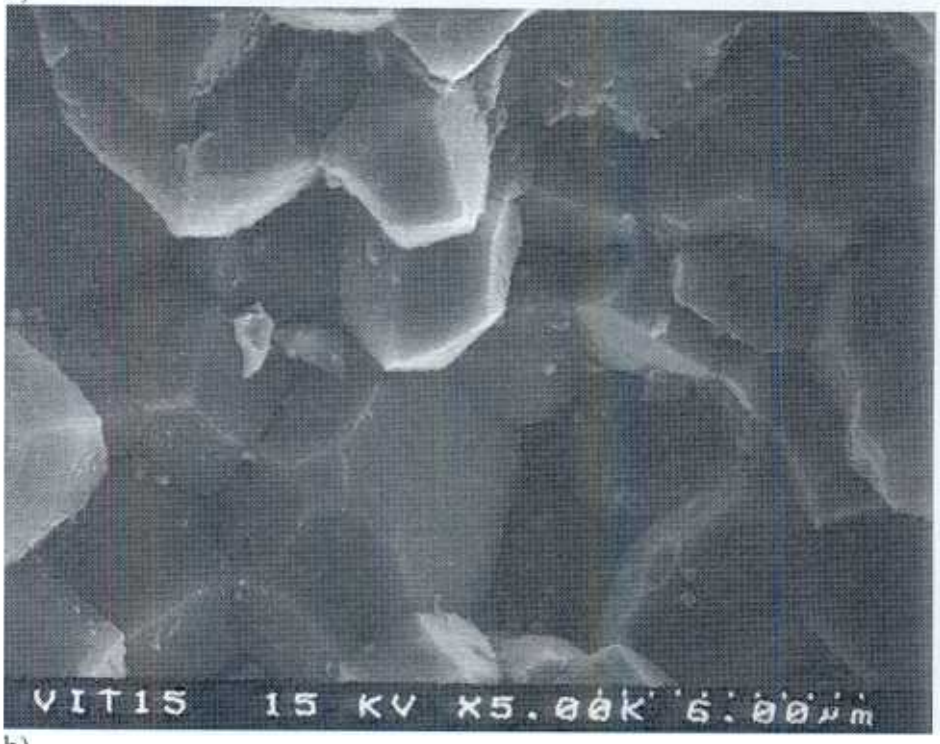

b)

Figure 33, Scanning electron micrographs of low load scratch tests on Vitox ceramic, a) single pass with 50 µm indenter, b) single pass with 50 µm indenter, c) 10 passes with 50 µm indenter, d) 10 passes with 50 µm indenter, e) 50 passes with 50 µm indenter, f) 100 passes with 50 µm indenter, g) 5 passes with 200 µm indenter, h) 20 passes with 200 µm indenter, i) 50 passes with 200 µm indenter, j) 100 passes with 200 µm indenter.

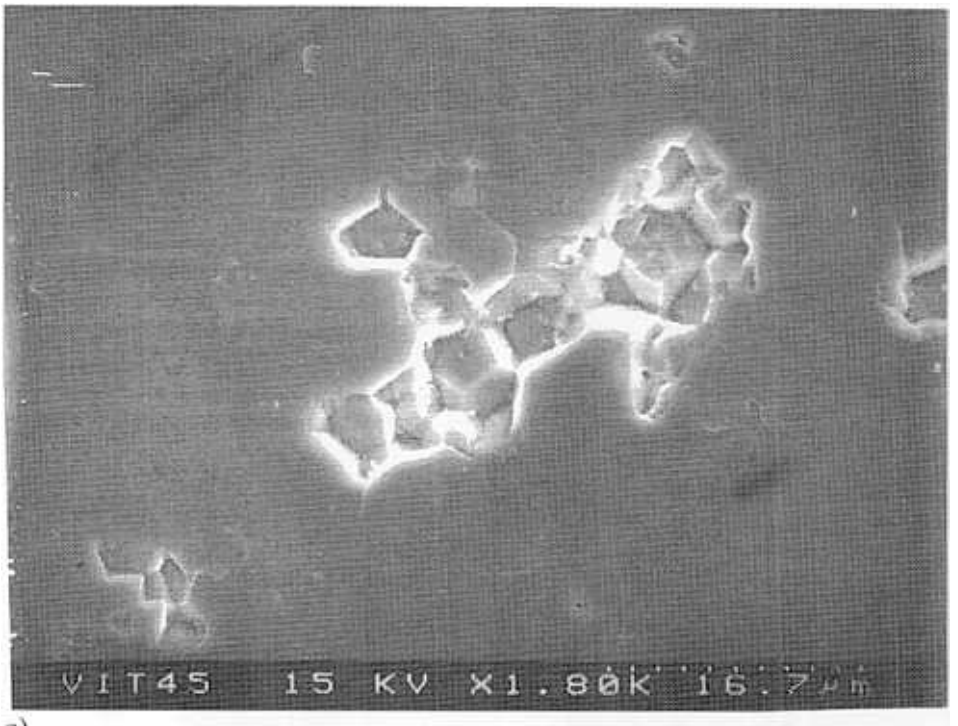

c)

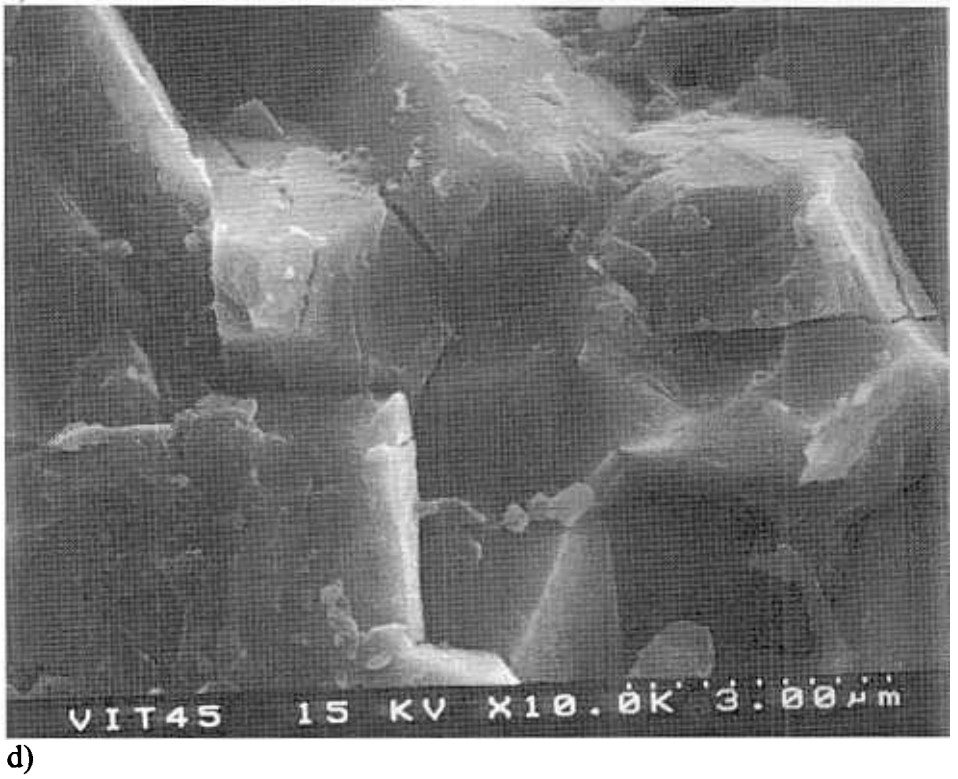

d)

Figure 33, Scanning electron micrographs of low load scratch tests on Vitox ceramic, a) single pass with 50 µm indenter, b) single pass with 50 µm indenter, c) 10 passes with 50 µm indenter, d) 10 passes with 50 µm indenter, e) 50 passes with 50 µm indenter, f) 100 passes with 50 µm indenter, g) 5 passes with 200 µm indenter, h) 20 passes with 200 µm indenter, i) 50 passes with 200 µm indenter, j) 100 passes with 200 µm indenter.

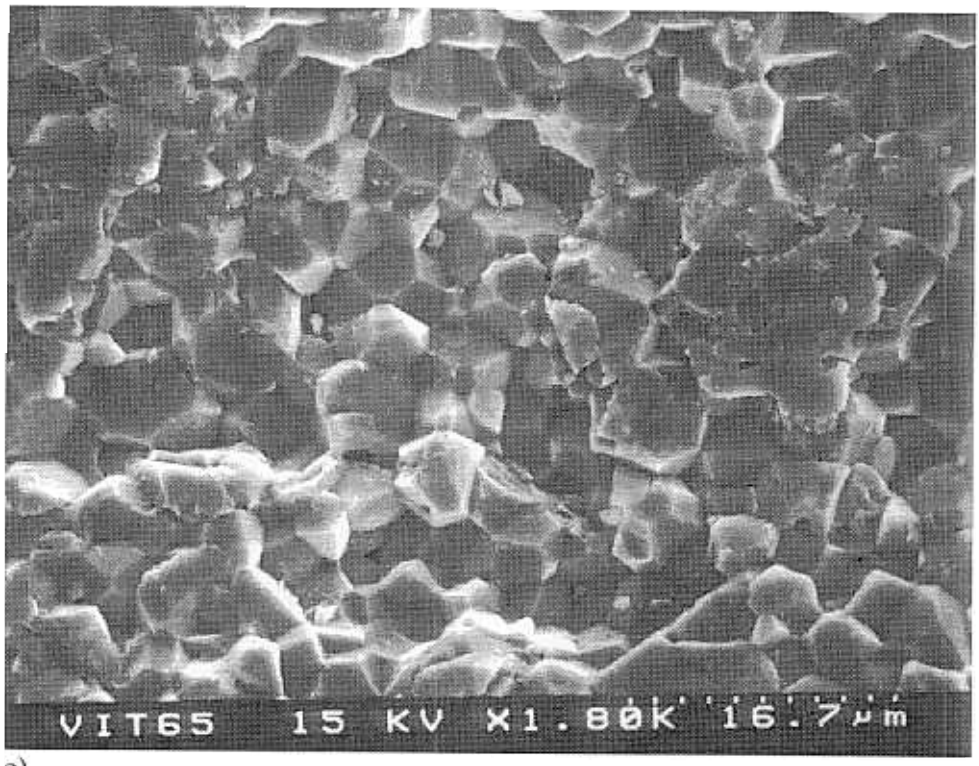

c)

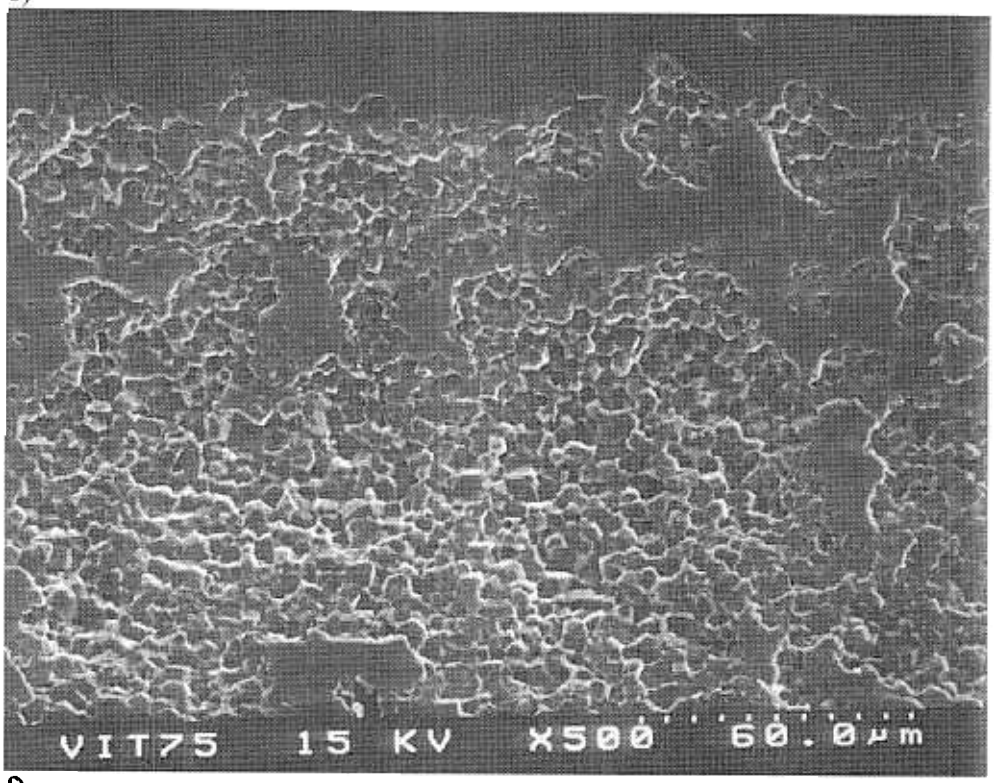

f)

Figure 33, Scanning electron micrographs of low load scratch tests on Vitox ceramic, a) single pass with 50 µm indenter, b) single pass with 50 µm indenter, c) 10 passes with 50 µm indenter, d) 10 passes with 50 µm indenter, e) 50 passes with 50 µm indenter, f) 100 passes with 50 µm indenter, g) 5 passes with 200 µm indenter, h) 20 passes with 200 µm indenter, i) 50 passes with 200 µm indenter, j) 100 passes with 200 µm indenter.

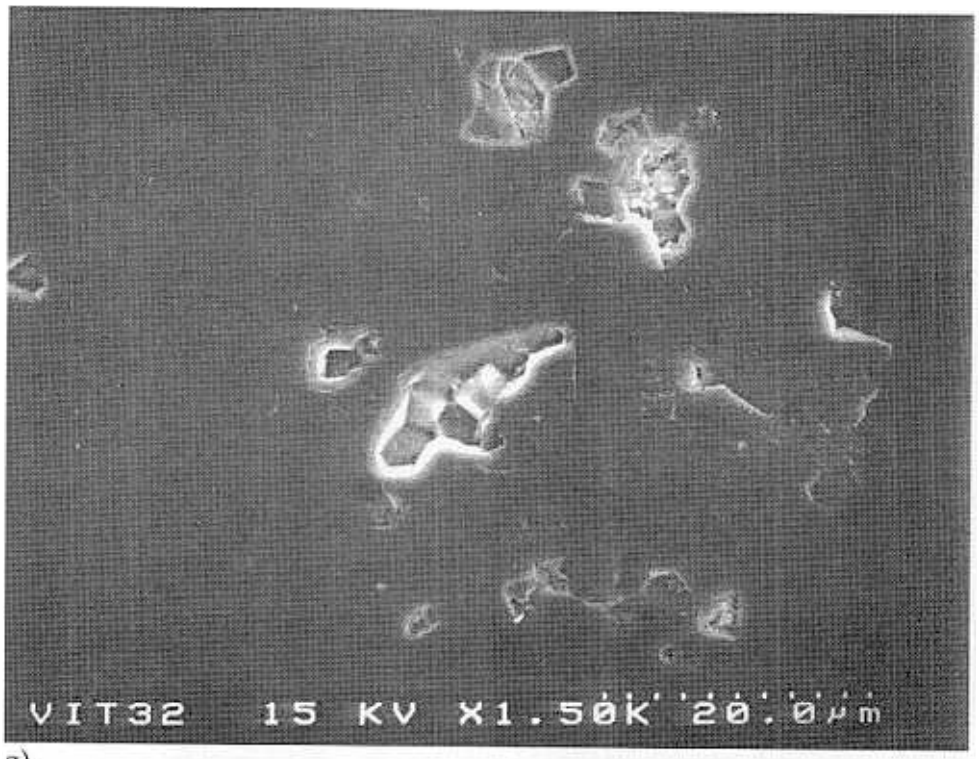

g)

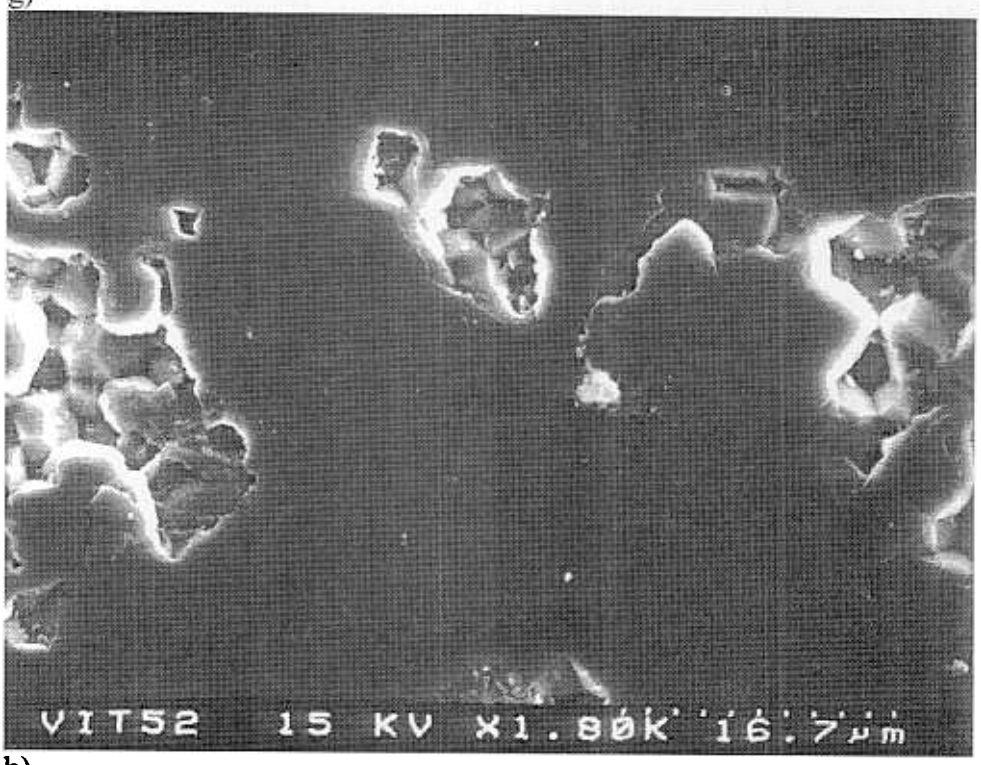

h)

Figure 33, Scanning electron micrographs of low load scratch tests on Vitox ceramic, a) single pass with 50 µm indenter, b) single pass with 50 µm indenter, c) 10 passes with 50 µm indenter, d) 10 passes with 50 µm indenter, e) 50 passes with 50 µm indenter, f) 100 passes with 50 µm indenter, g) 5 passes with 200 µm indenter, h) 20 passes with 200 µm indenter, i) 50 passes with 200 µm indenter, j) 100 passes with 200 µm indenter.

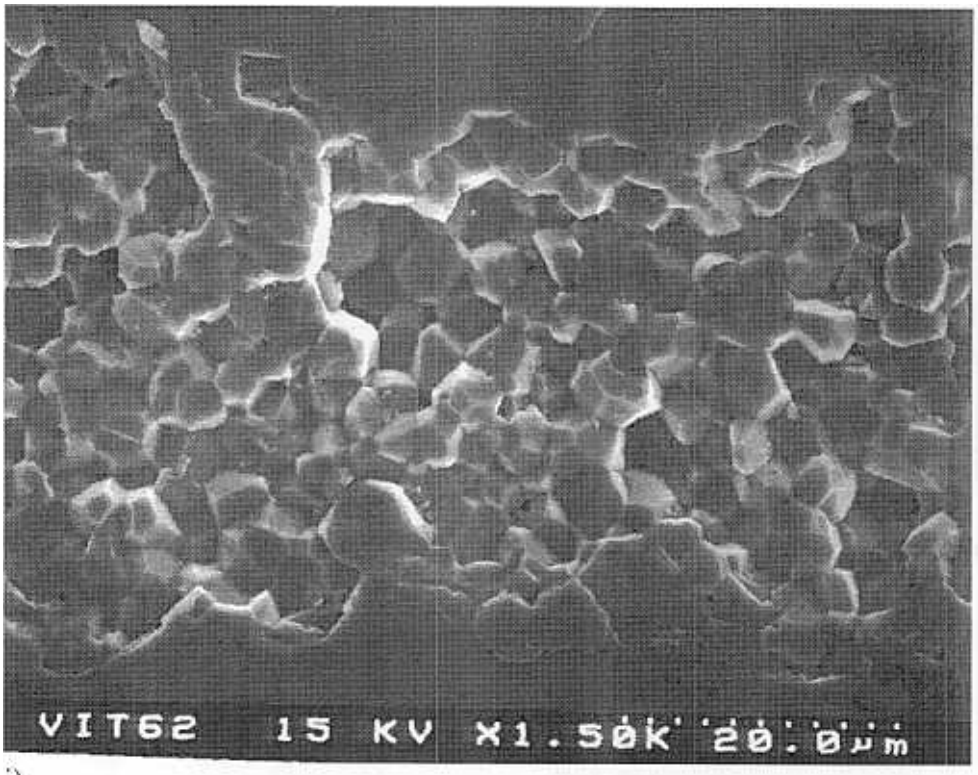

i)

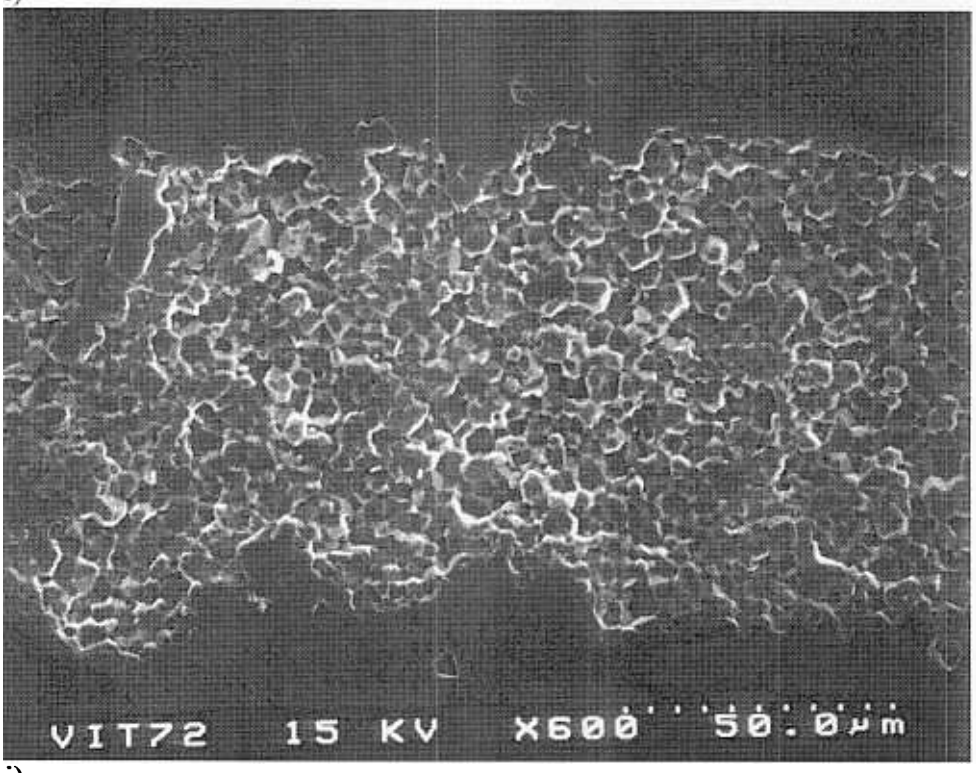

j)

Figure 33, Scanning electron micrographs of low load scratch tests on Vitox ceramic, a) single pass with 50 µm indenter, b) single pass with 50 µm indenter, c) 10 passes with 50 µm indenter, d) 10 passes with 50 µm indenter, e) 50 passes with 50 µm indenter, f) 100 passes with 50 µm indenter, g) 5 passes with 200 µm indenter, h) 20 passes with 200 µm indenter, i) 50 passes with 200 µm indenter, j) 100 passes with 200 µm indenter.

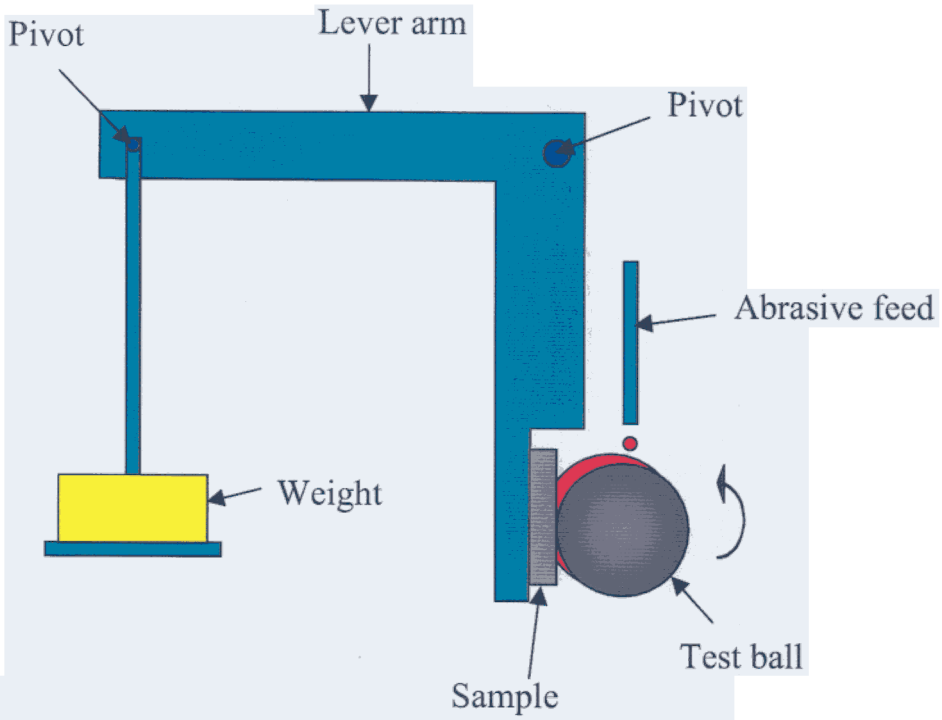

Figure 34, Schematic diagram of ball cratering equipment

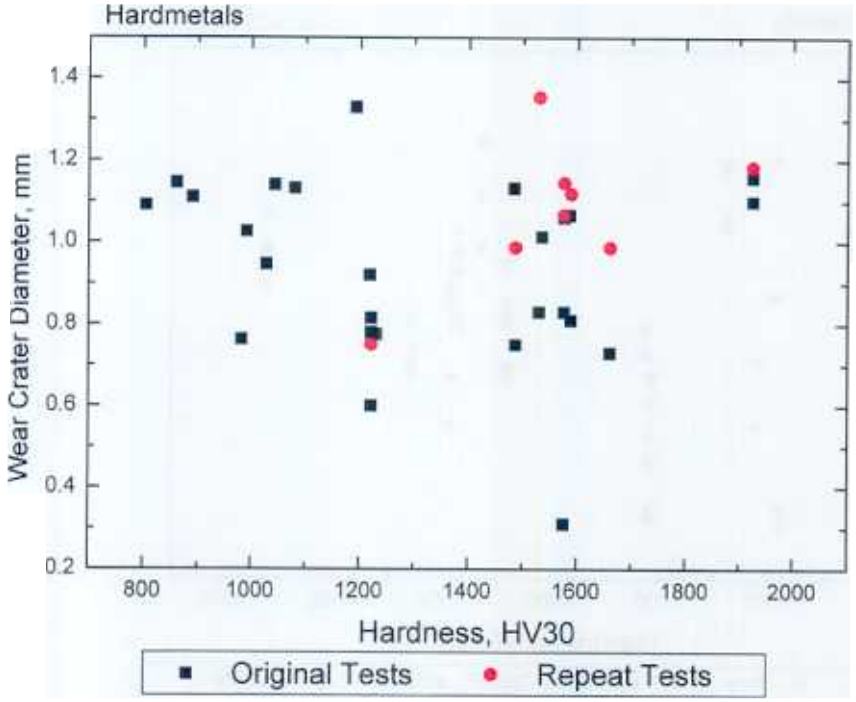

a)

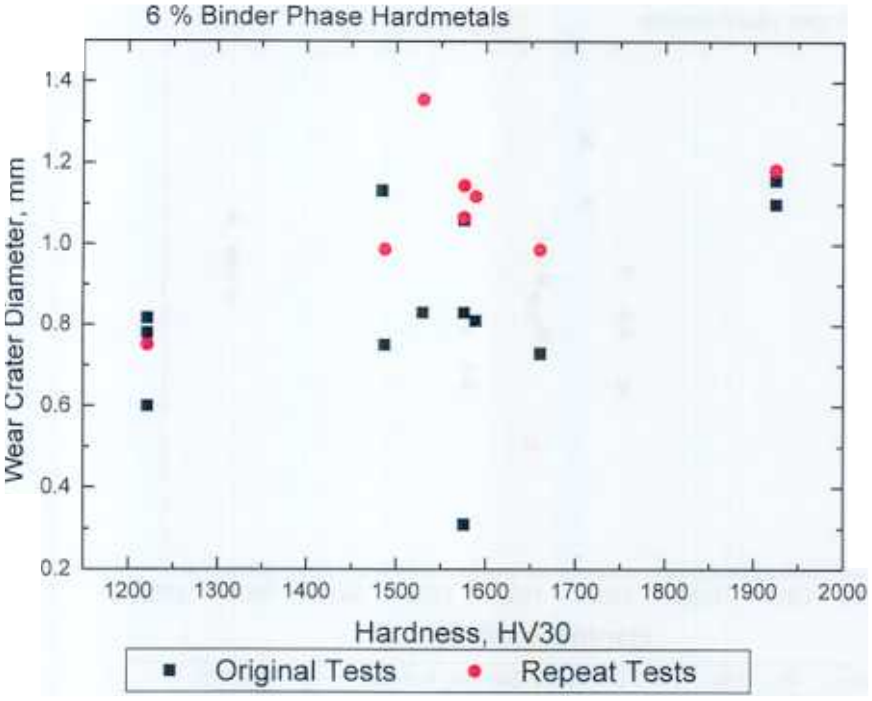

b)

Figure 35, Ball cratering results for hardmetal samples, a) all materials, b) 6 % binder phase only.

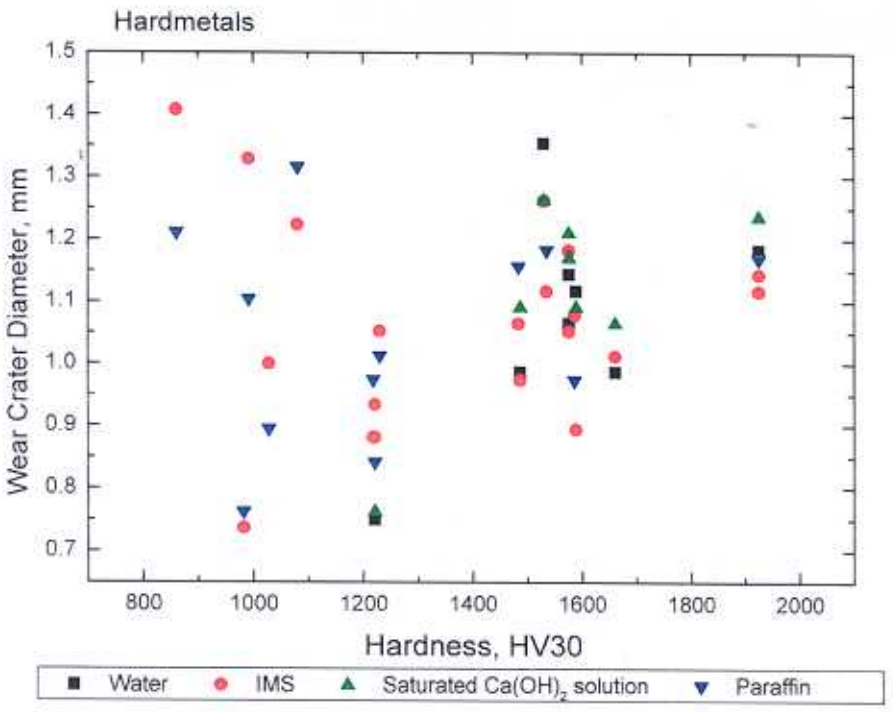

a)

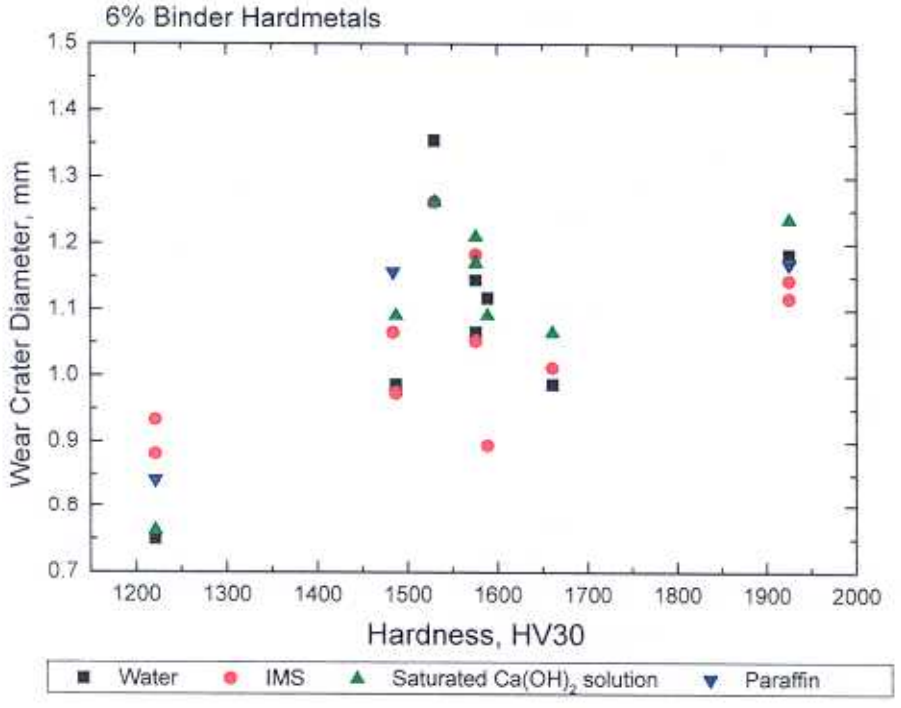

b)

Figure 36, Ball cratering results for hardmetal samples in different abrasive media, a) all materials, b) 6 % binder phase only.

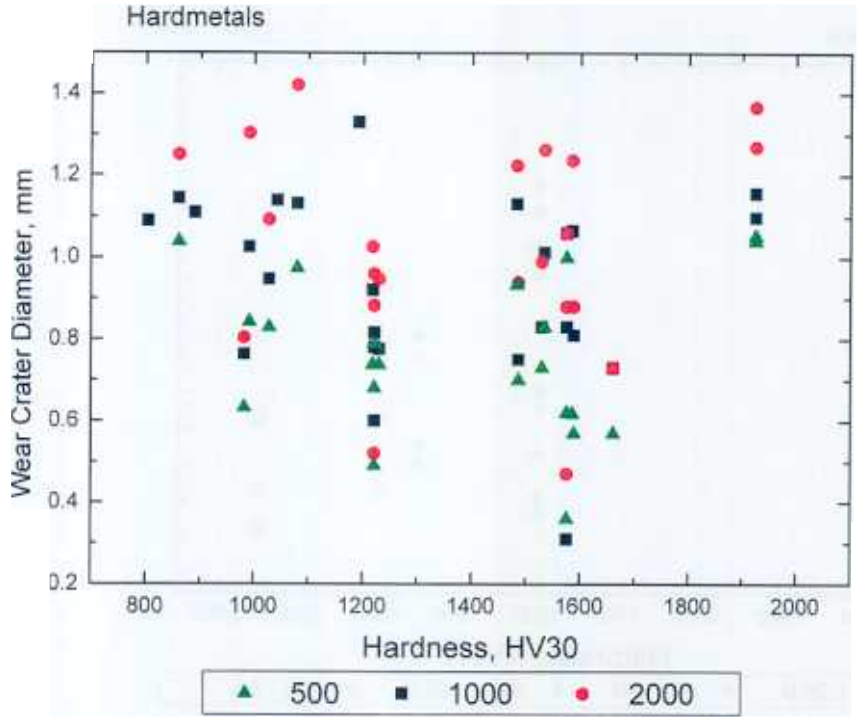

Figure 37, Ball cratering results for hardmetal samples for different test durations (number of ball revolutions).

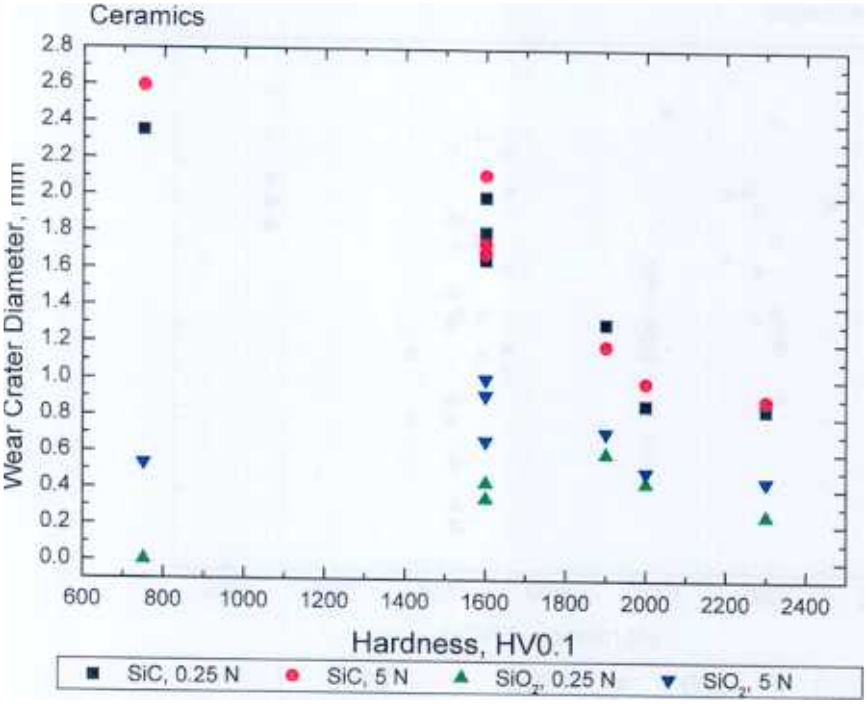

a)

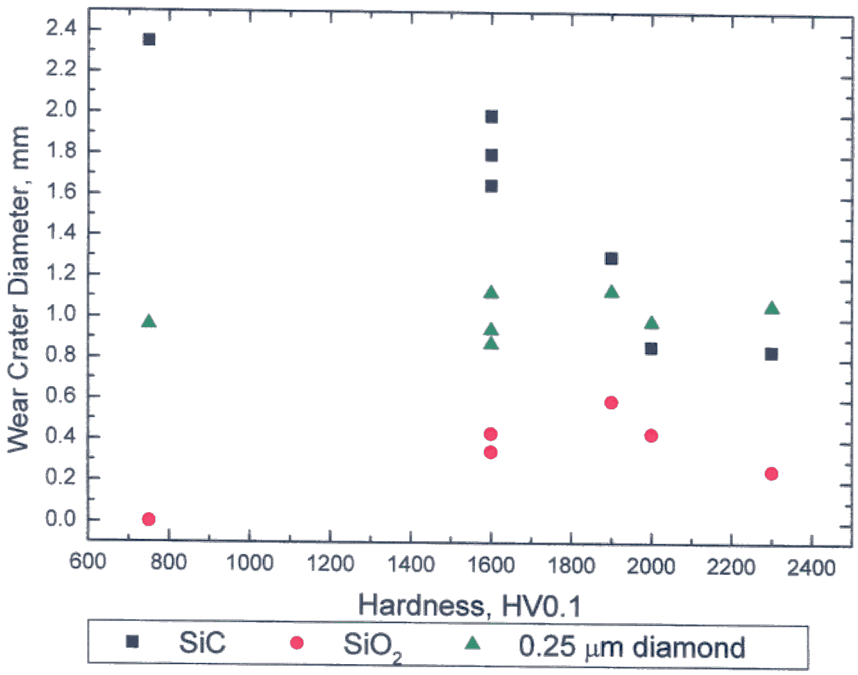

b)

Figure 38, Ball cratering results for ceramic samples, a) SiC and SiO2 abrasive and different loads, b) three different abrasives.

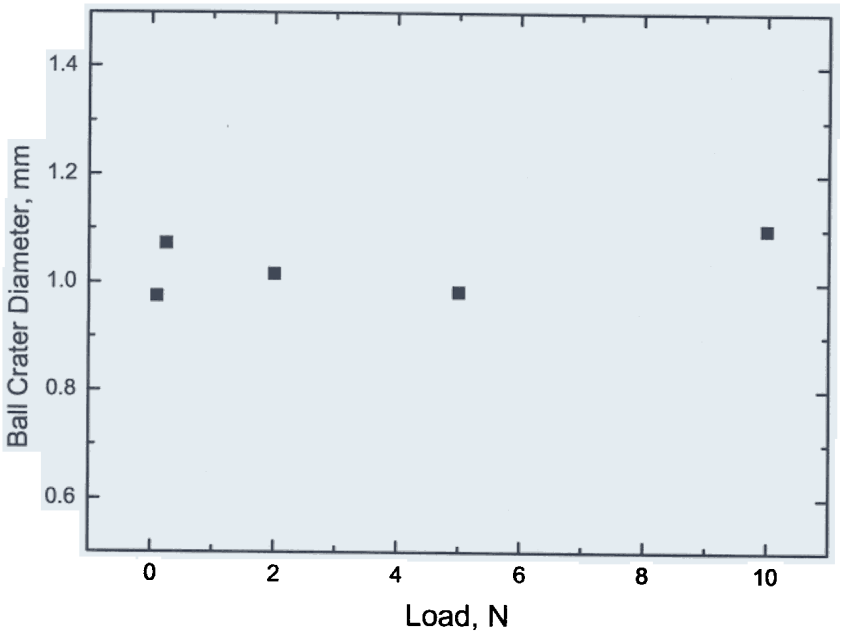

Figure 39, Ball cratering results for hardmetal sample at different loads.

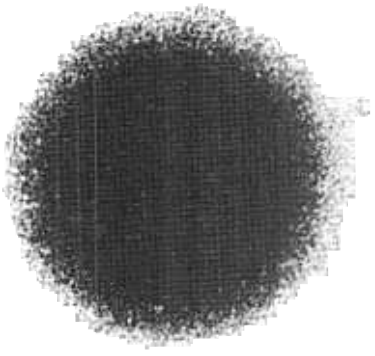

2000 Revolutions, 1221 HV30

a)

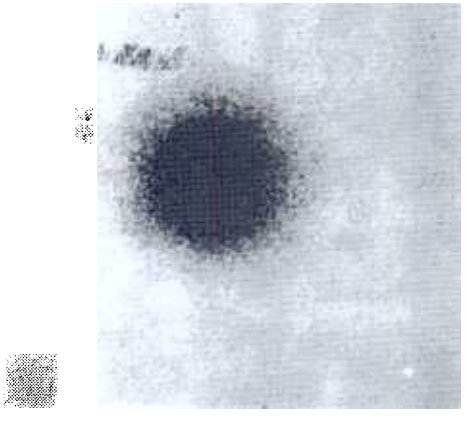

2000 Revolutions, 1580 HV30

b)

2000 Revolutions, 1930 HV30

mm

c)

Figure 40, Optical micrographs of ball craters on three hardmetals. Magnification marker refers to all three micrographs.

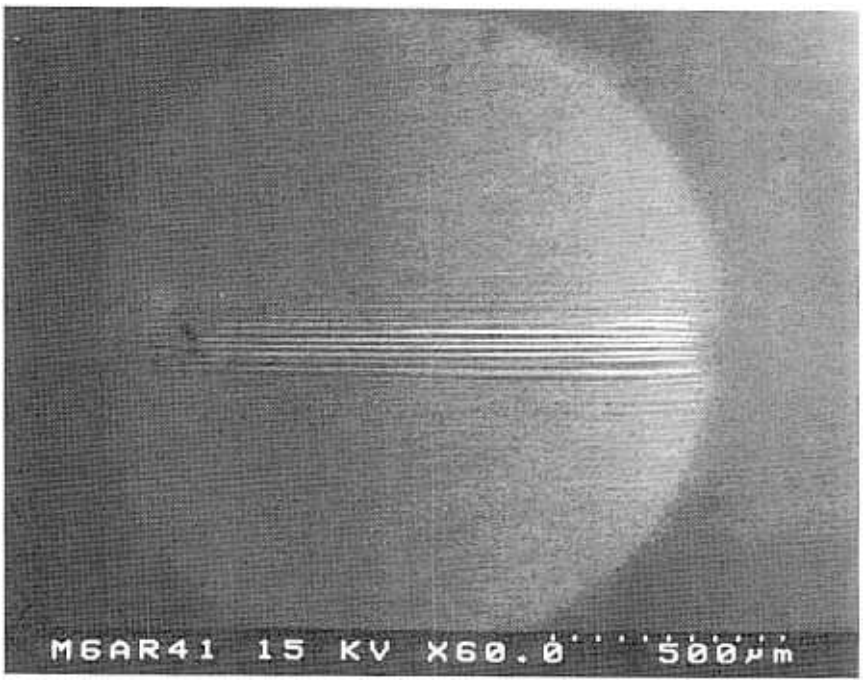

Figure 41, Scanning electron micrograph of ball crater on M6 hardmetal.

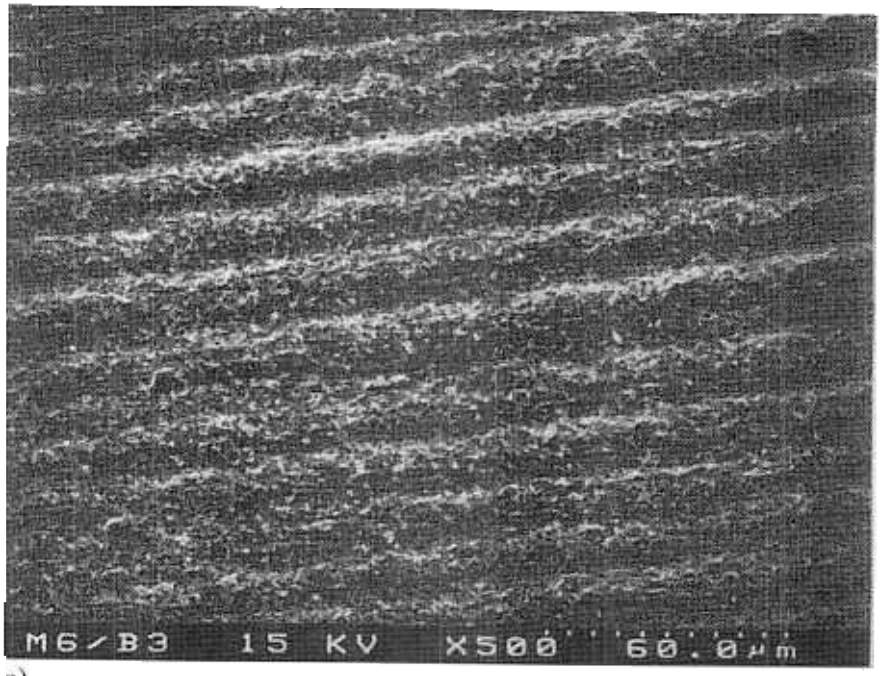

a)

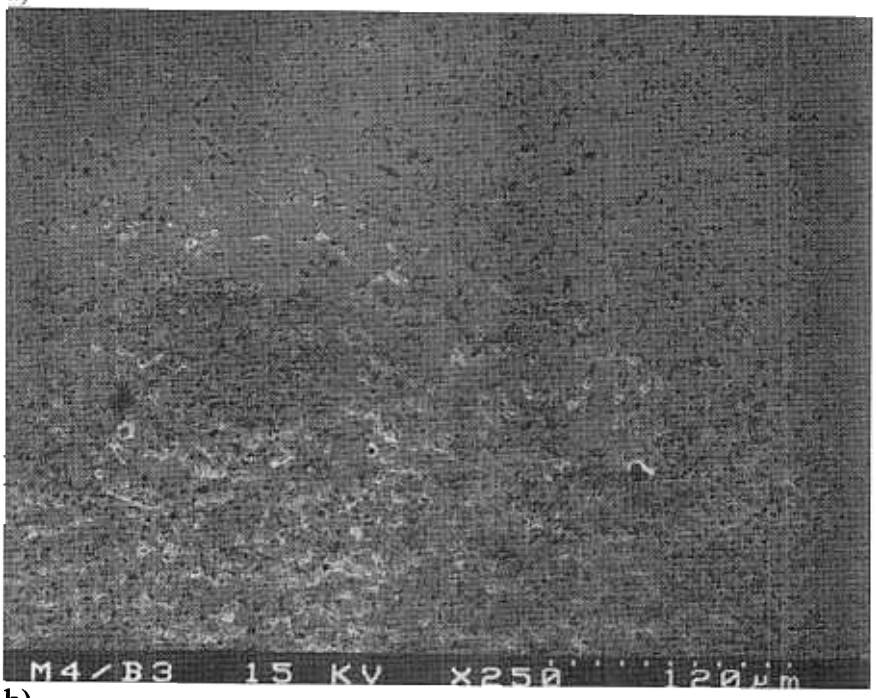

b)

Figure 42, Scanning electron micrographs of worn surface from ball craters on a) M6 hardmetal, b) M4 hardmetal, c) M4 hardmetal, d) M4 hardmetal, e) WCG23 hardmetal, f) M4 hardmetal, g) M6 hardmetal.

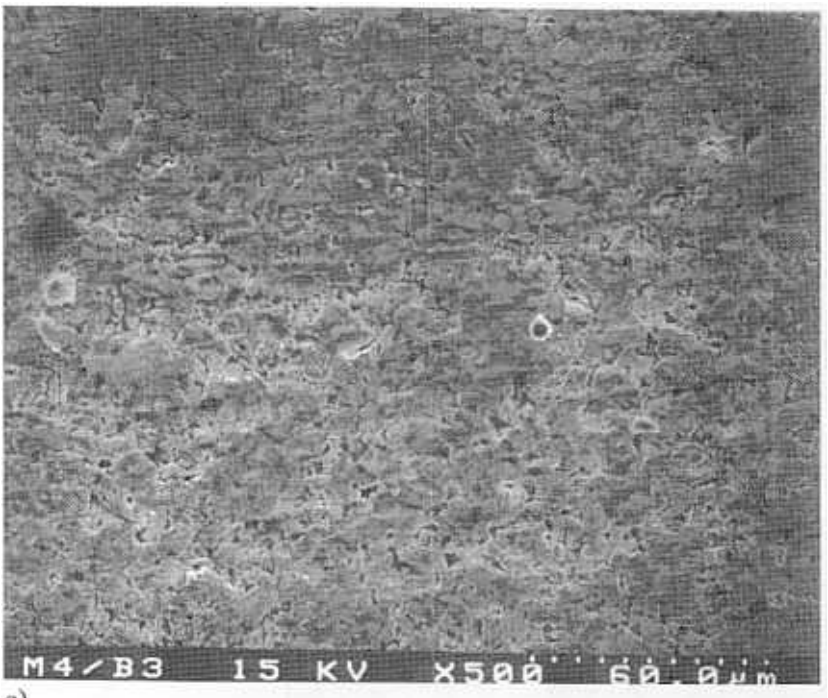

c)

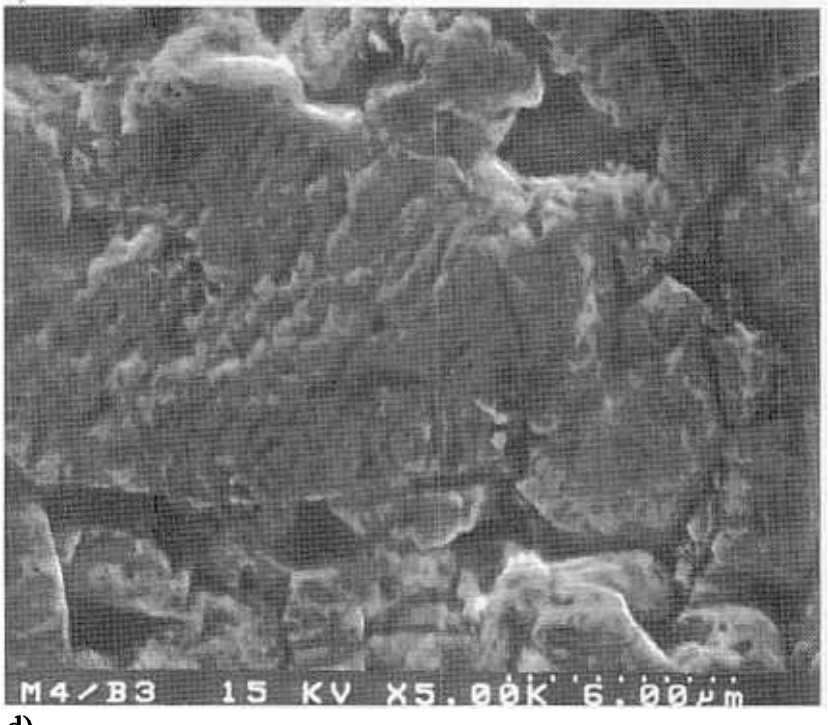

d)

Figure 42, Scanning electron micrographs of worn surface from ball craters on a) M6 hardmetal, b) M4 hardmetal, c) M4 hardmetal, d) M4 hardmetal, e) WCG23 hardmetal, f) M4 hardmetal, g) M6 hardmetal.

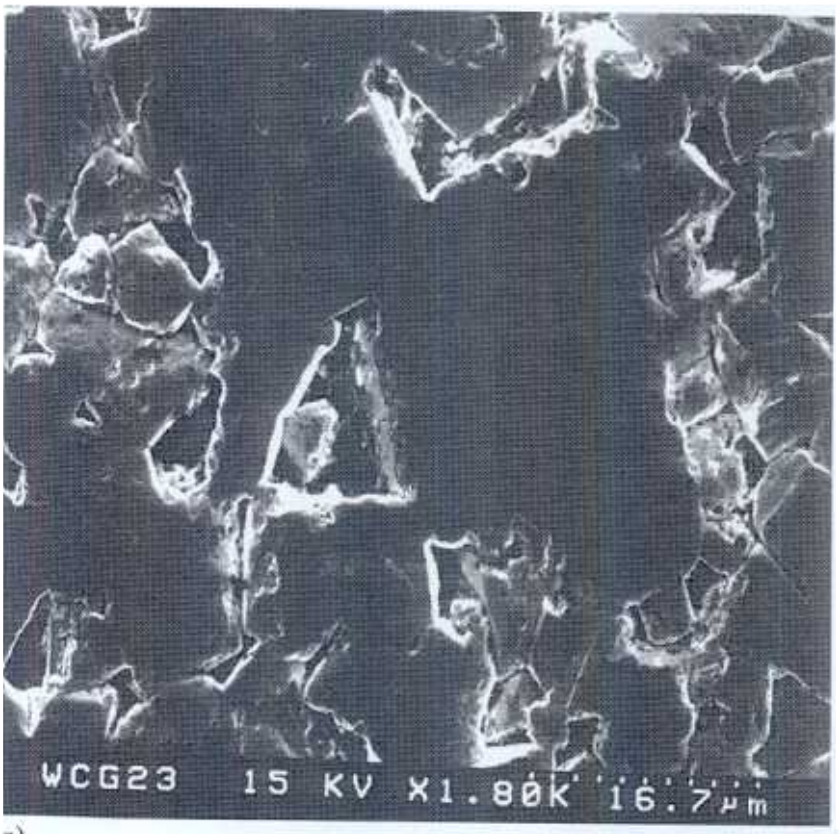

e)

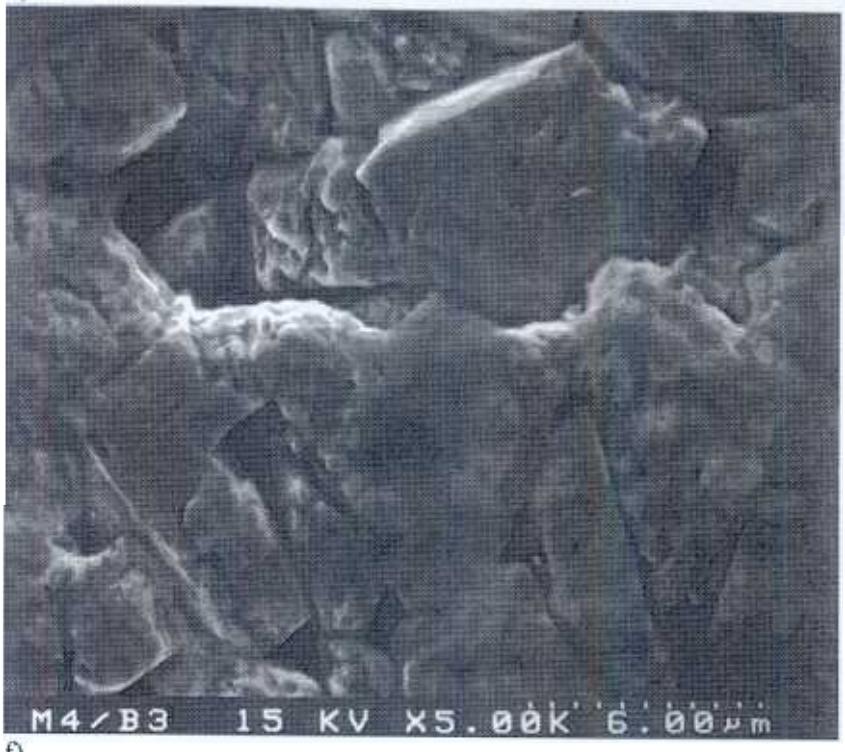

f)

Figure 42, Scanning electron micrographs of worn surface from ball craters on a) M6 hardmetal, b) M4 hardmetal, c) M4 hardmetal, d) M4 hardmetal, e) WCG23 hardmetal, f) M4 hardmetal, g) M6 hardmetal.

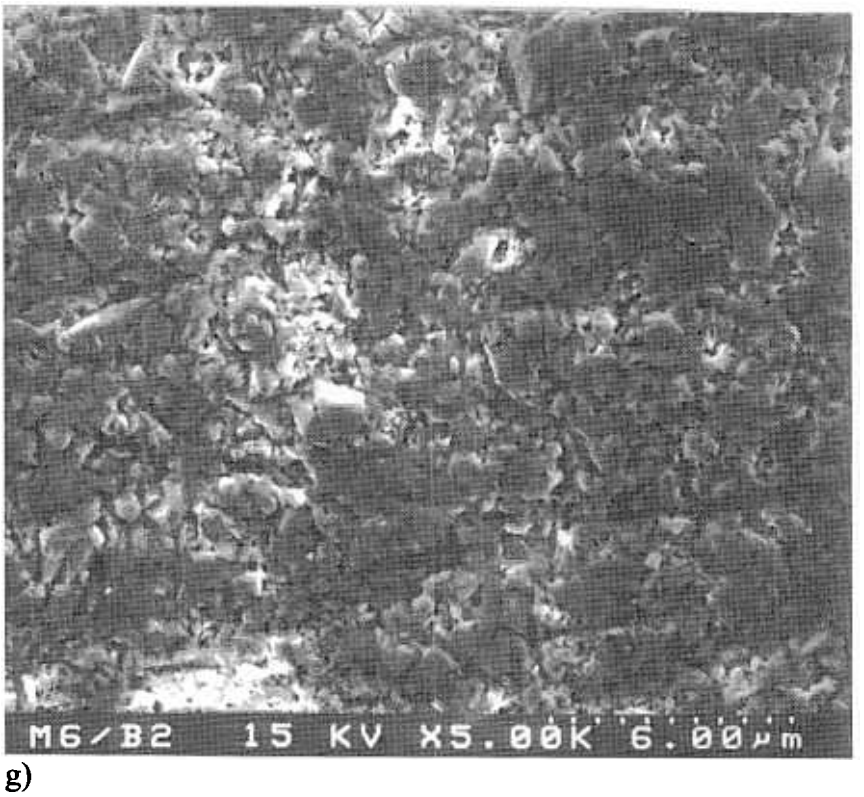

g)

Figure 42, Scanning electron micrographs of worn surface from ball craters on a) M6 hardmetal, b) M4 hardmetal, c) M4 hardmetal, d) M4 hardmetal, e) WCG23 hardmetal, f) M4 hardmetal, g) M6 hardmetal.

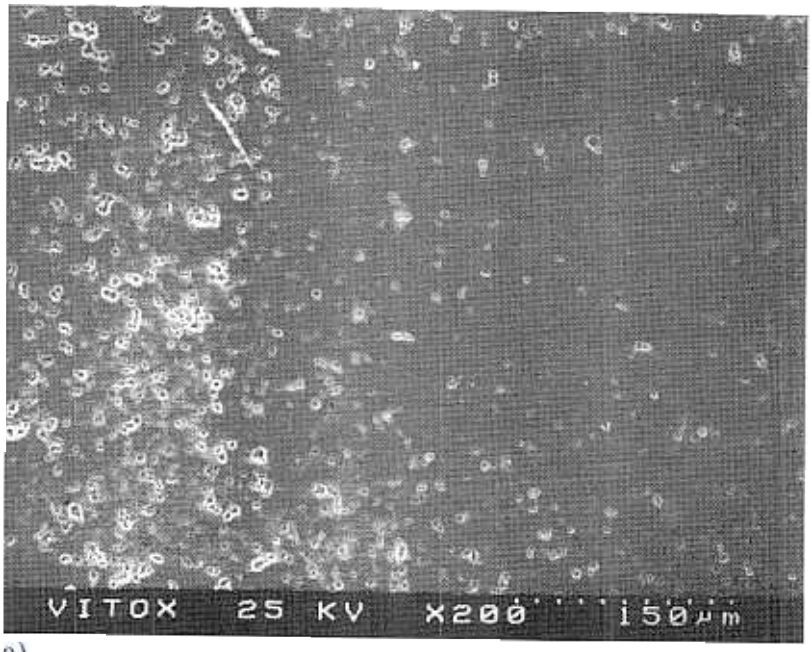

a)

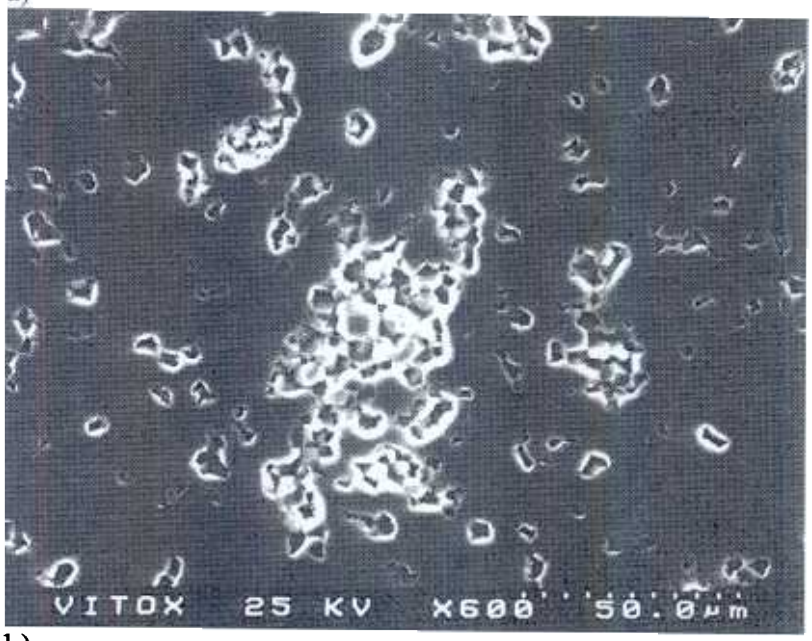

b)

Figure 43, Wear surface of ball crater on Vitox sample.

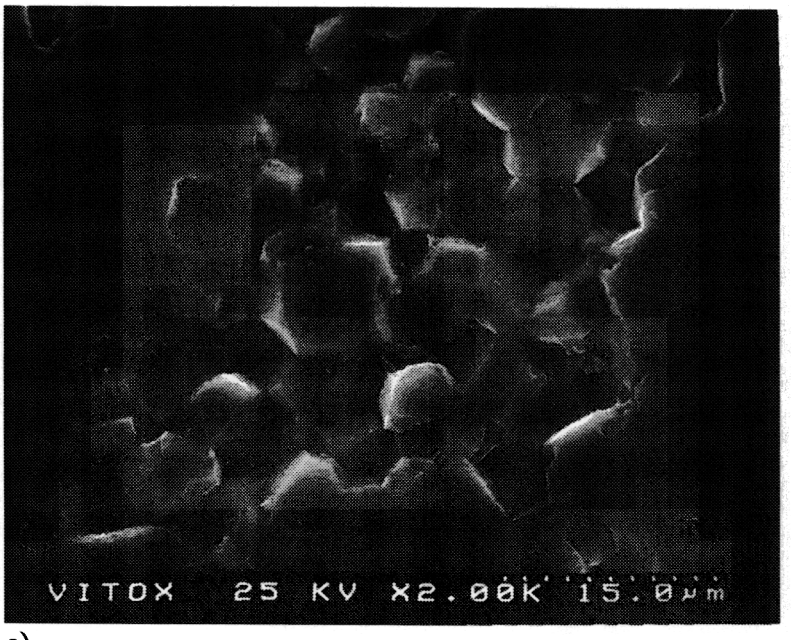

c)

Figure 43, Wear surface of ball crater on Vitox sample.

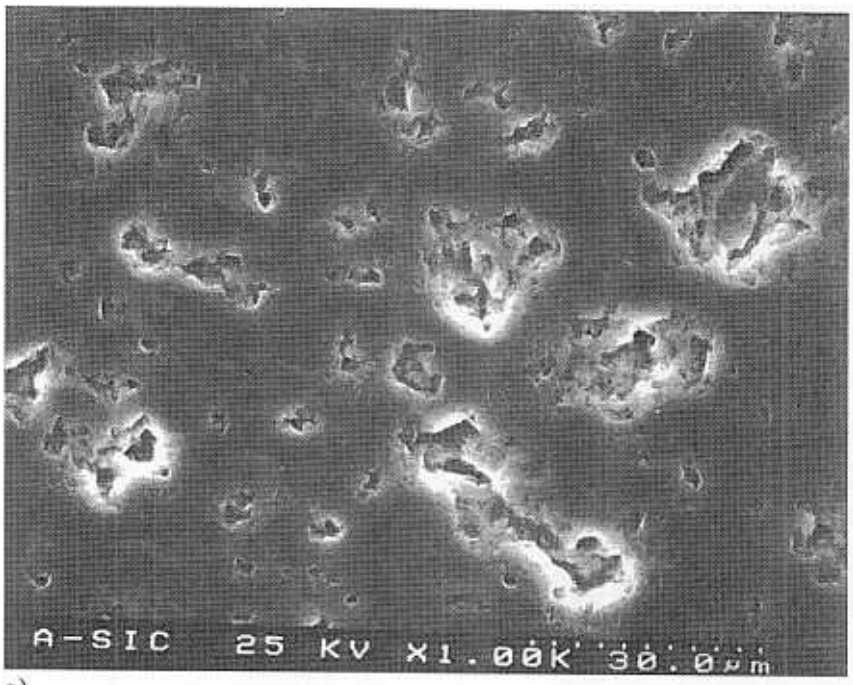

a)

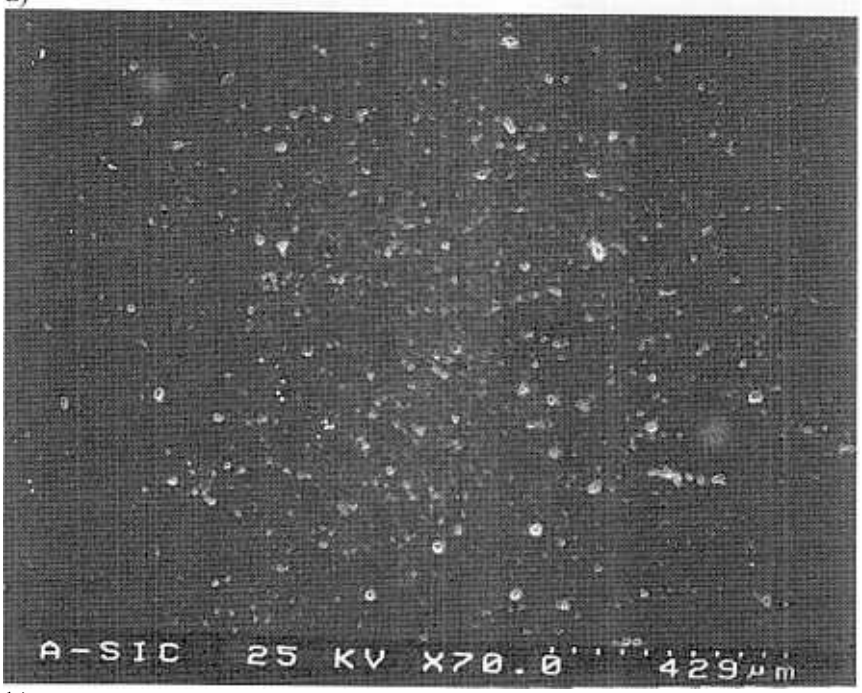

b)

Figure 44, Wear surface of ball crater on α-SiC sample.

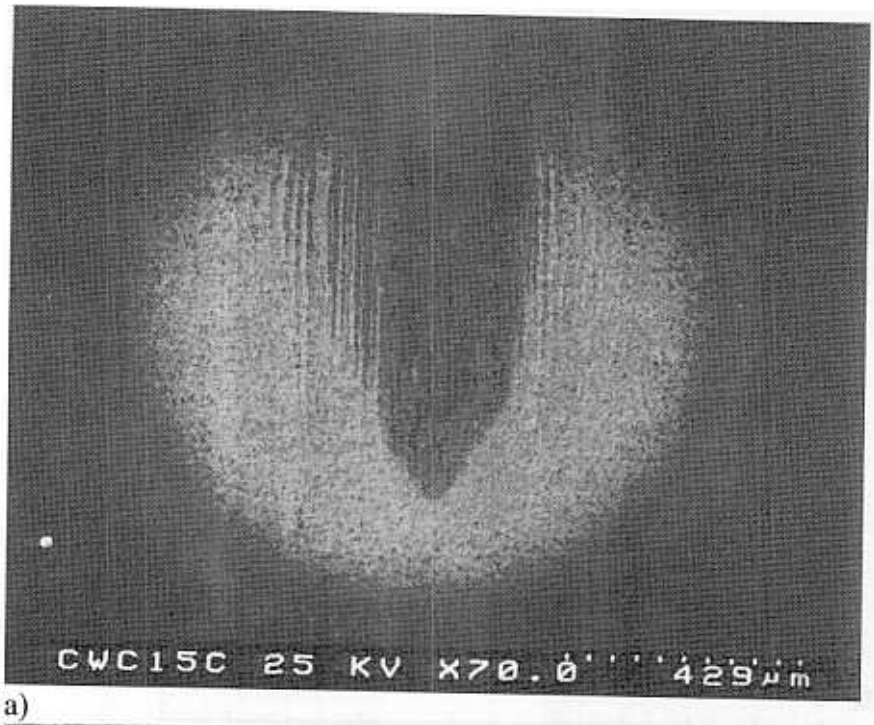

a)

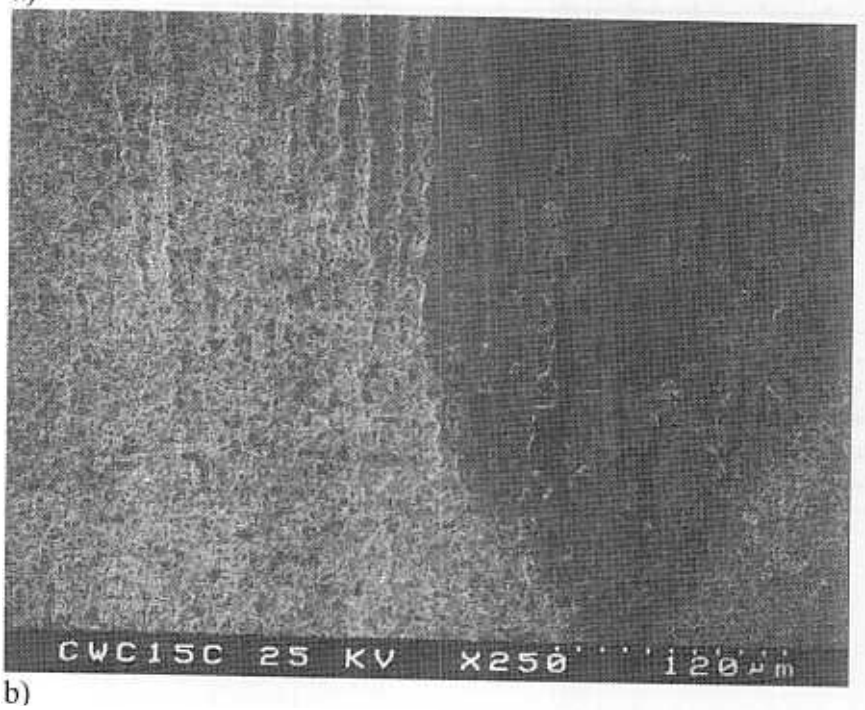

b)

Figure 45, Ball crater on CWC15C sample tested at 5 N load, a) complete crater, b) enlargement of central region.

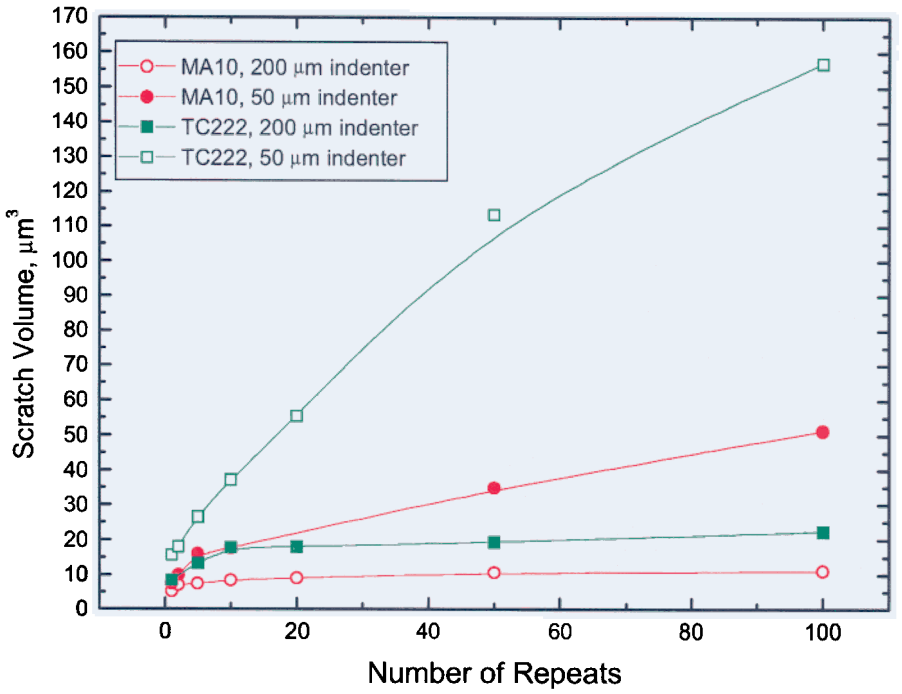

Figure 46, Variation of scratch volume with number of repeat passes for selected hardmetal samples.

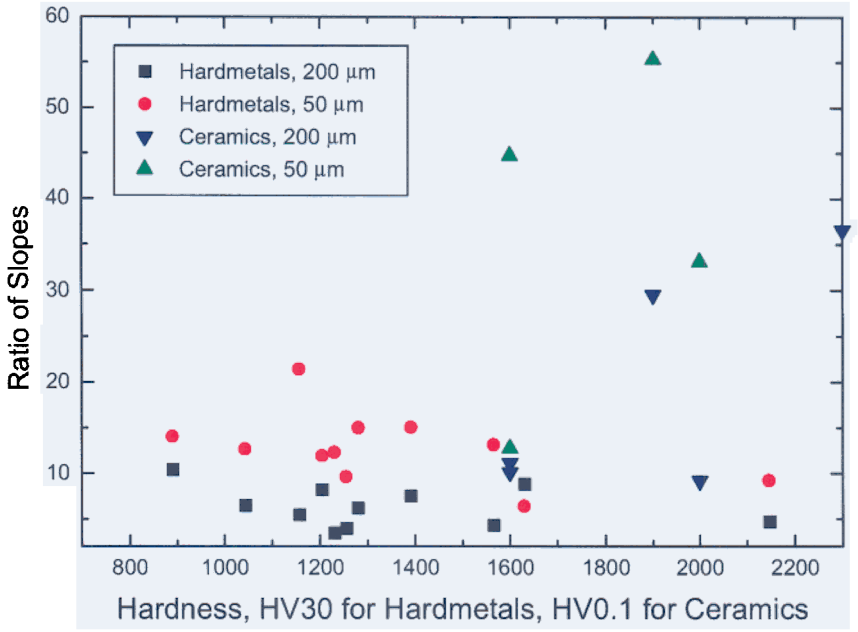

Figure 47, Slope parameter (ratio of slopes in graph) plotted against hardness for ceramics and hardmetals.